NASA TECHNICAL NOTE

NASA TN D-8206

NASA TN D-8206

REVIEW OF DRAG CLEANUP TESTS IN LANGLEY FULL-SCALE TUNNEL (FROM 1935 TO 1945) APPLICABLE TO CURRENT GENERAL AVIATION AIRPLANES

Paul L. Coe, Jr.

Langley Research Center
Hampton, Va. 23665

NATIONAL AERONAUTICS AND SPACE ADMINISTRATION • WASHINGTON, D. C. • JUNE 1976

1. Report No.	2. Government Accession No.	3. Recipient's Catalog No.
NASA TN D-8206		

4. Title and Subtitle	5. Report Date
REVIEW OF DRAG CLEANUP TESTS IN LANGLEY FULL-SCALE TUNNEL (FROM 1935 TO 1945) APPLICABLE TO CURRENT GENERAL AVIATION AIRPLANES	June 1976
	6. Performing Organization Code
7. Author(s)	8. Performing Organization Report No.
Paul L. Coe, Jr.	L-10735
	10. Work Unit No.
9. Performing Organization Name and Address	505-10-11-07
NASA Langley Research Center Hampton, Va. 23665	11. Contract or Grant No.
	13. Type of Report and Period Covered
12. Sponsoring Agency Name and Address	Technical Note
National Aeronautics and Space Administration Washington, D.C. 20546	14. Sponsoring Agency Code

15. Supplementary Notes

16. Abstract

Results of drag cleanup tests conducted in the Langley full-scale tunnel during the period from 1935 to 1945 have been summarized for potential application to current propeller-driven general aviation airplanes. Data from tests on 23 airplanes indicate that the drag increments produced by many individual configuration features – such as, power-plant installation, air leakage, cockpit canopies, control-surface gaps, and antenna installations – are not large; however, when the increments are summed, the resulting total drag increase is significant. On the basis of results of the investigation, it appears that considerable reduction in drag can be obtained by proper attention to details in aerodynamic design and by adherence to the guidelines discussed in the present paper.

17. Key Words (Suggested by Author(s))	18. Distribution Statement
Drag cleanup General aviation	Unclassified – Unlimited Subject Category 02

19. Security Classif. (of this report)	20. Security Classif. (of this page)	21. No. of Pages	22. Price*
Unclassified	Unclassified	97	$4.75

*For sale by the National Technical Information Service, Springfield, Virginia 22161

REVIEW OF DRAG CLEANUP TESTS IN LANGLEY FULL-SCALE TUNNEL (FROM 1935 TO 1945) APPLICABLE TO CURRENT GENERAL AVIATION AIRPLANES

Paul L. Coe, Jr.
Langley Research Center

SUMMARY

Results of drag cleanup tests conducted in the Langley full-scale tunnel during the period from 1935 to 1945 have been summarized for potential application to current propeller-driven general aviation airplanes. Data from tests on 23 airplanes indicate that the drag increments produced by many individual configuration features – such as, power-plant installation, air leakage, cockpit canopies, control surface gaps, and antenna installations – are not large; however, when the increments are summed, the resulting total drag increase is significant. On the basis of results of the investigation, it appears that considerable reduction in drag can be obtained by proper attention to details in aerodynamic design and by adherence to the guidelines discussed in the present paper.

INTRODUCTION

The Langley Research Center of the National Aeronautics and Space Administration is currently engaged in a broad research program to provide the technology required for the design of safe, efficient general aviation airplanes. Recently, considerable interest has been expressed in drag reduction for general aviation airplanes. (See ref. 1.) Reductions in drag would be expected to offer significant improvements in fuel economy and performance, and would thereby insure a strong competitive position in the domestic and foreign market for light airplanes.

From 1935 to 1945, a large number of full-scale military airplanes were subjected to drag cleanup tests in the Langley full-scale tunnel. Such tests identified sources of drag due both to poor design and to manufacturing processes, and in addition, allowed the determination of suitable modifications for these poor design features. For example, cleanup tests for the Army P-39 fighter resulted in modifications which reduced the drag coefficient of the airplane by about 35 percent and indicated a potential increase in the maximum speed of the airplane of over 44 knots. The results of cleanup tests for 23 of the configurations studied were summarized in reports by C. H. Dearborn, Abe Silverstein,

and Roy H. Lange (refs. 2 and 3). Unfortunately, these summary reports were originally issued as NACA Wartime Reports with restricted distribution, and they are now generally unavailable.

It is believed that many of the results and design guidelines derived from the foregoing tests are directly applicable to current propeller-driven general aviation airplanes. The present paper was therefore prepared to collate information from the two previous reports in a readily available publication. The results of references 2 and 3 have been technically edited, and items having no application to general aviation airplanes (such as drag of armament installations) have been omitted.

SYMBOLS

In order to facilitate international usage of data presented, dimensional quantities are given in both the International System of Units (SI) and in U.S. Customary Units. Measurements were made in U.S. Customary Units.

A_e	duct exit area, m^2 (ft^2)
A_i	duct inlet area, m^2 (ft^2)
A_r	radiator frontal area, m^2 (ft^2)
b	wing span, m (ft)
C_D	drag coefficient, $\frac{F_D}{qS}$
ΔC_D	drag-coefficient increment
$C_{D,w,o}$	wing profile drag coefficient at zero lift
$\Delta C_{D,w,o}$	difference between measured and calculated wing profile drag coefficients
c	local wing chord, m (ft)
$\bar{c}$	reference wing chord, m (ft)
$c_{d,o}$	two-dimensional wing section drag coefficient at zero lift
C_L	lift coefficient, $\frac{F_L}{qS}$

F_D	drag force, N (lb)
F_L	lift force, N (lb)
P	power, W (hp)
p_t	total pressure, N/m^2 (lb/ft^2)
Δp_t	change in total pressure, N/m^2 (lb/ft^2)
p_∞	free-stream static pressure, N/m^2 (lb/ft^2)
Q	volumetric flow rate of air, m^3/sec (ft^3/min)
$Q_{REQ'D}$	required volumetric flow rate of air, m^3/sec (ft^3/min)
q	free-stream dynamic pressure, N/m^2 (lb/ft^2)
S	wing area, m^2 (ft^2)
s	distance along wing surface measured from stagnation point, m (ft)
t	maximum wing section thickness for a given spanwise location, m (ft)
y	spanwise distance along wing measured from airplane center line, m (ft)
α	angle of attack, deg

Abbreviations:

L.E.	leading edge
rpm	revolutions per minute

AIRPLANES AND EQUIPMENT

Three-view sketches of the 23 airplanes tested are presented in figure 1, and photographs showing the airplanes mounted for tests in the wind tunnel are presented in figure 2. The photographs show most of the airplanes in the condition as received at the

Langley full-scale tunnel (designated original, or service, condition); however, a few configurations are shown in various stages of modification as described in the figure titles. The basic geometric characteristics and power-plant characteristics of the airplanes are presented in tables I and II, respectively. Most of the configurations were early models, or prototypes, of fighter airplanes.

The tests were conducted in the 9.1-m by 18.3-m (30-ft by 60-ft) open-throat test section of the Langley full-scale tunnel. The tunnel is described in detail in reference 4.

METHODS AND TESTS

The results presented herein were obtained from tests at tunnel speeds ranging from 27 m/sec (88 ft/sec) to 45 m/sec (147 ft/sec). The usual procedure in the tests was first to fair or remove all protrusions on the airplane and seal all points where air leakage was suspected. With the airplane in this condition, which is referred to as the sealed and faired condition, force tests were made to determine the drag of the airplane at lift coefficients corresponding to those required for the high-speed flight condition. The seals and fairings were then progressively removed and the drag increment due to each change was determined. In some cases the order in which seals and fairings were removed affected the amount of drag measured, and an attempt was made in all tests to isolate as many drag items as possible. In most cases the motion of wool tufts attached to the airplane surface was observed as an aid to the determination and analysis of poor airflow conditions. Except as noted, all tests were made with the propellers removed from the airplanes.

In order to determine the drag associated with cooling airflow, force tests were conducted with cowling and/or duct inlets and outlets completely sealed, and with these inlets and outlets open. In conjunction with these tests, airflow quantities through the ducts and cowlings were determined from measurements of the static and total pressures ahead of and at the outlet of the cooling units.

The wing profile drag was determined for airplanes 1 to 11 from total- and static-pressure surveys in the wake of the wing, at various spanwise locations. These measurements were obtained at a tunnel speed of 38 m/sec (125 ft/sec). The technique used is described in detail in reference 5. As an aid in the analysis of wing drag, the boundary-layer transition point was determined from total-pressure measurements and by hot-wire techniques. These methods are described in detail in reference 6.

When geometric features contributing to excessive drag were identified, practical modifications to the airplanes were determined, and the effectiveness of the modifications was evaluated in subsequent force tests.

RESULTS AND DISCUSSION

The results of the drag cleanup tests provided valuable insight into configuration features which produce excessive drag, with emphasis on drag associated with power-plant installations, air leakage, landing-gear installations, cockpit canopies, wing surface irregularities, control-surface gaps, and antenna installations. In most cases the drag increment due to these individual items was small; however, the sum of the drag increments produced by the items was a significant part of the total drag of each configuration. Perhaps the most valuable contribution of the drag cleanup tests was the identification of features that contributed to excessive drag and the development of modifications which reduced the drag increments of these features. The increases in performance predicted for the modified airplanes were, in many instances, verified by flight tests. In some cases it was not practical to incorporate these features into the existing design; however, they were used successfully in the design of subsequent airplane configurations.

The drag coefficients of the airplanes in the service condition and the drag-coefficient increments produced by modifying or removing various airplane components are summarized in table III. Because of the diverse nature of the individual items and modifications considered, a brief discussion of specific test results is presented with appropriate figures in the appendixes as follows:

	Appendix	Figure
Power-plant installation	A	A1 to A31
Air leakage	B	B1 to B2
Wing surface irregularities	C	C1 to C3
Landing-gear installations	D	D1 to D8
Cockpit canopies	E	E1 to E4
Control-surface gaps	F	F1
Antenna installations	G	G1 to G3

A general discussion of the design features which contribute to excessive drag is given in a subsequent section.

Identification of Drag Sources for a Representative Airplane

Presented in table IV are results of tests for airplane 8 (Seversky XP-41). These results indicate the impressive level of drag which is produced by a number of airplane features. As previously mentioned, the initial tests consisted of measuring the drag of the airplane in a sealed and faired condition. As the seals and fairings associated with the power-plant installation were removed individually, the drag increments for the following items were identified (the values are given in percent of the drag of the airplane in the sealed and faired condition and the condition number is indicated in parentheses):

Original cowling and cooling airflow (3 and 12)	18.6 percent
Unfaired carburetor air scoop (7)	3.6 percent
Cooling airflow through accessory compartment (13)	3.0 percent
Projecting exhaust stacks (10)	3.6 percent
Intercooler (11)	6.6 percent
Oil cooler (5)	10.2 percent

The foregoing items associated with the power-plant installation increased the drag 45.6 percent above that for the sealed and faired condition.

The drag increments for the additional features required to bring the airplane to service condition were

Removing seals from gaps in cowling flaps (14)	5.4 percent
Ejector chute (9)	1.8 percent
Removing seals around landing-gear doors (4)	1.2 percent
Sanded walkway (8)	4.2 percent
Antenna (18)	4.8 percent
Blast tubes (17)	1.8 percent

The total drag associated with this group of protrusion, roughness, and leakage items was 19.2 percent of the drag for the sealed and faired condition.

The combined drag of the power-plant items and the protrusion, roughness, and leakage items increased the drag of the sealed and faired airplane by an impressive 64.8 percent. Additional drag was produced by features of the cockpit ventilator and cowling venturi, and the total drag of the service airplane was about 66 percent higher than the value for the sealed airplane. It is particularly important to note that although most items generally produced drag increments of only a few percent, these increments add up to an impressive total when summed.

Additional tests and careful analysis showed that the drag of the power-plant items could be reduced from 45.6 percent of the drag for the sealed and faired condition to 26.6 percent, and the drag of the roughness and leakage items could be reduced from 19.2 percent to 2.5 percent. These results are typical of the cleanup tests and indicate that considerable improvements in drag can be made by attention to details in aerodynamic design.

Design Features Contributing to Excessive Drag

The following selected examples illustrate some of the design features for which lack of attention to detail can cause excessive drag.

Power-plant installation.- The power-plant installation, which includes the engine and its accessories (i.e., cooling units, carburetor air scoop, supercharger, exhaust

stacks, etc.) was typically found to produce the largest drag increment of the items investigated. Specific examples of drag-coefficient increments associated with power-plant installations are presented in appendix A. The drag increments may be discussed in terms of drag produced by internal and external airflows.

The drag increment associated with internal airflow is primarily a function of the total-pressure loss in ducts. For example, in a cooling duct some total-pressure loss is attributed to the cooling unit itself; however, the actual pressure loss of the installation includes the losses associated with the entire duct system, including features related to flow turning. If heat transfer is ignored, the power absorbed in a duct is given by

$$P = Q \Delta p_t \tag{1}$$

Therefore, an efficient duct design is one for which total-pressure loss is minimized and volumetric flow rate does not exceed the amount required for satisfactory cooling. As previously noted, equation (1) was obtained by ignoring heat transfer; however, as shown in reference 7, some thrust is provided by the transfer of heat to the cooling air.

Reference 2 indicates that, in general, efficient duct design may be obtained by adhering to the following guidelines:

(1) Whenever possible, duct inlets should be located on a stagnation point. Inlets at other locations should be designed to recover the full total pressure corresponding to the flight speed.

(2) Bends, particularly in the high-speed section of the duct, should be avoided. If bends are required, guide vanes should be installed.

(3) The duct should have a smooth internal surface with cylindrical cross sections.

(4) In general, sudden changes in cross-sectional area should be avoided. Two-dimensional expansions should be limited to an included angle of 10°, and three-dimensional expansions should be limited to an included angle of 7°. An exception to this general rule is a low-velocity expansion just ahead of a high-resistance area, in which case the expansion angles may be considerably higher. Also, as explained in reference 8, the expansion angles can be higher if the streamwise curvature of the duct walls is used to reduce the adverse pressure gradients and if the cooling block is located downstream to straighten the flow.

(5) The volumetric flow rate of air passing through the duct should not exceed the amount required for cooling. Since the volumetric flow rate depends upon the flight condition, provisions should be made for controlling airflow rate.

(6) The volumetric flow rate of air through a duct can be efficiently controlled by varying the area of the duct outlet. Internal shutters should be avoided.

(7) The airflow should be discharged along the contour of the aerodynamic body at the duct outlet, and the afterbody at the duct outlet should be slightly undercut.

The drag penalties due to departures from the ideal streamline shape, which are implemented to meet power-plant installation requirements, are considered power-plant drag increments associated with external airflow. The drag increments produced by engine-associated protuberances may therefore be charged to the power-plant installation. It should be noted that in the case of engine exhaust stacks, a drag increment is caused by ejecting the exhaust gases at an angle relative to the airstream, as well as by the actual protuberance. Furthermore, experience has shown that directing the exhaust gases rearward may provide a thrust component which is equal to about 10 percent of the installed thrust. Failure to utilize this thrust force properly may be considered a drag penalty.

Air leakage.- The leakage of air through gaps in airplane surfaces may be properly associated with drag increments due to internal and/or external airflows. For example, leakage from air ducts essentially represents a reduction in momentum and is, therefore, a contributor to total-pressure loss. Furthermore, since leakage is generally normal to the airstream, it produces a significant disturbance to the external airflow and thereby increases the aerodynamic drag. Specific examples of drag-coefficient increments due to leakage are presented in appendix B. Because of the difficulty of isolating the drag contribution produced solely by leakage, additional results related to this problem are discussed under other headings. The significance of these results, in terms of drag penalties, emphasizes the importance of sealing surfaces across which a pressure differential exists.

Wing surface irregularities.- The wing profile drag, which includes the effects of skin friction and surface irregularities, was measured for airplanes 1 to 11. The increment in drag coefficient due to roughness, rivets, joints, construction deviations, and other items was estimated by subtracting the calculated drag coefficients (based on two-dimensional smooth airfoil data) from the measured profile drag coefficient. The resulting incremental drag coefficients and the measured boundary-layer transition points are presented in table V. Additional examples of the effects of surface irregularities and roughness on wing profile drag are shown and discussed in appendix C.

Investigations conducted to determine the location of the boundary-layer transition points for both the smooth wings and the service-condition wings of airplanes 1 to 11 showed that irregularities of the production wings were generally located behind the transition points, and were therefore in a region of turbulent flow. Comparison of the measured profile drag coefficients for the service-condition wings with the calculated profile drag coefficients of the smooth wings indicates that significant drag increments are attributable to wing surface irregularities, even when these irregularities are located

in the turbulent boundary layer. From the results presented in table V it is readily apparent that extreme care should be exercised in wing construction to avoid the excessive high drag penalties associated with surface irregularities. Furthermore, it should be noted that wing protuberances (for example, nonflush rivets) may fix the point of transition from laminar to turbulent flow on the wing if the protuberance is located ahead of the natural transition point of the corresponding smooth wing. For example, if transition for the smooth wing occurs at $0.30\bar{c}$, then the addition of a row of nonflush rivets at $0.20\bar{c}$ may fix the boundary-layer transition at the $0.20\bar{c}$ location. However, if transition for the smooth wing normally occurs at $0.15\bar{c}$, then the addition of a row of rivets at $0.20\bar{c}$ should not affect the location of the transition point. When the transition point is moved forward by the presence of the protuberances, a significant drag increment is caused by the increased region of turbulent flow and a smaller drag increment is produced by the form drag of the protuberance itself. Therefore, for configurations with surface irregularities ahead of the boundary-layer transition point, the incremental values of drag would be even larger than those shown in table V. A detailed study of the effects of surface irregularities on wing profile drag is presented in reference 9.

Landing-gear installation.- The drag increments associated with landing gear were determined from differences between the drag of the airplanes with the original retracted gears and that of the airplanes in a smooth condition with gears retracted, all doors and cover plates sealed, and protruding portions faired. The results consistently indicated that considerable drag increments were produced by airflow disturbances caused by exposed components and air leakage. It should be noted that even in the completely faired condition, inadequate sealing produced considerable drag due to leakage. The results obtained for specific landing-gear installations are discussed in appendix D.

Cockpit canopies.- Sharp edges and short afterbodies on airplane canopies have been found to produce significant regions of flow separation, which in turn leads to increased drag. The results of tests conducted to reduce the drag increments produced by cockpit-canopy installations are discussed in appendix E.

Control-surface gaps.- When seals and metal fairings were removed from the gaps associated with control surfaces, significant drag increments were measured. Such control-surface drag can result from several sources. Air can leak through unsealed gaps from the high-pressure side of the surface to the low-pressure side where it can exhaust normal to the stream and act as a jet spoiler. The blunt rear of the fixed fin or stabilizer can also cause considerable drag, both directly as profile drag and indirectly by inducing airflow through the airframe if there are lightening holes in the rear spar. Reference 10 indicates that such profile drag can be reduced markedly by reducing the thickness of the airfoil at the blunt base of the fixed surface, so that it is thinner than the maximum thickness of the control surface.

Specific examples of drag-coefficient increments due to control-surface gaps are presented in appendix F.

Antenna installations.- The drag increment associated with antenna installations is comprised of an increment due to the wires and an increment due to the mast. If external antennas are required, it is suggested that (1) the wires be positioned parallel to the flow and (2) the mast have a thin airfoil section. Specific examples of drag-coefficient increments due to antenna installations are presented in appendix G.

CONCLUDING REMARKS

Results of drag cleanup tests conducted in the Langley full-scale tunnel during the period from 1935 to 1945 have been summarized for potential application to current propeller-driven general aviation airplanes. Data from tests on 23 airplanes indicate that the drag increments produced by many individual configuration features – such as, power-plant installation, air leakage, cockpit canopies, control-surface gaps, and antenna installations – are not large; however, when the increments are summed, the resulting total drag increase is significant. On the basis of results of the investigation, it appears that considerable reduction in drag can be obtained by proper attention to details in aerodynamic design and by adherence to the guidelines discussed in the present paper.

Langley Research Center
National Aeronautics and Space Administration
Hampton, Va. 23665
April 1, 1976

APPENDIX A

DRAG DUE TO POWER-PLANT INSTALLATIONS

Specific examples of drag-coefficient increments associated with power-plant installations are discussed according to the following outline:

APPENDIX A

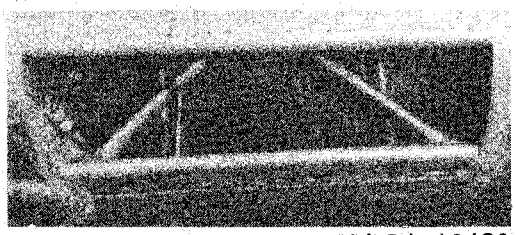

NACA 18429

(a) Inlet.

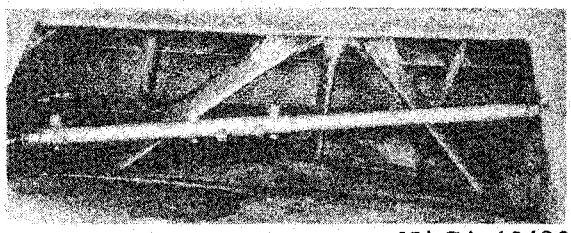

NACA 18430

(b) Outlet.

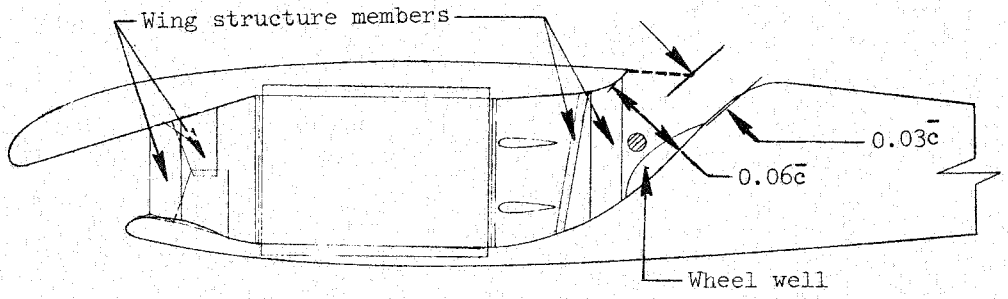

(c) Longitudinal section.

Figure A1.- Wing duct on airplane 9 (Bell XP-39).

Cooling for airplane 9 was provided by a radiator located in the wing duct without outlet control. In the original duct the height of the outlet opening was approximately 6 percent of the reference chord, and a drag-coefficient increment of 0.0023 was attributed to the cooling airflow. By reducing the outlet opening to about 3 percent of the reference chord, sufficient air quantity for cooling in the high-speed condition was obtained, and the drag increment due to cooling airflow was reduced to 0.0008. For this installation further reductions in drag may have been obtained by removal of the structural members interior to the duct.

APPENDIX A

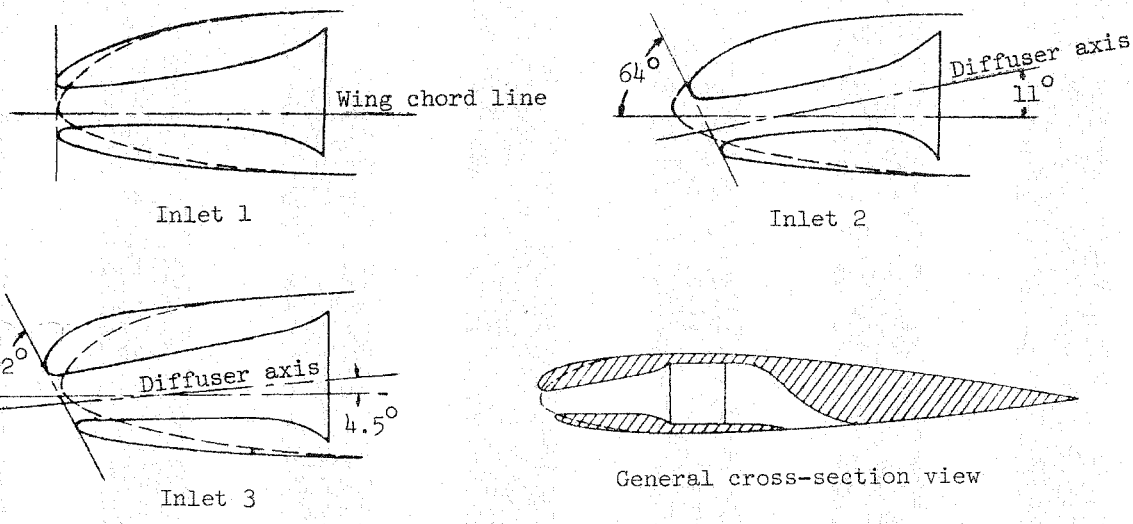

Inlet	C_L	ΔC_D	$P_t - P_\infty$
1	0.12	0.0006	0.95q
	.89		.22q
2	0.12	0.0022	0.86q
	.89		.87q
3	0.12	0.0011	0.95q
	.89		.68q

Figure A2.- Inlets for wing cooling ducts and associated cooling drag on airplane 18 (General Research Model).

Various inlets were tested for the wing cooling ducts of airplane 18. Inlet 1 had a relatively sharp lip and an inlet plane perpendicular to the wing chord and diffuser axis. This inlet showed the lowest drag at low lift coefficients. At high lift coefficients the internal flow separated from the lower lip and resulted in a loss in pressure recovery at the face of the radiator. Inlet 2 was designed to obtain higher pressure recoveries at high lift coefficients. However, at low lift coefficients the pressure recovery for inlet 2 was less than that for inlet 1 because of flow separation just inside the upper lip. This problem also caused inlet 2 to have the highest drag of those tested. Inlet 3 represents a compromise between considerations of high pressure recovery and low drag for a wide range of flight conditions. The drag-coefficient increments presented are for airflow quantities considered satisfactory for the high-speed condition.

APPENDIX A

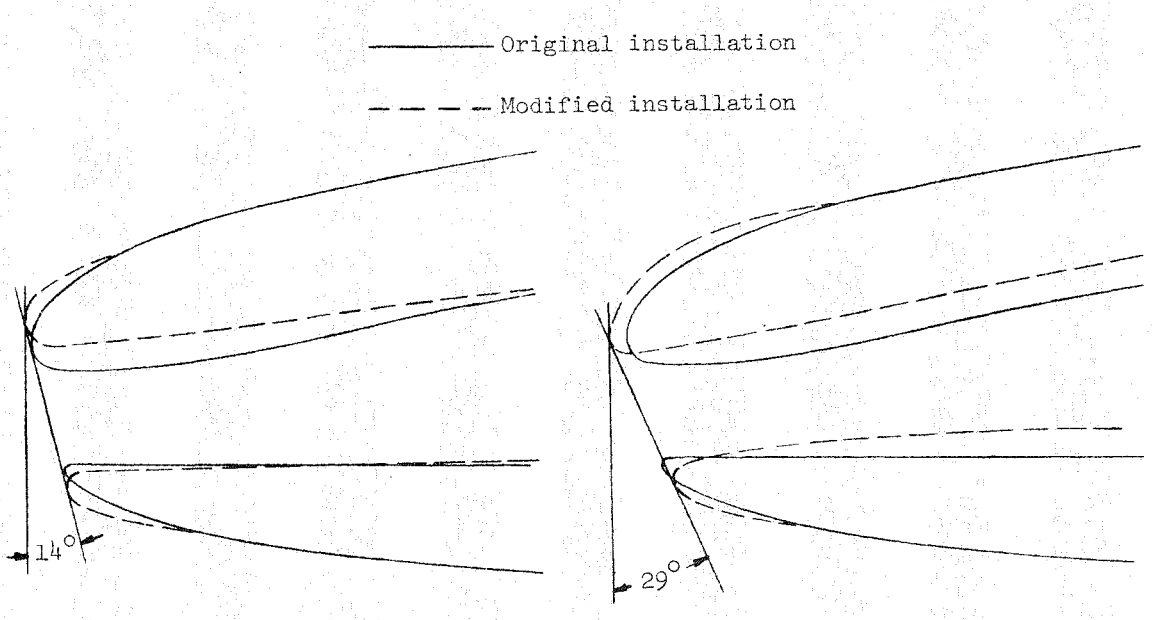

(a) Right inlet. (b) Left inlet.

Figure A3.- Wing duct inlets on airplane 22 (Bell P-63).

Propeller operating tests conducted with airplane 22 showed that the slipstream rotation caused a misalinement of the wing duct inlet and the airstream. This resulted in serious losses in total-pressure recovery. To remedy this condition, modified inlets were installed with the plane of the inlet on the side of the upgoing propeller blade tilted 15° farther downward than the plane of the inlet on the side of the downgoing propeller blade. A further modification, which consisted of increasing the inlet area by about 33 percent, was made to lower the ratio of inlet velocity to free-stream velocity. For the high-speed condition the modified inlets decreased the drag coefficient by 0.0005 and increased the total pressure at the faces of the radiators by 15 percent. Cooling was improved for both the high-speed and the climb conditions with the modified inlets.

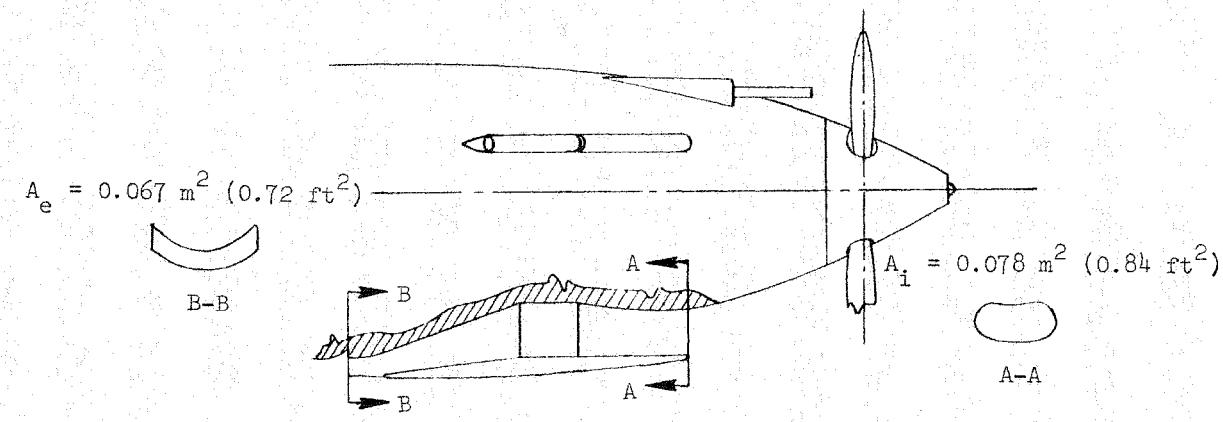

(a) Original installation.

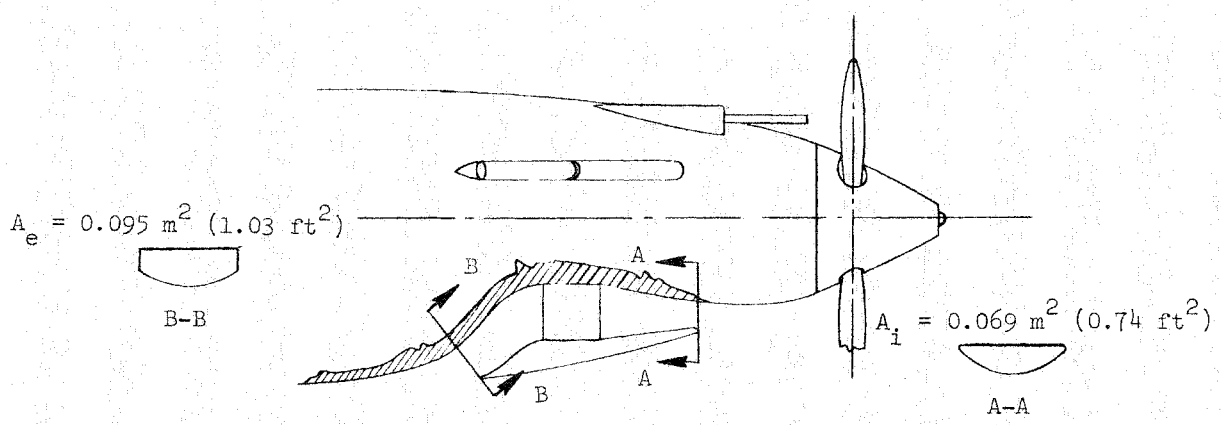

(b) Modified installation.

Figure A4.- Cooling installations on airplane 7 (Curtiss XP-40).

In its original condition the radiator on airplane 7 was located under the engine, and the air was taken in by means of the large scoop which protruded below the normal fuselage line. This installation increased the airplane drag coefficient by 0.0034. By raising the installation so that it did not protrude beyond the normal fuselage lines, the drag-coefficient increment was reduced to 0.0017 and the same airflow as that for the original installation was obtained.

APPENDIX A

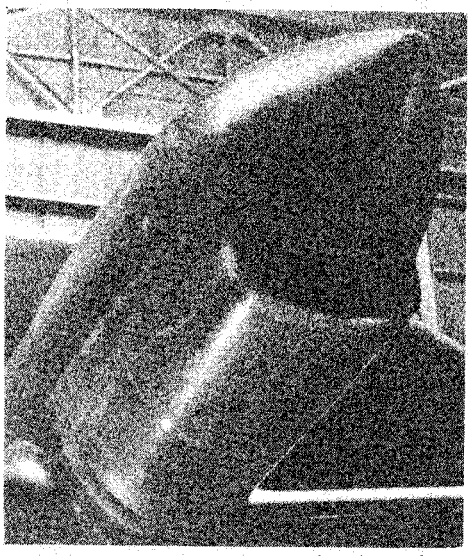

NACA 18907

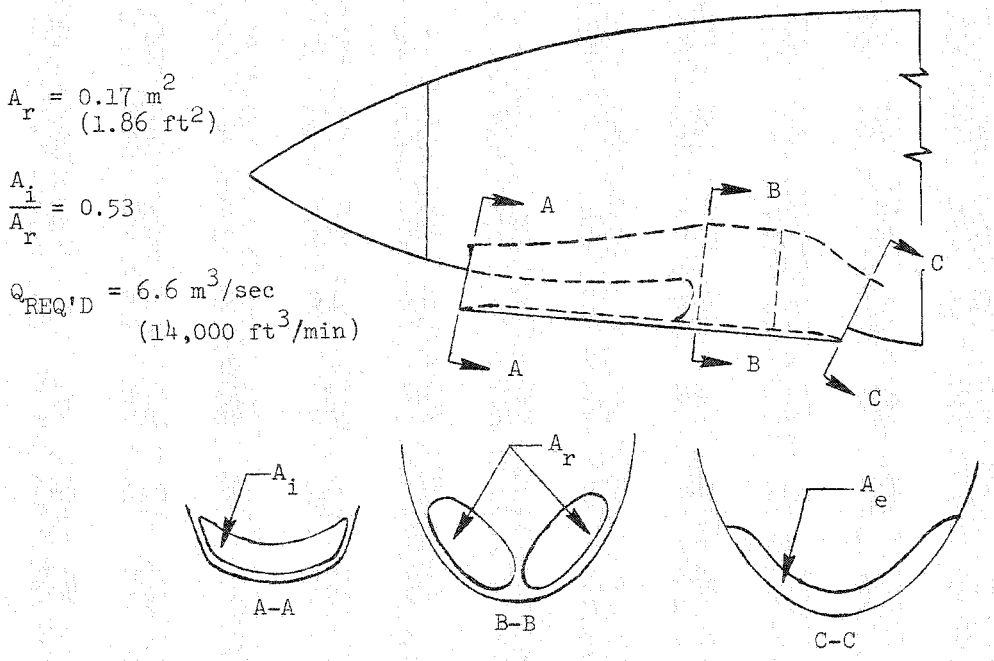

(a) Photograph and sketch of forward underslung radiator installation.

Figure A5.- Radiator installations and associated cooling drag on airplane 11 (Curtiss XP-46).

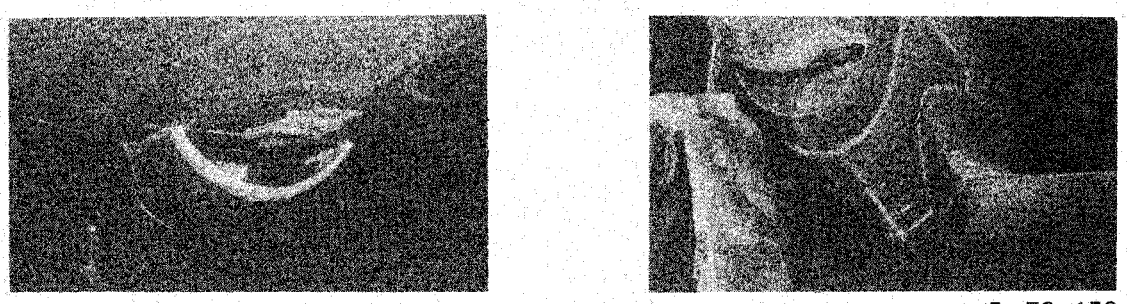

Inlet Outlet L-76-159

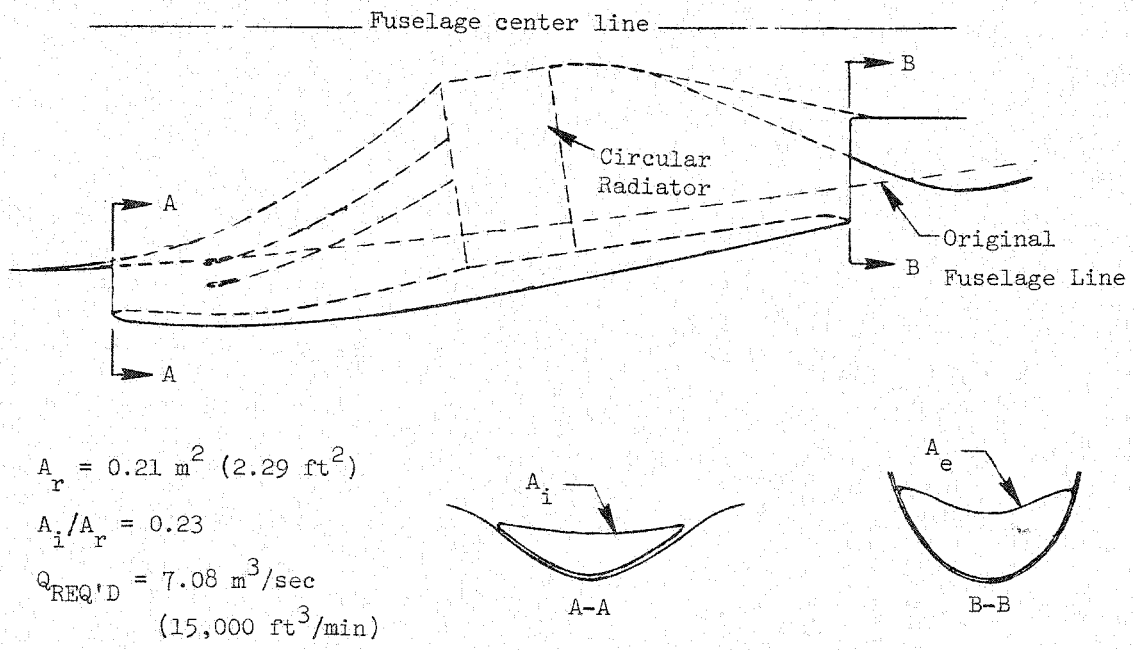

(b) Photographs and sketch of rear underslung radiator installation.

Figure A5.- Continued.

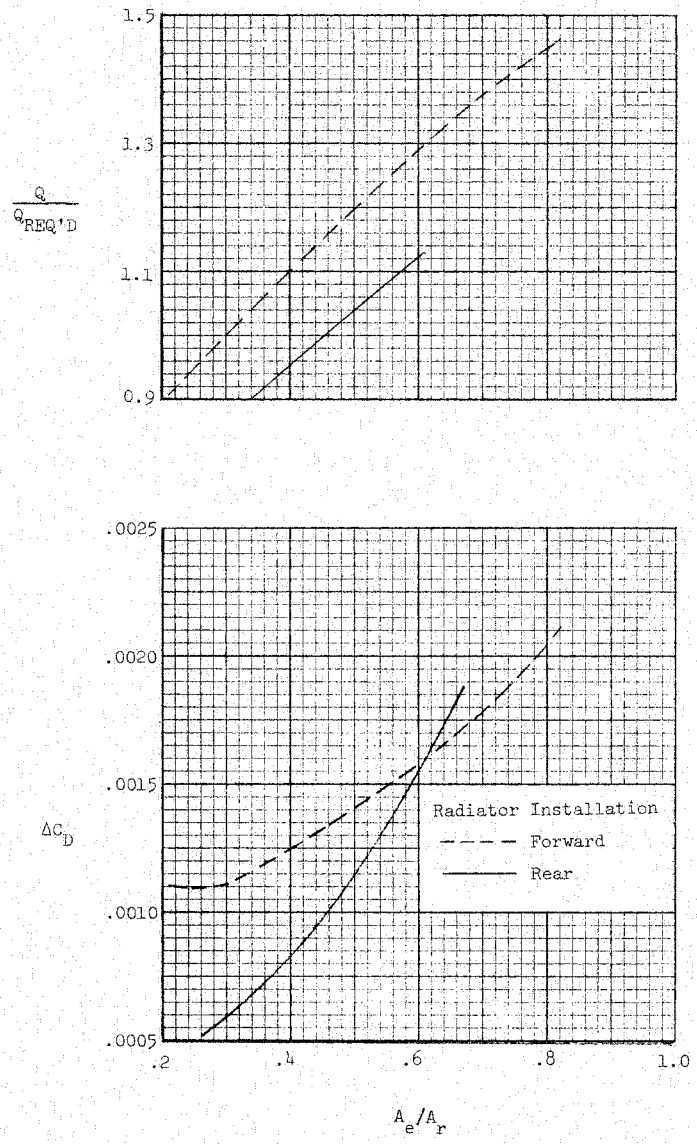

(c) Volumetric flow rate and drag-coefficient increment as a function of exit area for forward and rear radiator installations.

Figure A5.- Concluded.

A study was conducted for two radiator installations designated forward and rear according to their location on the fuselage of airplane 11. The results show respective drag-coefficient increments of 0.0011 and 0.0010 for the forward and the rear installations (figs. A5(a) and A5(b)) when both were adjusted to the correct airflow. The large increase in drag which would have occurred if outlet control were not used on these ducts is shown by the steep slope of the curve of drag increment as a function of exit area (fig. A5(c)).

APPENDIX A

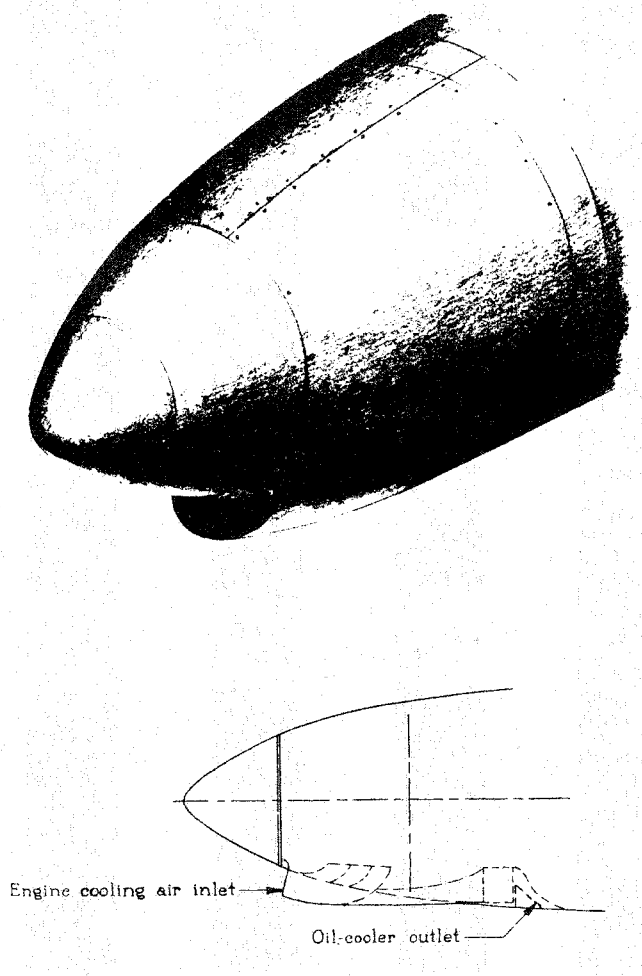

(a) Original long nose cowling.

Figure A6.- Nose cowlings on airplane 12 (Curtiss XP-42).

Airplane 12 had a relatively long propeller shaft extension in order to permit a cowling shape of high fineness ratio. The inlet of the original cowling was too small and had leading edges that were too sharp. The sudden change in direction and the extreme expansion of the high-velocity cooling air resulted in a total-pressure recovery in front of the engine cylinders of only 0.40q. In the high-speed condition the drag coefficient was 0.0040 greater for the original installation than for the sealed and smooth cowling with the scoop removed.

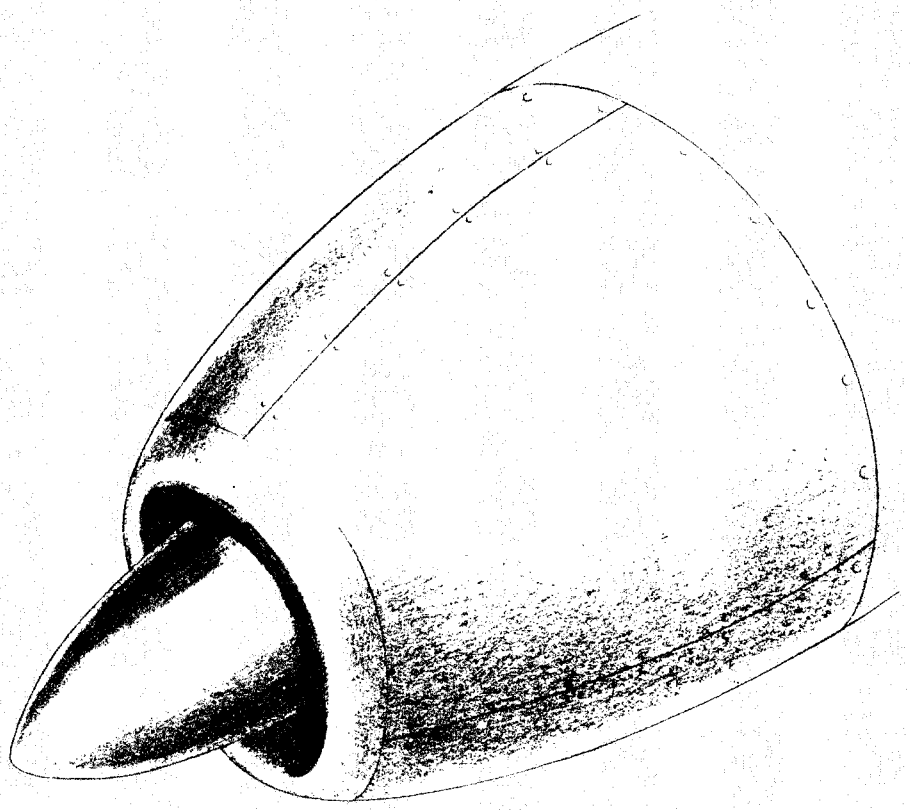

(b) Modified cowling with annular inlet and spinner.

Figure A6.- Continued.

A modified cowling with an annular inlet, designed to reduce the kinetic-energy losses of the cooling air and to avoid the large drag of the original cowling, was tested on airplane 12. The data showed that the drag-coefficient increment of this installation was reduced to 0.0025 when adjusted for the same airflow as the original installation. The total pressure at the rear of the diffuser was slightly less than 0.90q for these conditions.

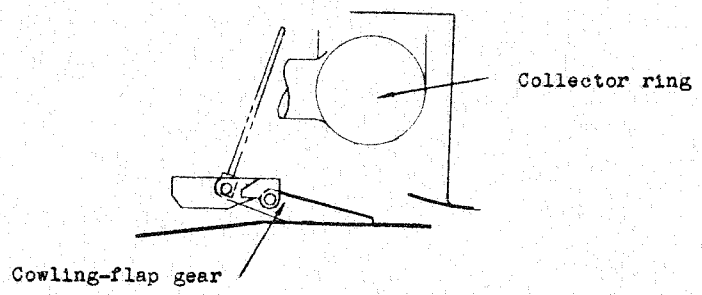

Section at original cowling outlet

Section at smooth cowling outlet

(c) Outlet of annular-inlet cowling.

Figure A6.- Continued.

The outlet of the annular-inlet cowling contained a cowling-flap actuating linkage, an exhaust collector ring, and a sharp lip just inside the cowling-flap outlet. Removal of these items provided a further reduction in drag coefficient of 0.0007. In addition, a bottom exit was provided by removing the oil cooler and enlarging the oil-cooler exit to allow greater cooling flow with the cowling flaps closed.

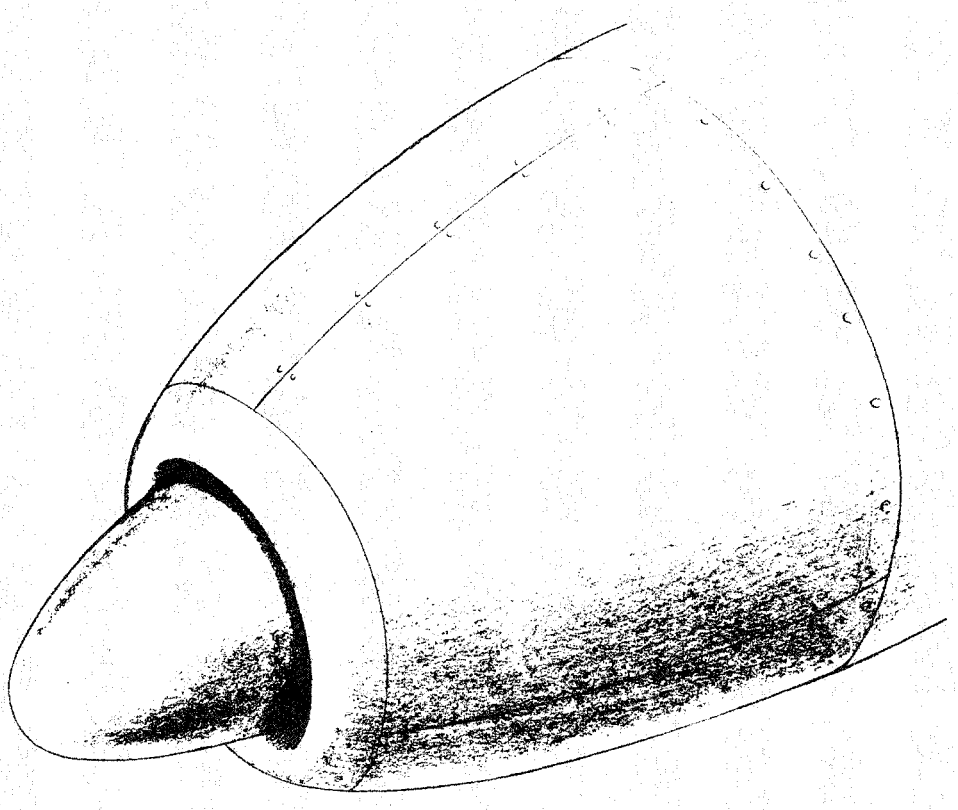

(d) Modified cowling with annular inlet and enlarged spinner.

Figure A6.- Concluded.

A further modification of the cowling inlet arrangement on airplane 12, consisting of an enlarged spinner which reduced the inlet area, produced a total drag-coefficient increment of only 0.0012 when compared with the sealed and smooth original cowling with the scoop removed. This increment was obtained for an airflow which was sufficient for the engine, carburetor, and oil cooler.

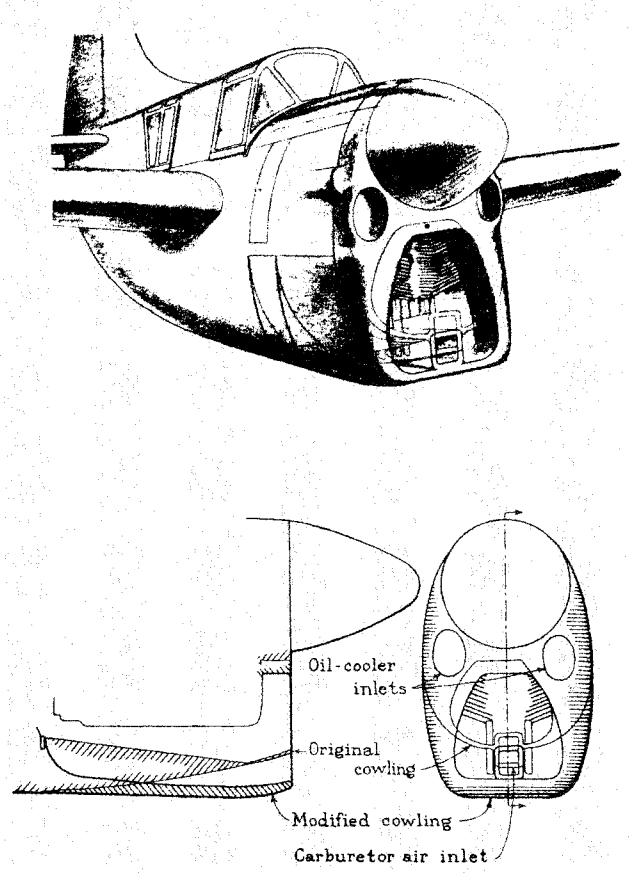

Figure A7.- Cooling installations on airplane 13 (Curtiss XS03C-1).

Flight tests showed that the inverted V-12 air-cooled engine of airplane 13 did not cool satisfactorily in any flight attitude in the original condition. Tests revealed that losses in the cooling system were excessive because of restricted inlet and outlet openings. The inlet was accordingly lowered and its area increased by about 28 percent. Additional outlet openings were installed on each side of the cowling. These modifications increased the power-on inlet total pressure by about 25 percent in the climb attitude, principally because the inlet was lowered into a region of higher slipstream velocity. In addition, the average total pressure in front of the engine cylinders was increased. The drag coefficient with propeller removed was decreased 0.0004 by the cowling modification. This reduction was attributed mainly to the improved shape of the cowling lip and the greater efficiency of the internal flow.

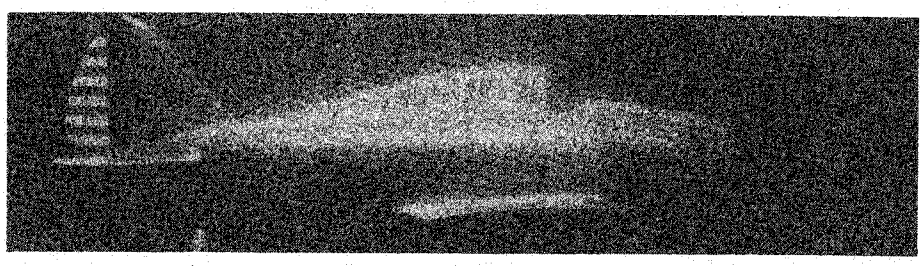

(a) Airplane 8 with original cowling.

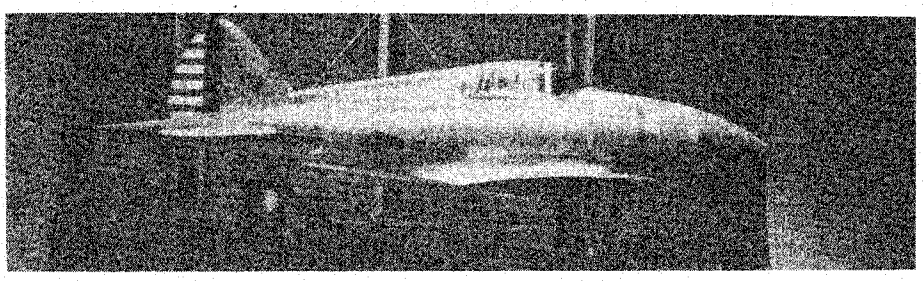

(b) Airplane 8 with streamlined nose fairing and afterbody extension.

L-76-160

Figure A8.- Cowlings and afterbody extension on airplane 8 (Seversky XP-41).

Air-cooled engine installations generally resulted in a blunt fuselage shape. This nonideal shape often resulted in flow separation caused by an adverse pressure gradient. The drag coefficient for airplane 8 with the original cowling and no cooling airflow was 0.0020 greater than the drag coefficient for the airplane with a solid streamline nose added. Lengthening the fuselage by means of a conical extension had no significant influence on the drag of the airplane with the streamline nose, but resulted in a reduction in drag coefficient of 0.0005 for the airplane with the original cowling.

APPENDIX A

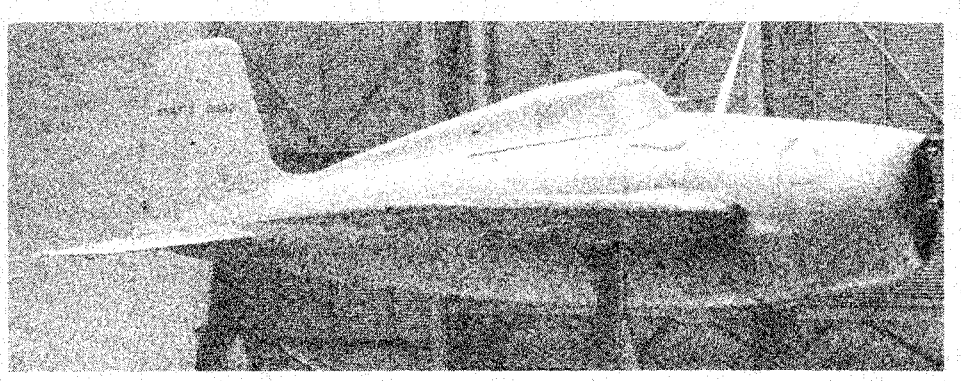

(a) Airplane 10 with original cowling.

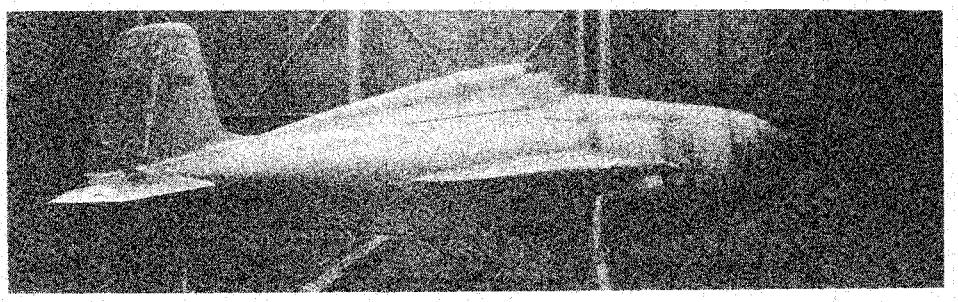

(b) Airplane 10 with streamlined nose fairing.

L-76-161

Figure A9.- Cowlings on airplane 10 (Grumman XF4F-3).

The drag coefficient of airplane 10, with the original cowling sealed (no cooling airflow), was 0.0013 greater than the drag coefficient of the airplane with a solid streamline nose fairing.

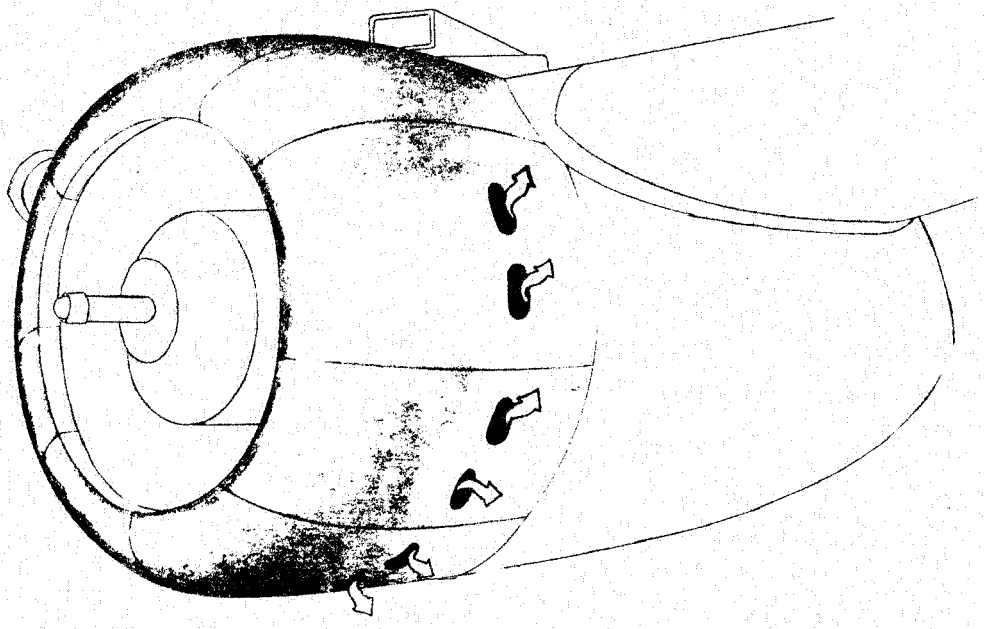

Figure A10.- Engine cowling on airplane 14 (Douglas A-20A).

Airplane 14 had unsatisfactory engine cooling in the climb condition. In an attempt to remedy this situation, holes were cut in the periphery of the cowling just behind the cylinder baffles. Subsequent tests showed that the cooling problem was not solved and that the flow disturbance caused by the airflow from the holes resulted in an increase in drag coefficient of 0.0041.

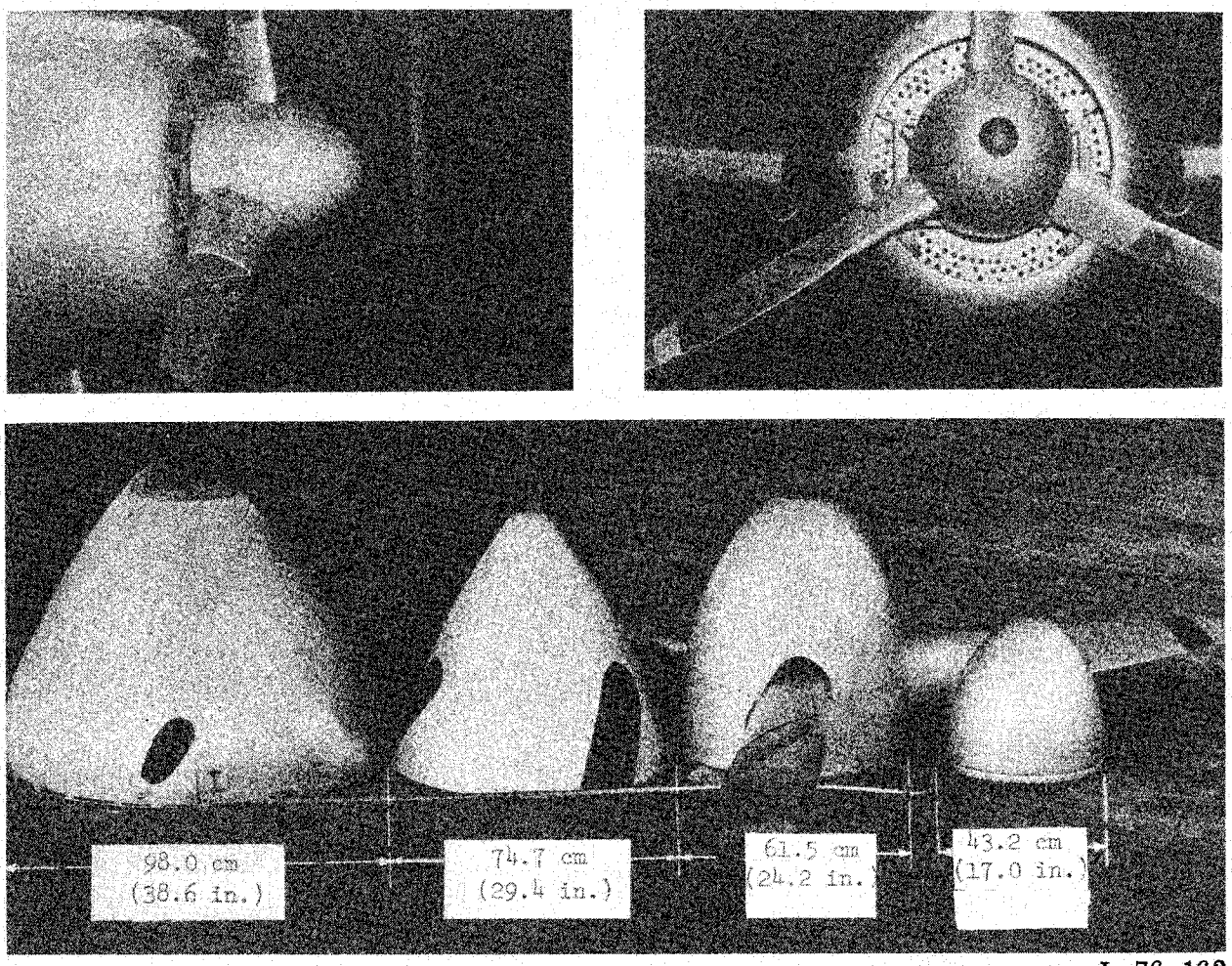

L-76-162

Figure A11.- Spinner arrangements on airplane 10 (Grumman XF4F-3).

Spinners of various sizes were evaluated on airplane 10 to obtain a better streamline shape. Powered tests showed that the 61.5-cm (24.2-in.) spinner, shown in the upper photographs, provided approximately a 3-percent increase in overall propulsive efficiency and provided sufficient cooling air. The larger spinners produced about the same increase in propulsive efficiency but did not provide adequate cooling air to the engine.

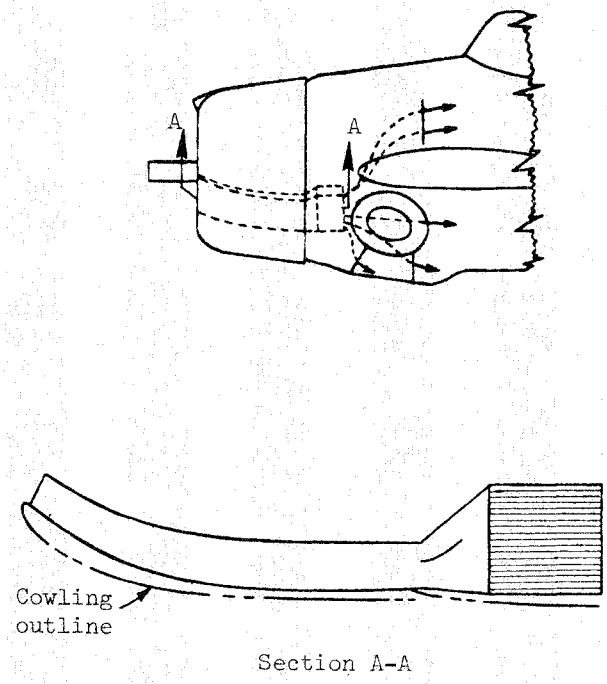

Figure A12.- Intercooler duct on airplane 10 (Grumman XF4F-3).

Airflow from the intercooler duct of airplane 10 was discharged into the wheel wells without any energy recovery. The total drag-coefficient increment for this installation was 0.0012. The drag was due both to internal duct losses and to leakage.

APPENDIX A

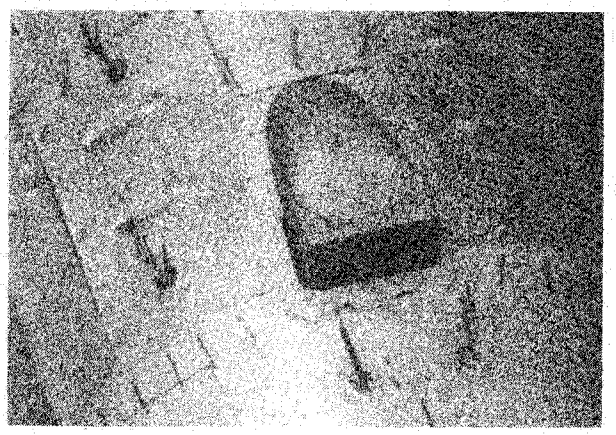

L-76-163

(a) Tuft photograph of original carburetor air scoop showing region of separated flow.

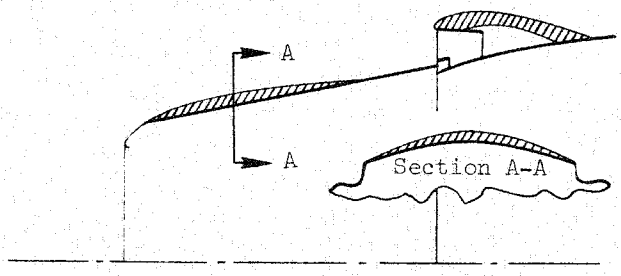

(b) Section view of modified installation.

Figure A13.- Carburetor air scoop on airplane 2 (Grumman XF4F-2).

Refairing the carburetor air scoop and cowling of airplane 2 reduced the airplane drag coefficient by 0.0010. This modification further helped to maintain the carburetor pressure up to high angles of attack.

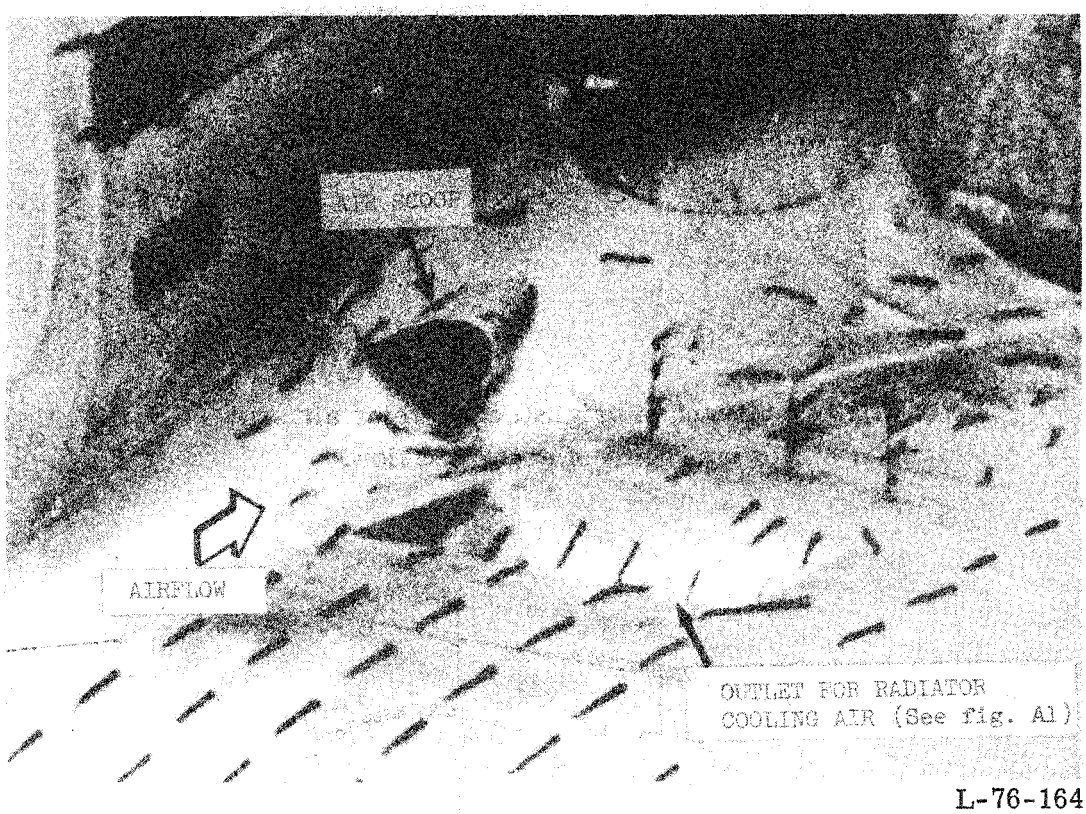

L-76-164

Figure A14.- Flow visualization of flow over carburetor air scoop on airplane 9 (Bell XP-39).

Small sharp-edge air scoops were used in the wing-fuselage fillets of airplane 9. These air scoops increased the airplane drag coefficient by 0.0019. This large drag increment was attributed to the sizable region of disturbed flow, as determined by flow visualization using surface tufts.

APPENDIX A

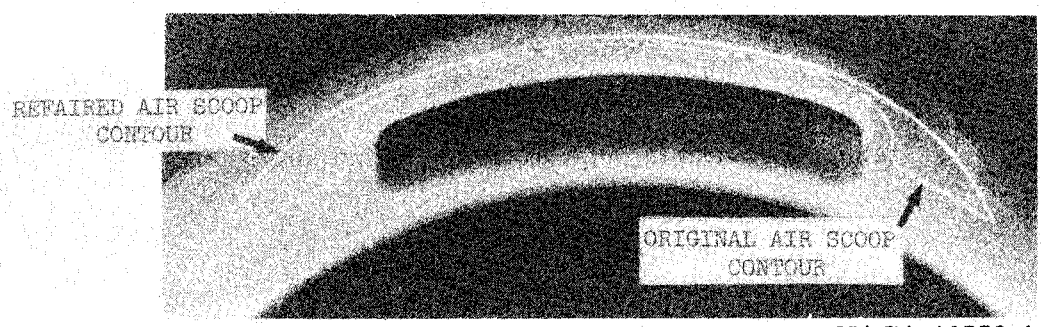

NACA 18559.1

Figure A15.- Carburetor air scoops on airplane 10 (Grumman XF4F-3).

Flow visualization studies for airplane 10 showed that in the power-off condition satisfactory flow existed over the carburetor air scoop. However, with the propeller operating, a flow separation was observed on one side of the scoop because of propeller slipstream rotation. To eliminate the flow separation, the sides of the scoops were faired out more gradually, and a reduction of the airplane drag coefficient by 0.0006 resulted.

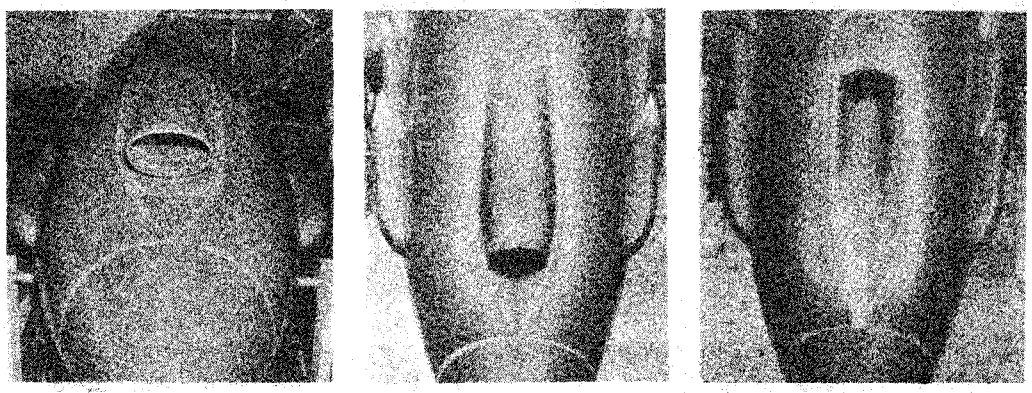

(a) Photographs of original and modified inlets.

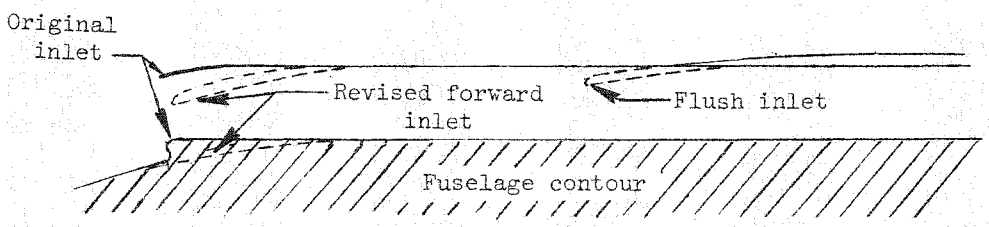

(b) Section view of original and modified inlets.

Figure A16.- Inlets for carburetor air scoops on airplane 11 (Curtiss XP-46).

Two modifications to the carburetor air scoop of airplane 11 were tested. The revised forward inlet resulted in an increment in drag coefficient of only 0.0001 for the correct airflow. Although the flush inlet also had very low associated drag, the ram pressure was significantly below the value of about 0.95q obtained with the revised forward inlet. The advantages of the revised forward inlet are thought to be due to the improved shape of the nose, which was more nearly parallel to the streamlines, and to the elimination of the lower lip on the original inlet.

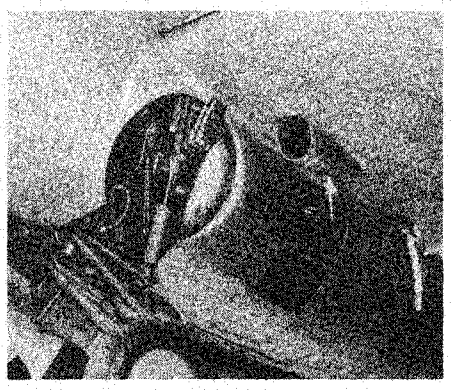

(a) Inlet.

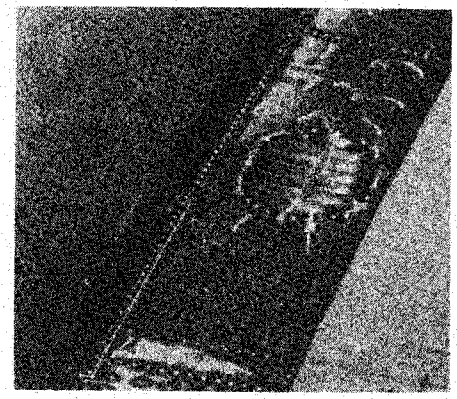

(b) Outlet.

L-76-166

Figure A17.- Oil cooler on airplane 2 (Grumman XF4F-2).

The air for the oil cooler of airplane 2 was taken in by means of a scoop on the undersurface of the wing. The air passed through a cross-flow wing duct, in which the oil cooler was located, and was discharged at an angle of about 45° (relative to the wing chord) through louvers on the upper surface of the wing. Surface tufts show the flow interference due to the inefficient discharge. A drag-coefficient increment of 0.0020 was measured for this installation.

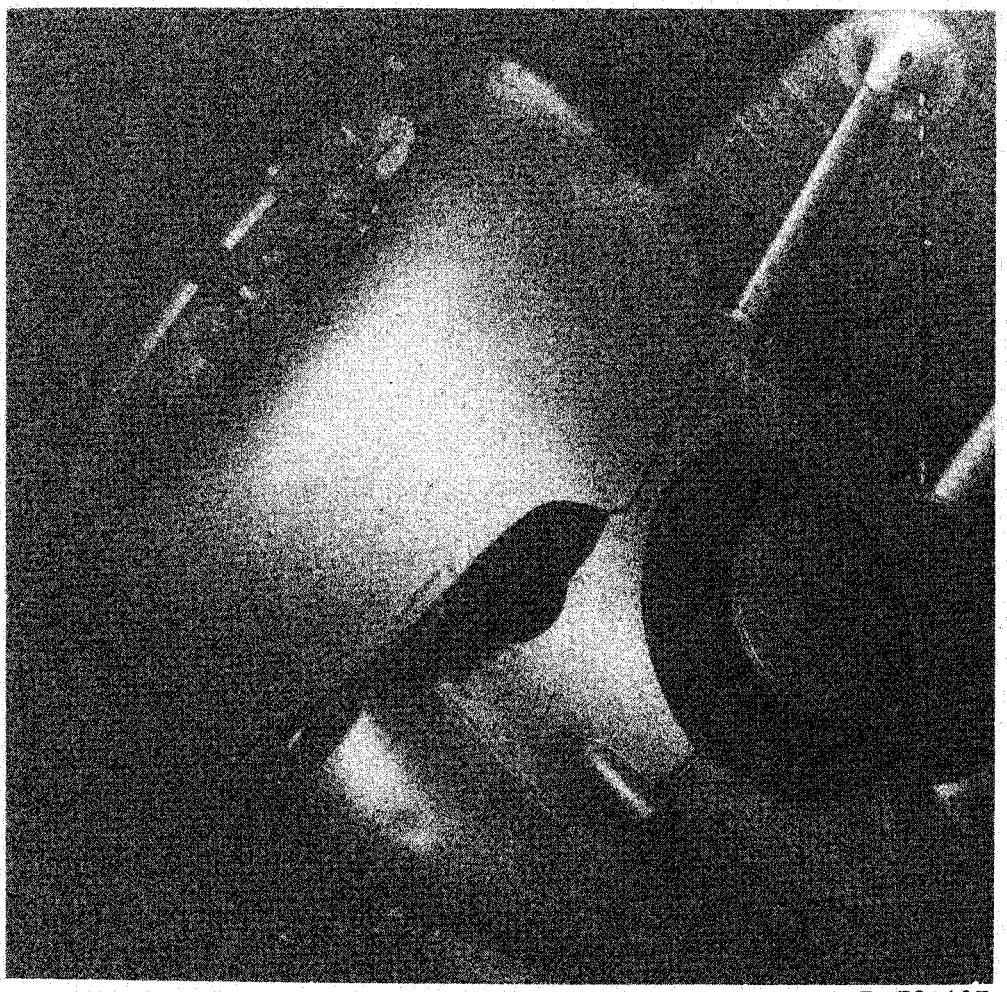

L-76-167

Figure A18.- Oil-cooler scoop on airplane 3 (Grumman F3F-2).

The oil-cooler scoop of airplane 3 was located at the bottom of the fuselage on the rear of the cowling. A drag-coefficient increment of 0.0007 was measured for this installation.

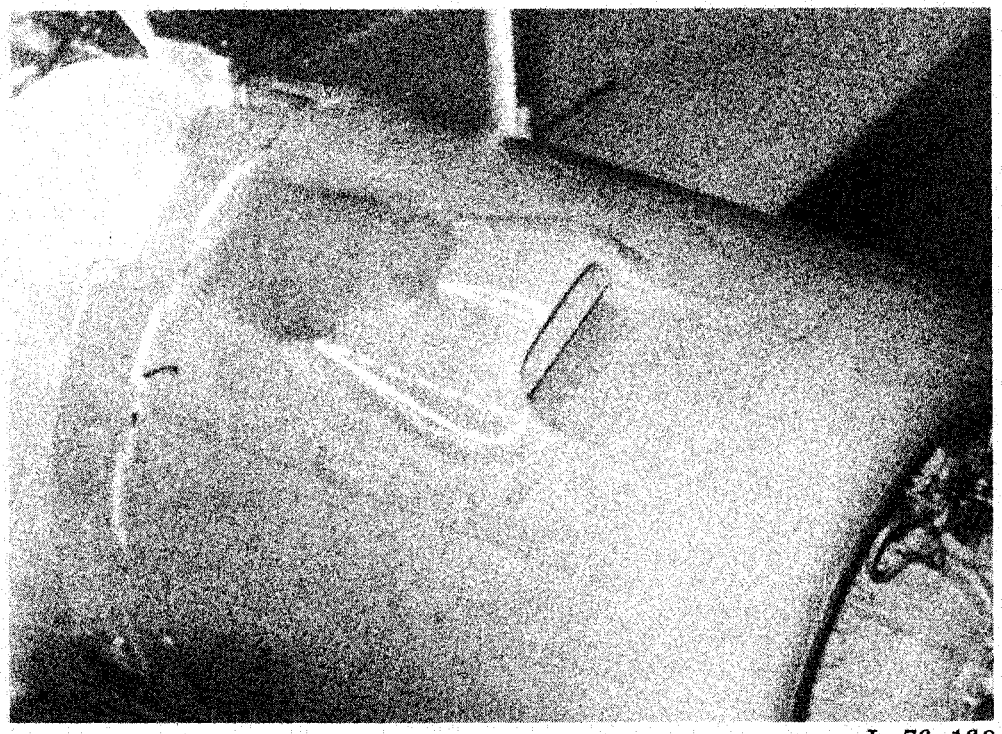

L-76-168

Figure A19.- Oil-cooler scoop on airplane 4 (Vought SB2U-1).

The oil-cooler scoop on airplane 4 was placed on the top of the cowling. The incremental drag coefficient produced by the installation was 0.0007. This increment was reduced to 0.0003 by refairing the scoop as shown.

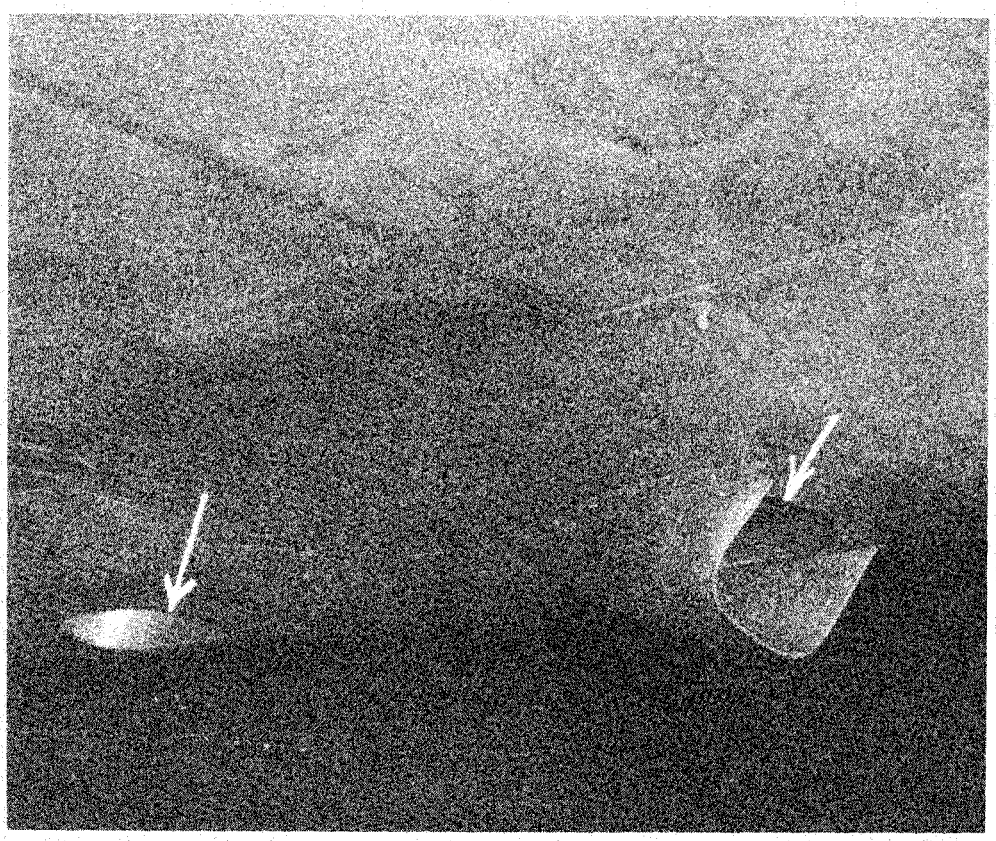

L-76-169

(a) Original installation.

Figure A20.- Oil-cooler installations on airplane 8 (Seversky XP-41).

The oil-cooler installation on airplane 8 consisted of a sharp-edge scoop located on the bottom of the fuselage which diverted air at a rather sharp angle up into oil-cooler ducts located in the fuselage. This air was then discharged at an angle of about 60° relative to the fuselage axis. This oil-cooler installation failed to supply sufficient airflow for oil cooling and increased the airplane drag coefficient by 0.0017.

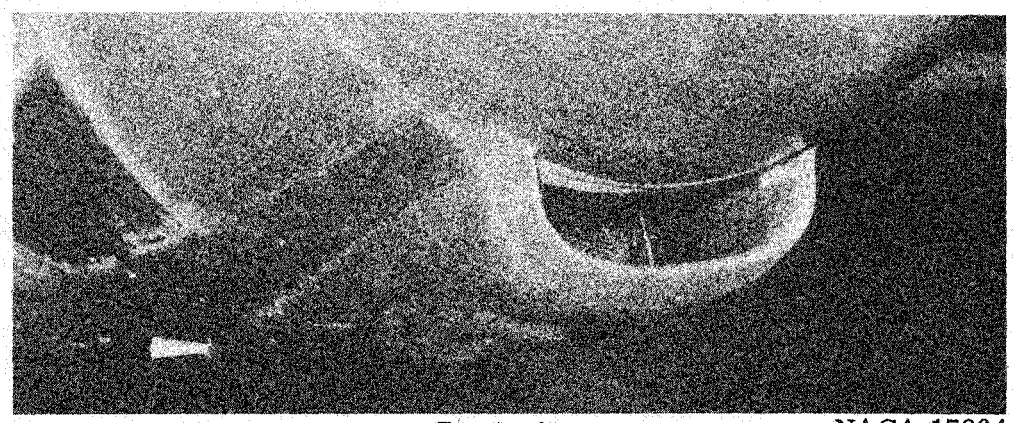

Front view NACA 17864

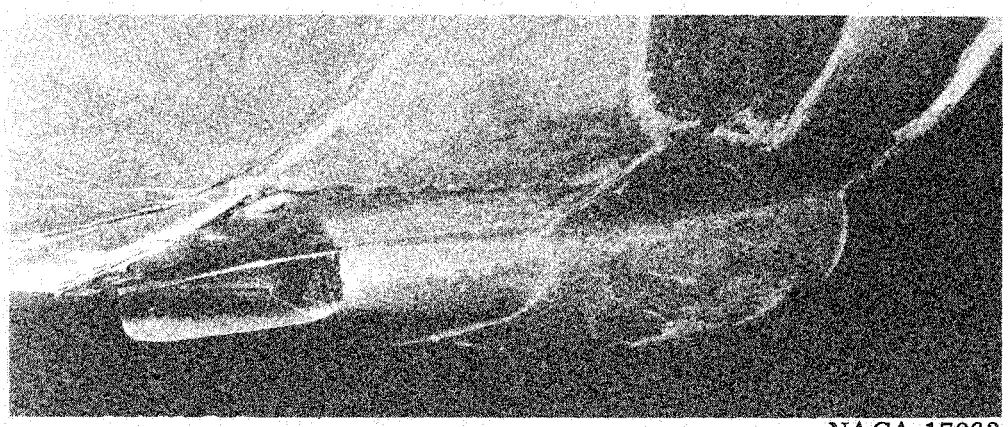

Rear view NACA 17863

(b) Modified installation.

Figure A20.- Concluded.

A modified oil-cooler installation, consisting of an underslung radiator designed to be attached to the bottom of the cowling, was tested on airplane 8. When the required quantity of airflow passed through the cooler, the incremental drag coefficient for this installation was 0.0009.

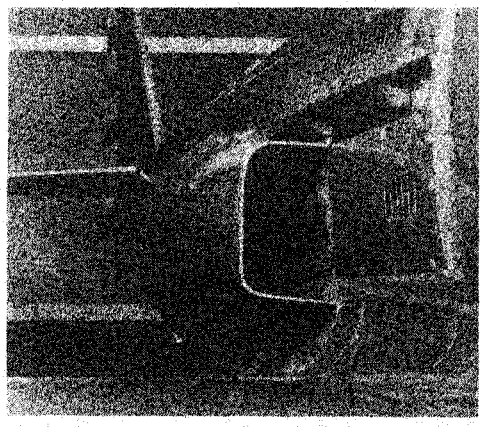

(a) Inlet.

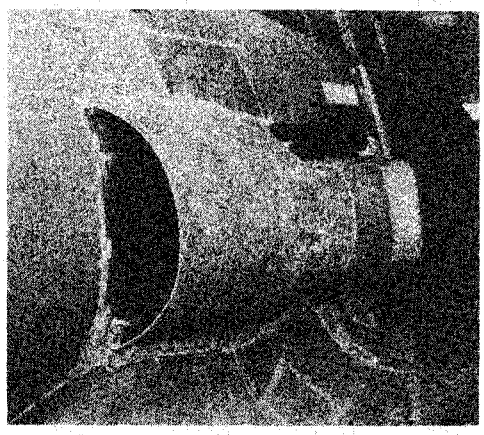

(b) Outlet.

L-76-170

Figure A21.- Oil cooler on airplane 9 (Bell XP-39).

The large-scoop oil cooler used on airplane 9 increased the airplane drag coefficient by 0.0040. This installation was later changed to a wing duct installation for which the airplane drag coefficient was increased by only 0.0011.

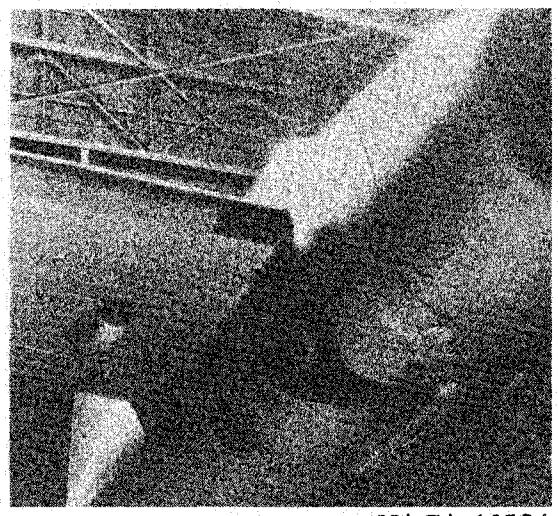

NACA 18524

Figure A22.- Oil cooler on airplane 10 (Grumman XF4F-3).

The oil coolers for airplane 10 were located in streamline ducts on the lower surfaces of the wings outboard of the fuselage. This oil-cooler installation increased the airplane drag coefficient by 0.0008. When the cooler units were streamlined, a drag-coefficient increment of 0.0001 was measured. These results indicate that streamlined blisters located at noncritical positions may not produce large drag increments.

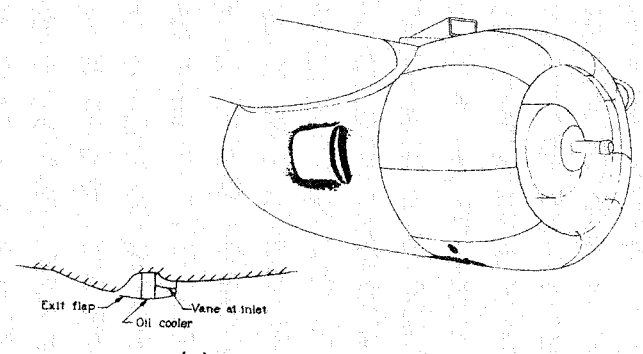

(a) Original installation.

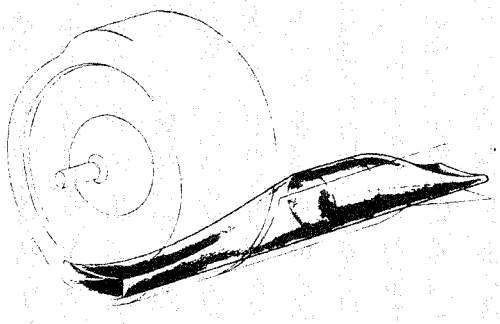

(b) Modified installation.

Figure A23.- Oil-cooler installations on airplane 14 (Douglas A-20A).

The original oil-cooler installation on airplane 14 resulted in an increment in drag coefficient of 0.0018, and the total-pressure recovery at the oil-cooler face was only 0.40q. The oil-cooler modifications consisted of an inlet that was flush with the face of the cowling and a gradually expanding diffuser. The resulting drag-coefficient increment of this modified installation was reduced to 0.0008, and the total-pressure recovery at the oil-cooler face was increased to 0.95q.

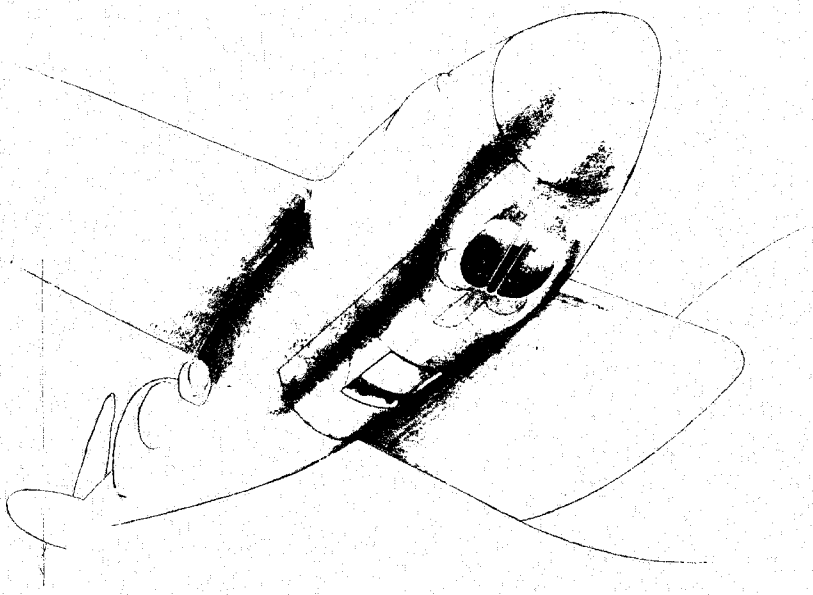

Figure A24.- Oil cooler on airplane 15 (Lockheed YP-38).

The oil-cooler installation of airplane 15 produced a moderate drag-coefficient increment of 0.0008. However, the total-pressure recovery at the oil-cooler face was only 0.33q. This result was attributed to the high oblique angle of the inlet relative to the local flow.

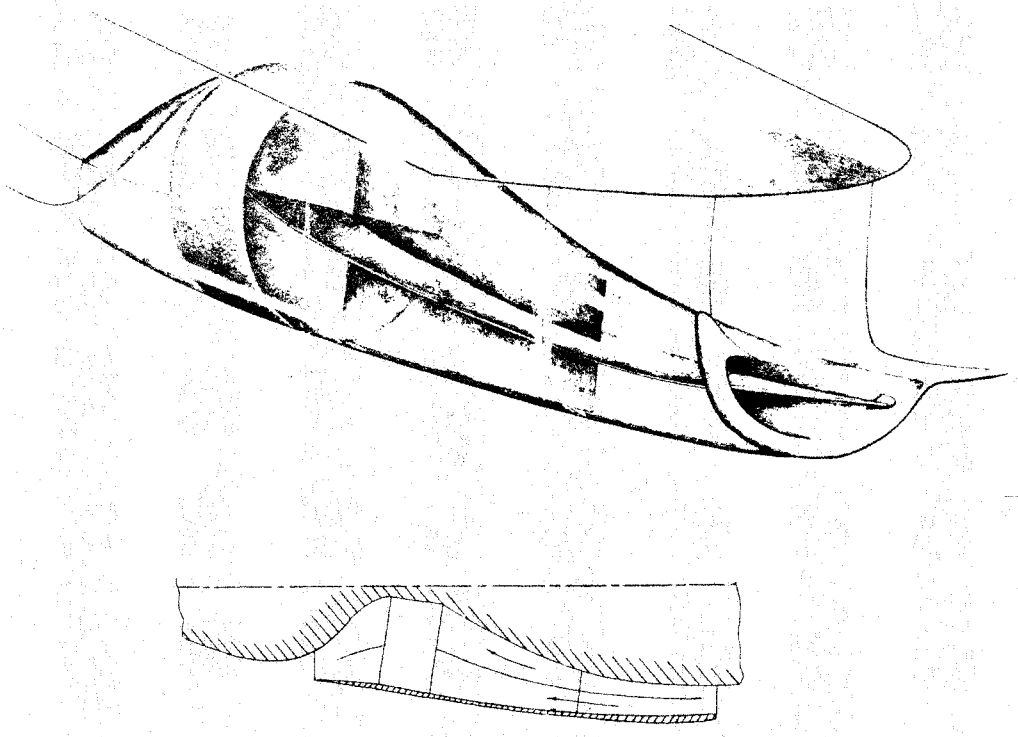

Figure A25.- Oil cooler on airplane 18 (General Research Model).

Dividing vanes were installed in the underslung duct of airplane 18 to reduce the pressure losses at the radiator resulting from flow separation of a thick boundary layer at the inlet. The airplane drag coefficient was reduced by 0.0004 by this modification. In addition, the pressure recovery at the radiator face was increased from 0.69q to 0.83q at $\alpha = 0.2^{o}$, and from 0.84q to 0.92q at $\alpha = 10.4^{o}$.

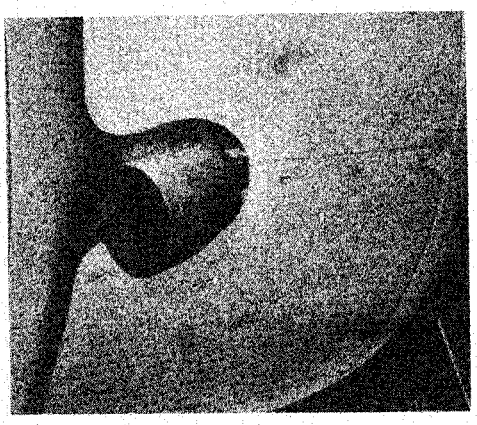

(a) Airplane 5; $\Delta C_D = 0.0010$.

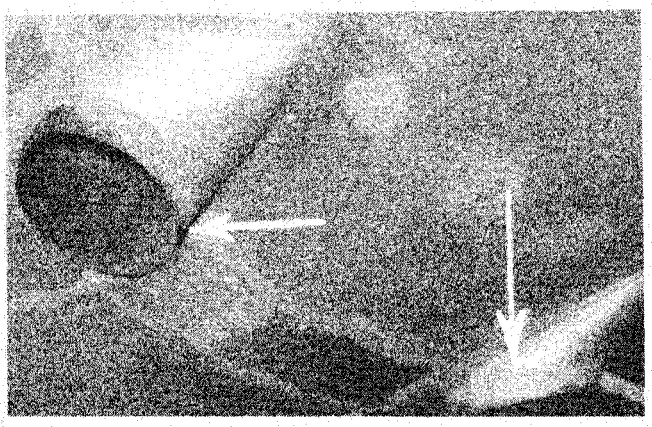

(b) Airplane 8; $\Delta C_D = 0.0005$.

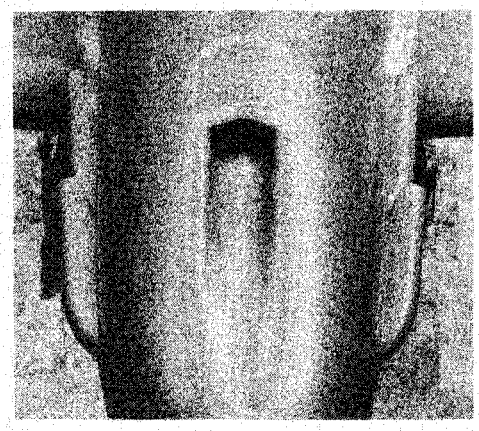

(c) Airplane 11; $\Delta C_D = 0.0003$.

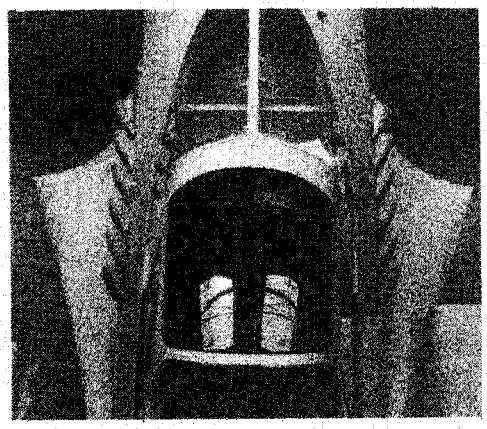

(d) Airplane 9; $\Delta C_D = 0.0014$.

L-76-171

Figure A26.- Exhaust-stack drag for airplanes 5 (Douglas XBT-2), 8 (Seversky XP-41), 9 (Bell XP-39), and 11 (Curtiss XP-46).

Large-bore exhaust stacks such as those used on airplane 5 produced excessive drag; however, some drag reduction may be provided by introducing fairings as shown for airplane 8. Analysis has shown that significant drag reduction and thrust increases may be obtained by using an exhaust-stack installation as shown for airplane 11; however, the individual exhaust-stack arrangement used on airplane 9 contributed an excessive drag increment which was attributed to the relatively large-diameter exhaust pipes used.

APPENDIX A

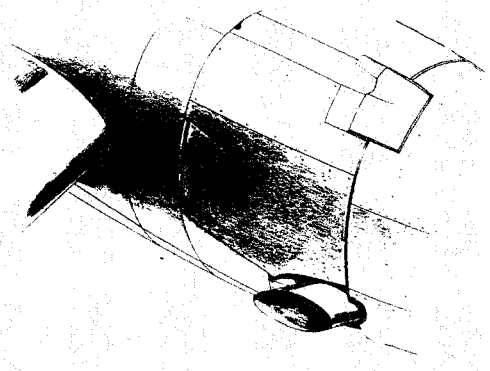

(a) Airplane 17.

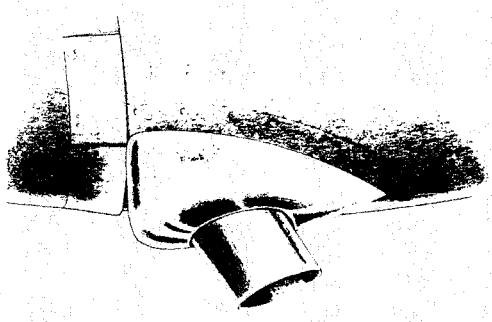

(b) Airplane 19.

Figure A27.- Exhaust stacks on airplanes 17 (Grumman XTBF-1) and 19 (Curtiss SB2C-1).

The large protrusion of the large-bore stovepipe exhaust stacks on airplanes 17 and 19 and the air leakage around them increased the drag coefficient by 0.0008 and 0.0021, respectively. Engine operating tests were conducted for airplane 19 with both the original exhaust-stack installation and a modified installation which used individual jet exhaust stacks. Analysis of the results indicated that the increased thrust and reduced drag obtained through use of the individual jet exhaust stacks would provide airplane 19 with about a 5-percent increase in speed.

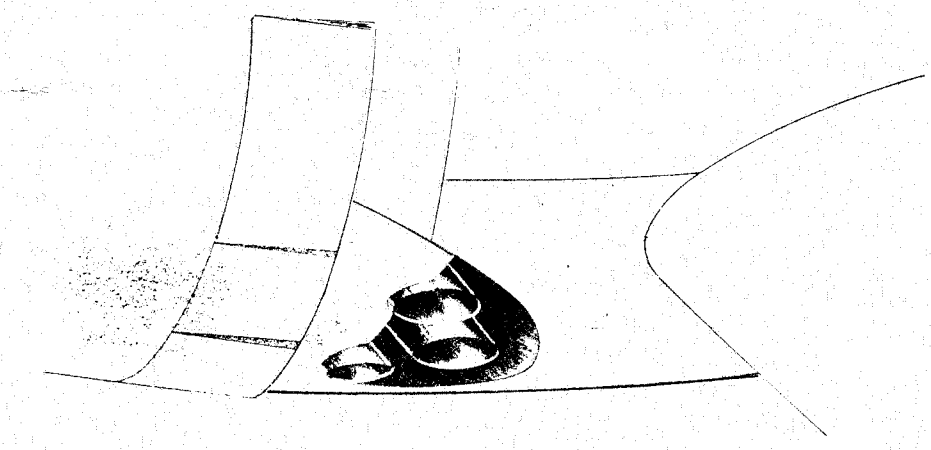

Figure A28.- Exhaust stack on airplane 20 (Vought-Sikorsky F4U-1).

Removing the seal from the exhaust opening of airplane 20 increased the drag coefficient by 0.0010. The form drag of the installations has been avoided in this design; however, the large amount of air leakage through the opening around the exhaust stacks accounted for the excessive drag of the installation.

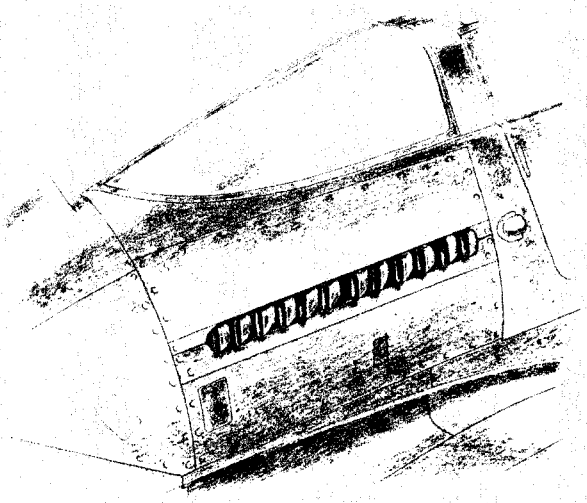

(a) Airplane 22.

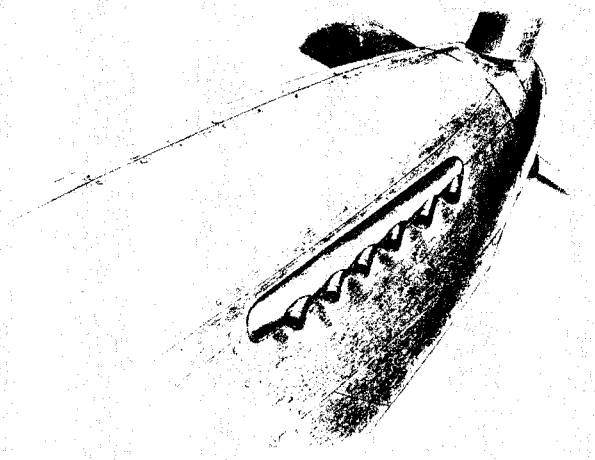

(b) Airplane 23.

Figure A29.- Exhaust stacks on airplanes 22 (Bell P-63) and 23 (North American P-51B).

Removing the sealed metal fairings that enclosed the exhaust stacks of airplanes 22 and 23 increased the drag coefficients by 0.0005 and 0.0007, respectively.

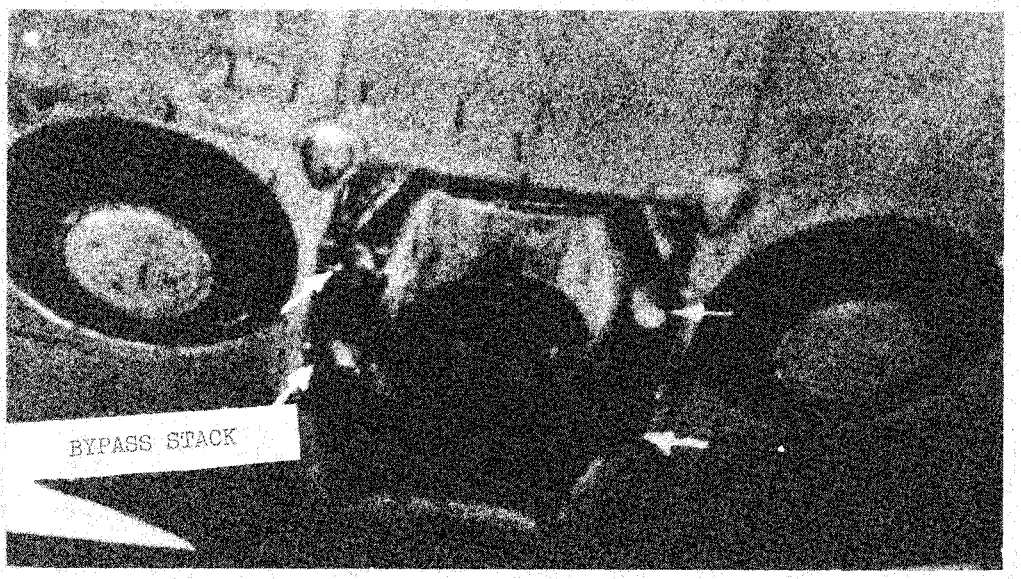

L-76-172

Figure A30.- External turbosupercharger installation on airplane 9 (Bell XP-39).

The external turbosupercharger installation used on airplane 9 produced an increment in drag coefficient of 0.0033. Of this increment, 0.0020 was attributed to the supercharger, 0.0010 was attributed to the bypass stacks, and 0.0003 was attributed to the system used to cool the exhaust lines from the engine to the supercharger.

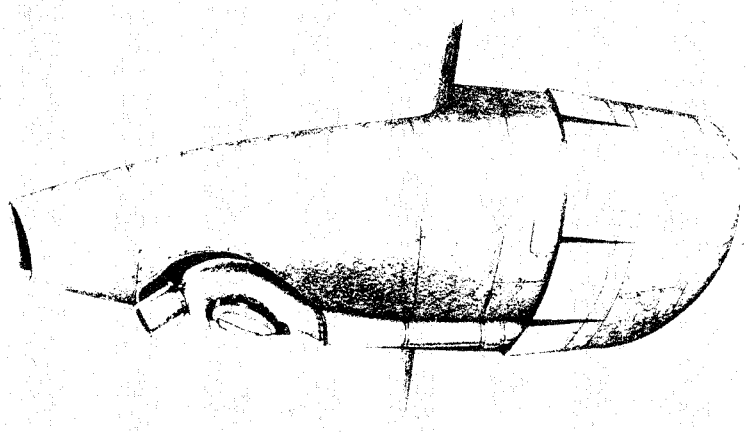

(a) Original installation.

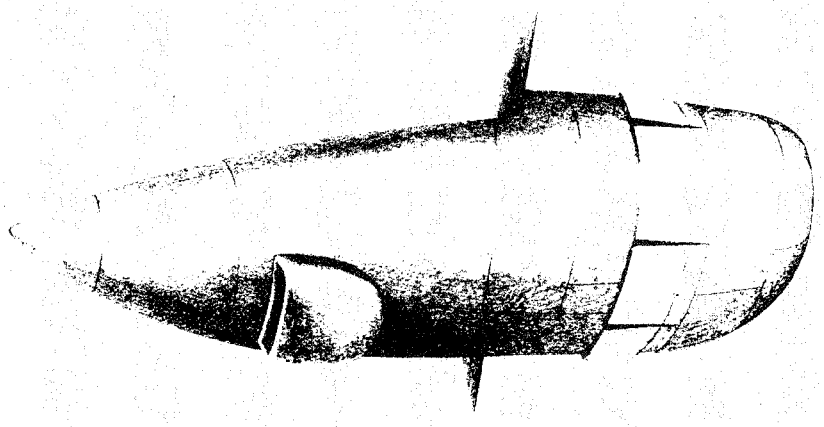

(b) Submerged installation.

Figure A31.- Supercharger installations on airplane 16 (Consolidated B-24 D).

Because of size constraints, only the isolated engine-nacelle installation of airplane 16 was tested. The results from these tests indicated that the complete four-engine configuration would experience an increment in drag coefficient of 0.0040 due to the original supercharger installation. Submerging the supercharger and sealing the openings at the aft end of the nacelles reduced this increment to 0.0027. Thrust recovery obtained by redirection of the exhaust gases was expected to further enhance the effectiveness of this modification under operational conditions; however, the submerged installation would have required some shroud cooling.

APPENDIX B

DRAG DUE TO AIR LEAKAGE

Specific examples of incremental drag coefficients due to air leakage are discussed herein.

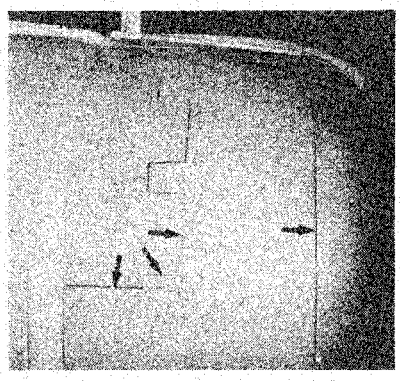

(a) Airplane 5 (Douglas XBT-2);
$\Delta C_D = 0.0008$.

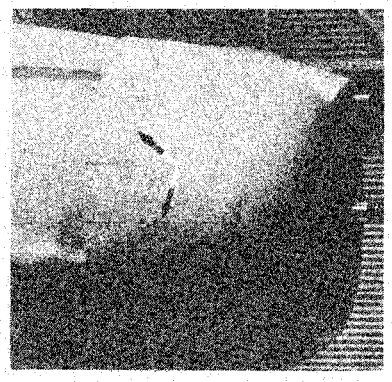

(b) Airplane 10 (Grumman XF4F-3);
$\Delta C_D = 0.0003$.

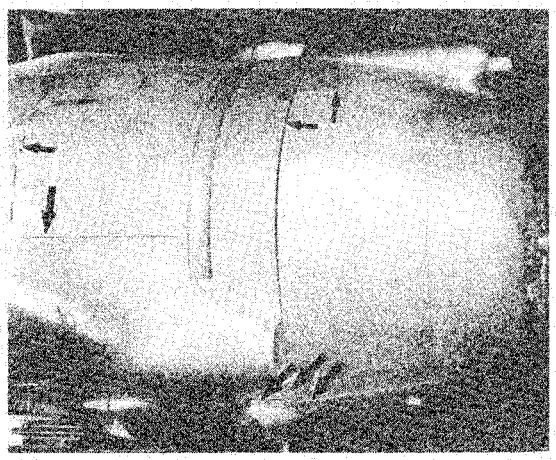

(c) Airplane 8 (Seversky XP-41);
$\Delta C_D = 0.0009$.

L-76-173

Figure B1.- Air leakage through cowling gaps.

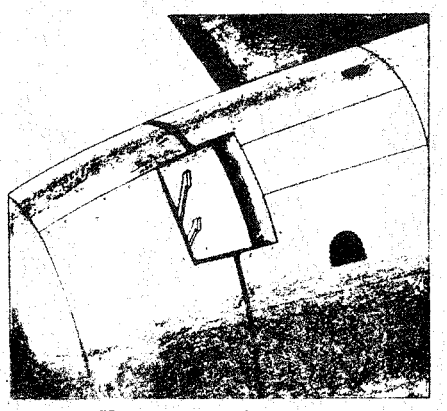

Upper cowling flap

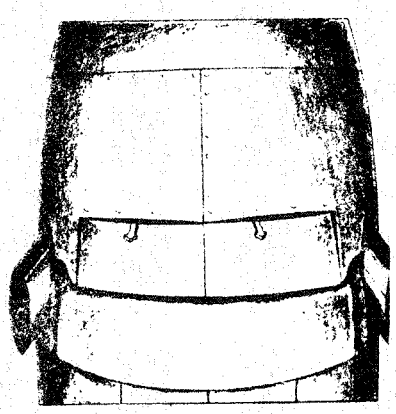

Lower cowling flaps

(d) Airplane 17 (Grumman XTBF-1); $\Delta C_D = 0.0004$.

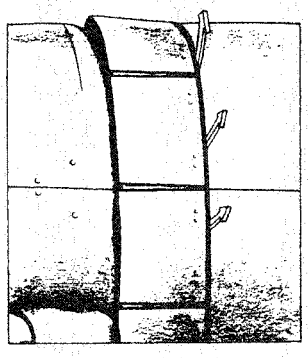

(e) Airplane 19 (Curtiss SB2C-1); $\Delta C_D = 0.0005$.

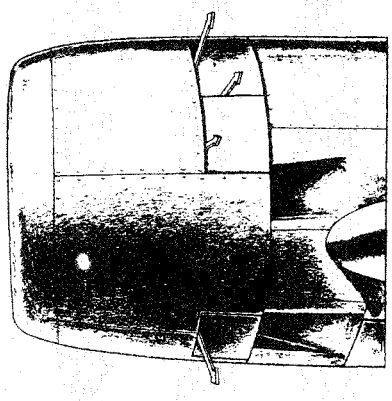

(f) Airplane 21 (Grumman F6F-3); $\Delta C_D = 0.0005$.

Figure B1.- Concluded.

Incremental drag coefficients due to air leakage were obtained when the doped-tape seals were removed from cowling gaps and hinges. The arrows indicate sources of leakage that produced a loss in momentum, disturbed the external airflow, and in turn resulted in an increase in drag.

APPENDIX B

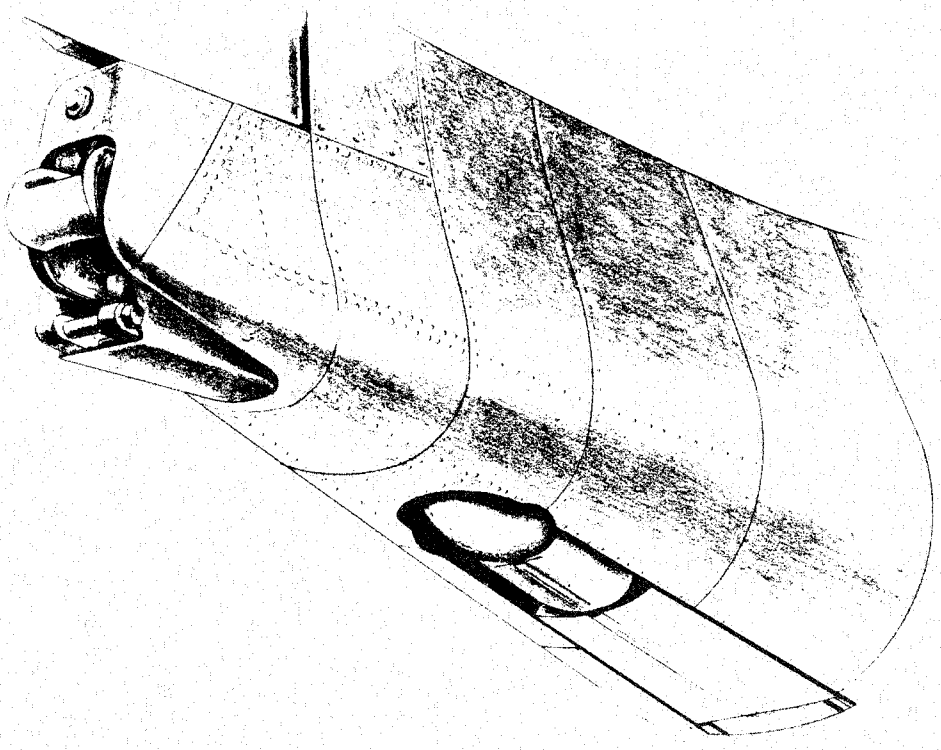

Figure B2.- Tail wheel and arresting hook openings on airplane 21 (Grumman F6F-3).

Removing seals and fairings from the openings at the tail wheel and arresting hook of airplane 21 increased the drag coefficient by 0.0005. This increment was largely due to leakage through these openings. The drag could have been reduced or eliminated by internal sealing of the bulkhead in front of the tail-wheel well.

APPENDIX C

DRAG DUE TO WING SURFACE IRREGULARITIES

Examples of the effects of surface irregularities and roughness on wing profile drag are discussed herein.

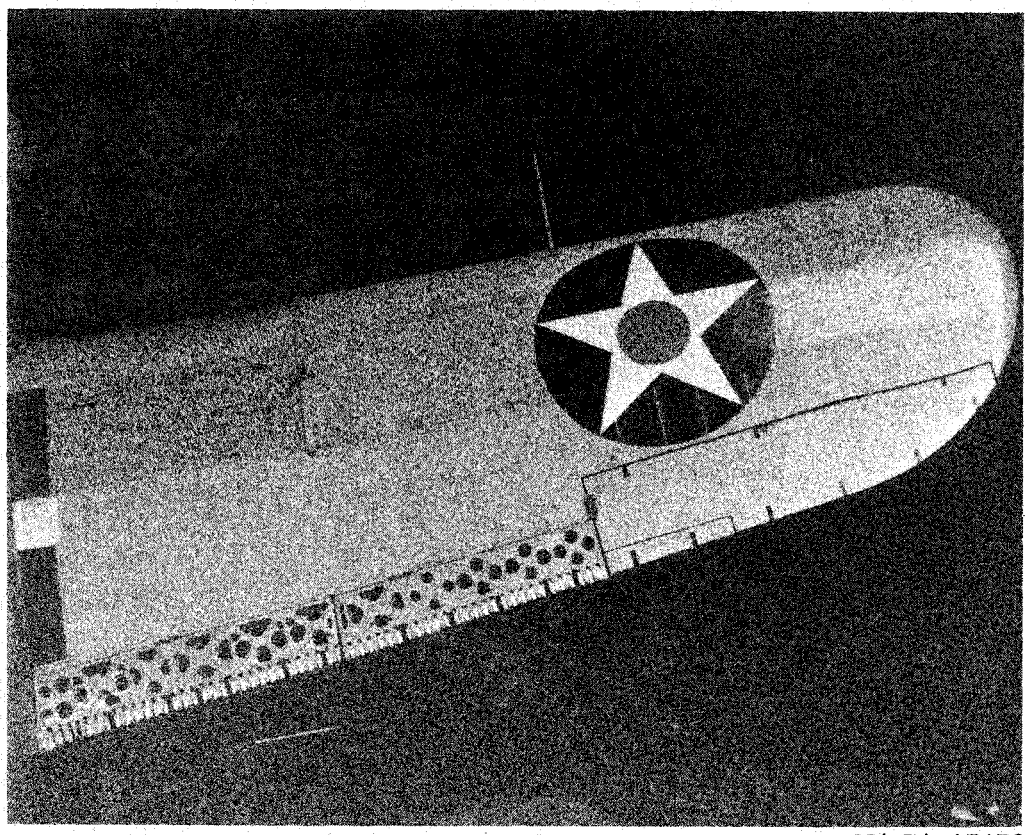

NACA 17173

Figure C1.- Perforated flaps on airplane 6 (Brewster XSBA-1).

The use of perforated trailing-edge flaps (split dive brake) on airplane 6 resulted in a drag increment of 0.0016.

APPENDIX C

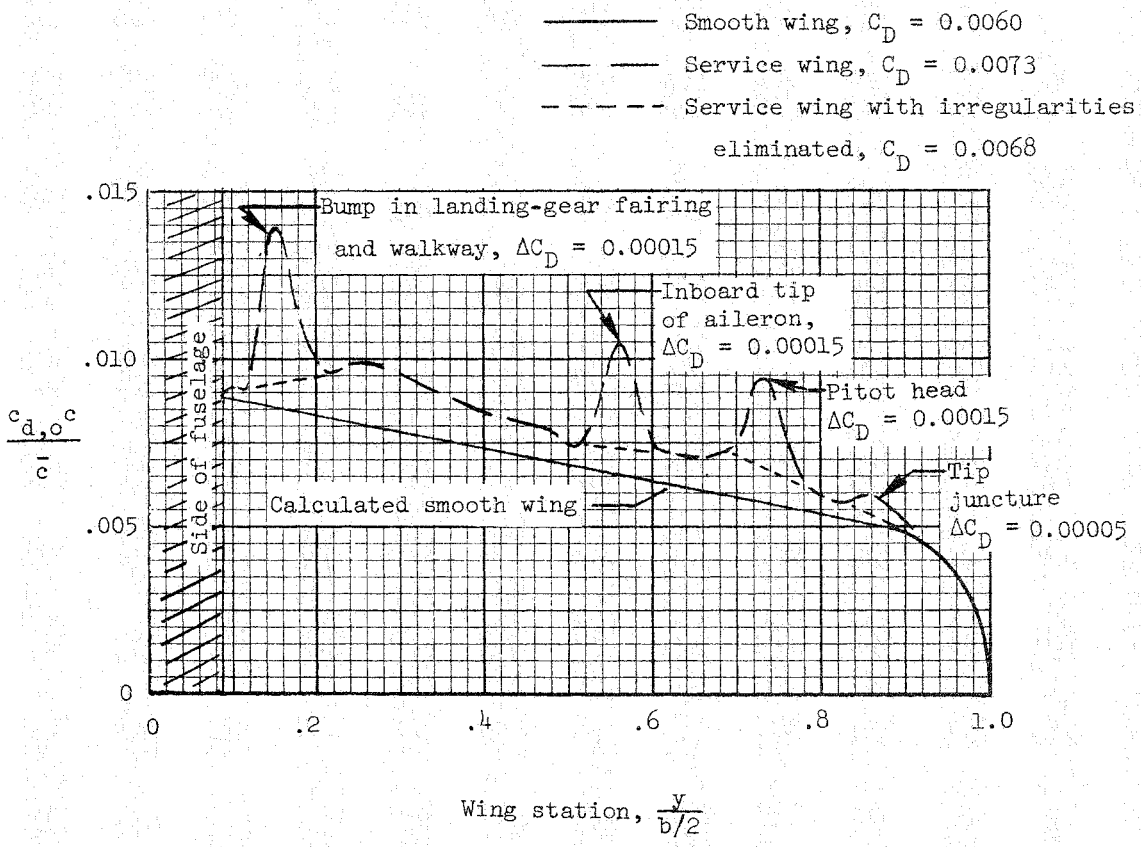

Figure C2.- Wing profile drag for airplane 9 (Bell XP-39).

The results obtained for the wing of airplane 9 are typical of the effects of small protuberances, gaps, and roughness on wing profile drag. The wing was flush riveted and had butt joints on the lateral seams and lap joints on the longitudinal seams.

APPENDIX C

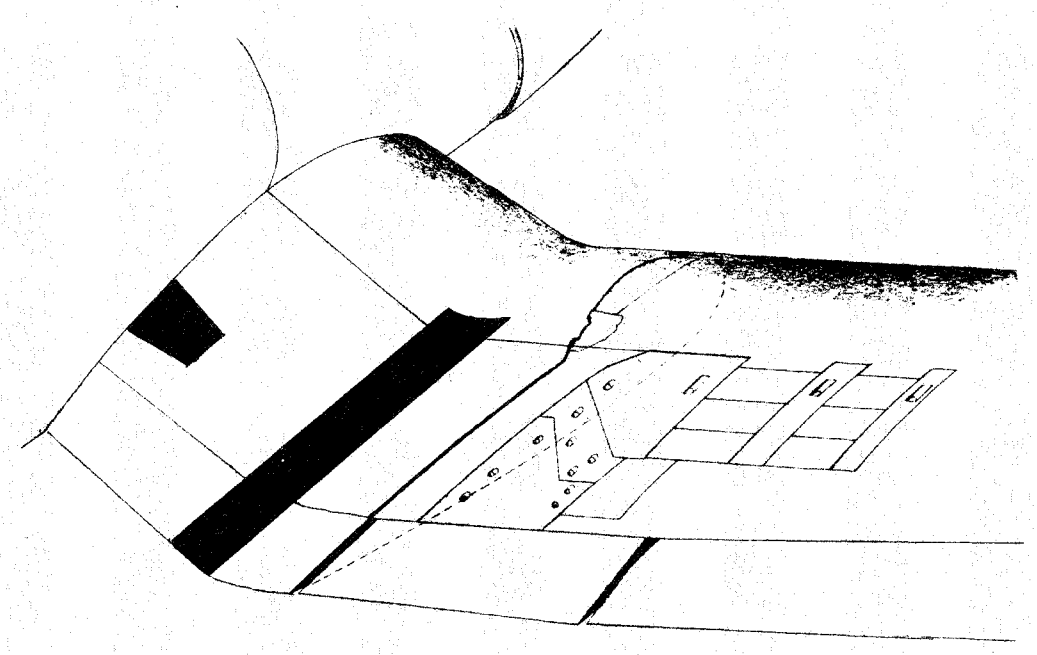

Figure C3.- Wing irregularities of airplane 20 (Vought-Sikorsky F4U-1).

The combination of irregularities and leakage for the wing of airplane 20 resulted in a drag-coefficient increment of 0.0022. Of this total, 0.0010 was attributed to the sanded walkway. The remainder of this increment was attributed to a large number of cover plates, access doors, and butt joints, and to air leakage.

APPENDIX D

DRAG DUE TO LANDING-GEAR INSTALLATIONS

Drag results for specific landing-gear installations are discussed herein.

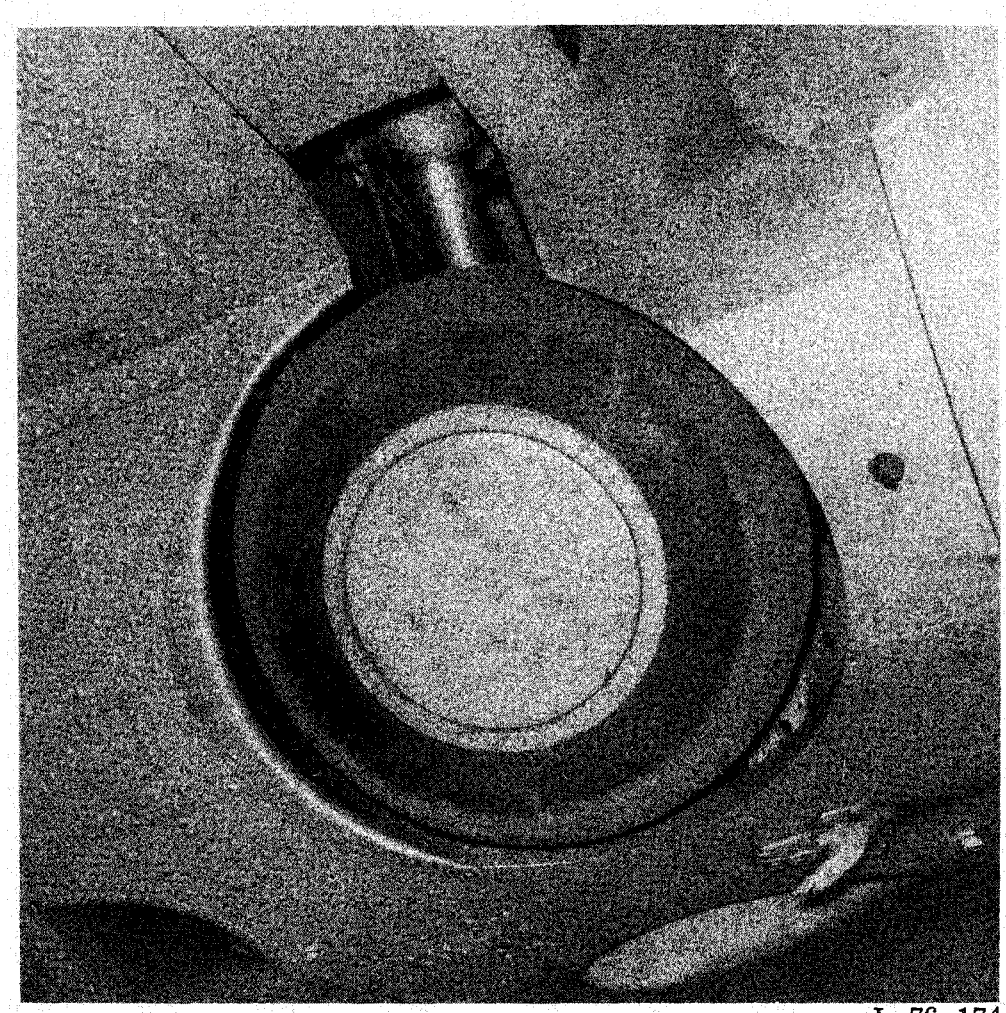

L-76-174

Figure D1.- Landing-gear installation on airplane 1 (Brewster XF2A-1).

The fuselage-located landing-gear installation of airplane 1 produced a drag-coefficient increment of 0.0016. This increment was due to air leakage and to the flow disturbances caused by the protrusion of the wheels beyond the normal fuselage line.

APPENDIX D

(a) Original condition.

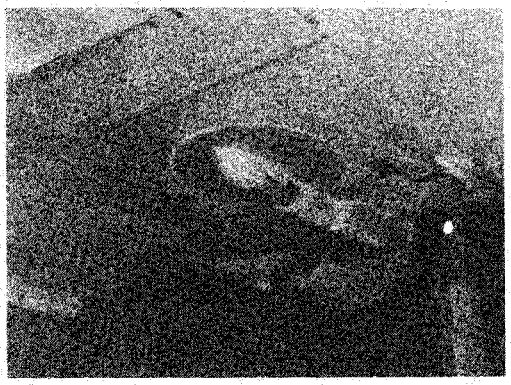

(b) Faired oleo struts and wheel cover plates.

L-76-175

Figure D2.- Landing-gear installations on airplane 4 (Vought SB2U-1).

The landing-gear installation of airplane 4 resulted in a drag-coefficient increment of 0.0019. Fairing of the oleo struts and rounding the edges of the rear halves of the wheel wells reduced the landing-gear drag-coefficient increment to 0.0015. Use of sealed wheel cover plates, together with the faired oleo struts, reduced the landing-gear increment to 0.0005.

APPENDIX D

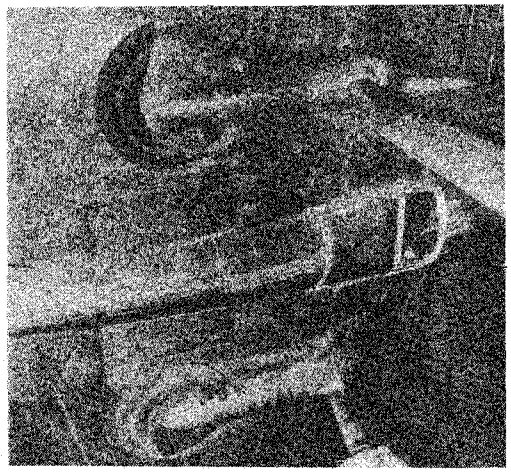

(a) Original condition.

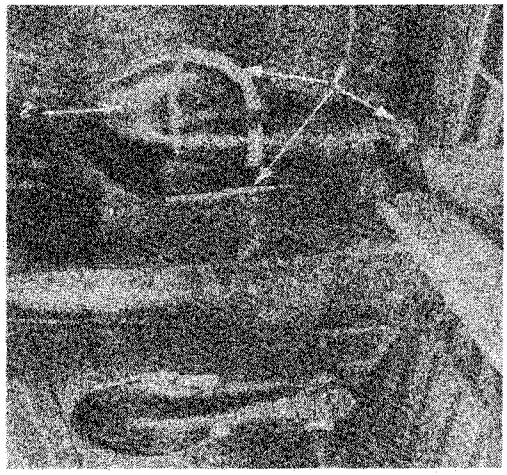

(b) Faired and sealed oleo struts and extended wheel covers.

L-76-176

Figure D3.- Landing-gear installations on airplane 7 (Curtiss XP-40).

Sealing the gaps on the landing gear of airplane 7 reduced the airplane drag coefficient by 0.0007. Additional use of extended wheel covers reduced the airplane drag coefficient by 0.0009.

APPENDIX D

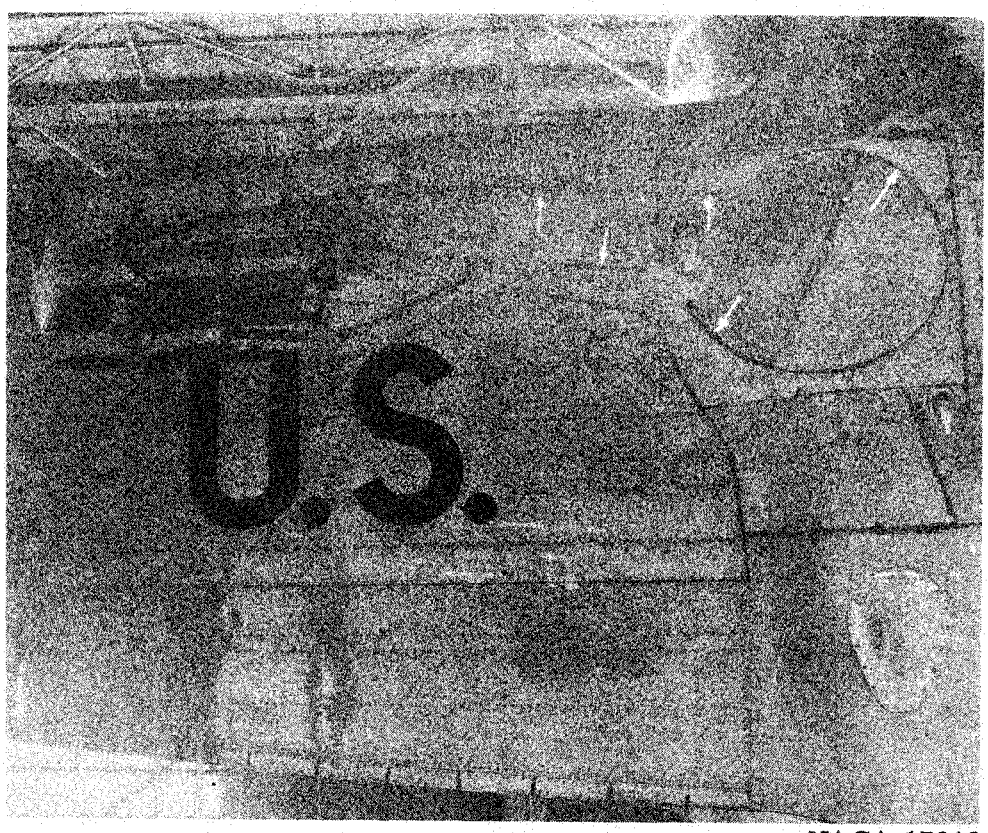

NACA 17816

Figure D4.- Landing-gear installation on airplane 8 (Seversky XP-41).

The landing-gear installation of airplane 8 allowed the oleo strut to be retracted into the wing and included wheel cover plates. The increment in drag coefficient due to this installation was only 0.0002.

APPENDIX D

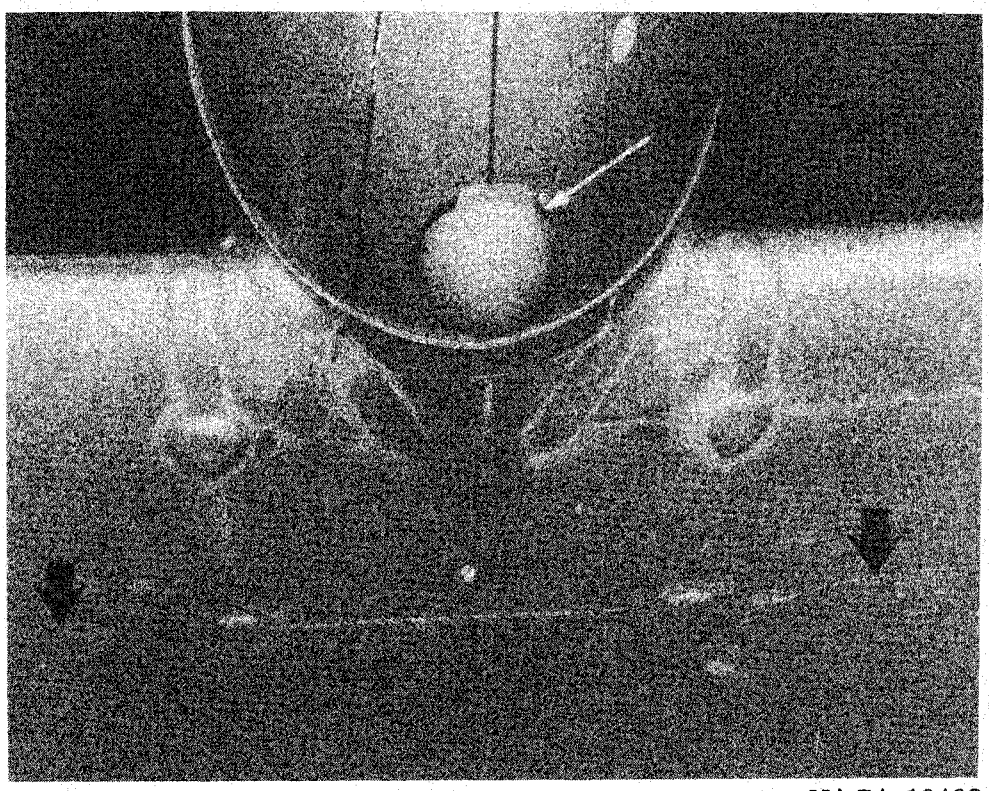

NACA 18462

Figure D5.- Landing-gear installation on airplane 9 (Bell XP-39).

The tricycle gear on airplane 9 had a nose wheel which did not fully retract into the fuselage and had main wheels which protruded from the wing by an amount equal to about one-third of the tire thickness, as shown in the photograph. The increment in drag coefficient for this landing-gear installation was 0.0019. Subsequent modifications provided for full nose-gear retraction and allowed the main gear to be fully submerged in coverless wheel wells. However, the modified installation also had a high drag-coefficient increment of 0.0016.

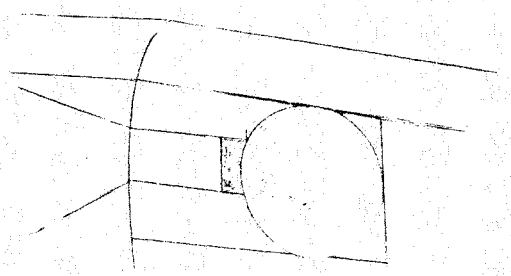

(a) Completely sealed wheel well.

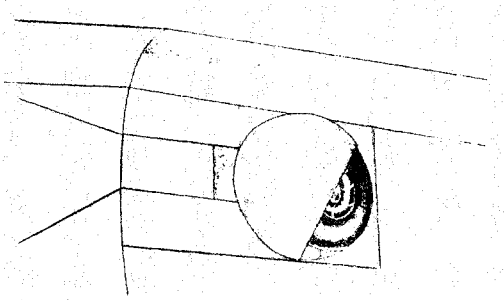

(b) Partially enclosed wheel well.

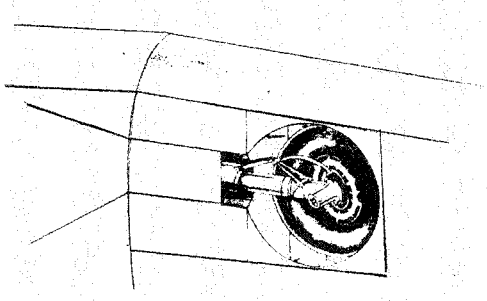

(c) Original wheel well.

Figure D6.- Landing-gear installations on airplane 17 (Grumman XTBF-1).

Completely sealing the open wheel well of airplane 17 decreased the drag coefficient by 0.0014. Partial enclosure of the wheel well decreased the airplane drag coefficient by 0.0007.

APPENDIX D

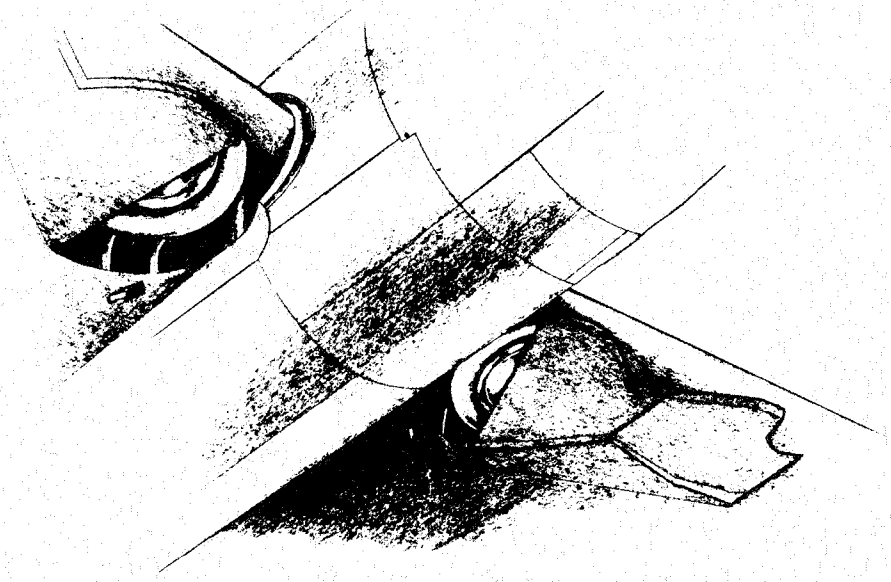

Figure D7.- Landing-gear installation on airplane 19 (Curtiss SB2C-1).

The partially open wheel wells on airplane 19 produced a drag-coefficient increment of 0.0005.

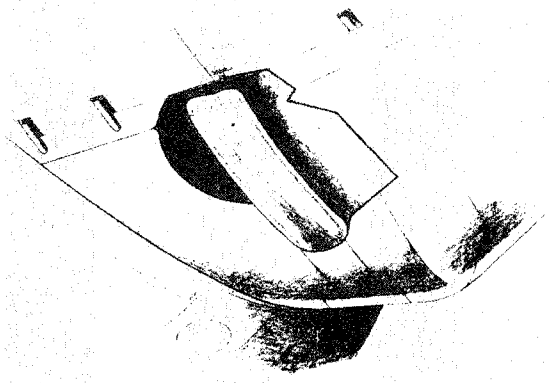

(a) Original full-length fairing.

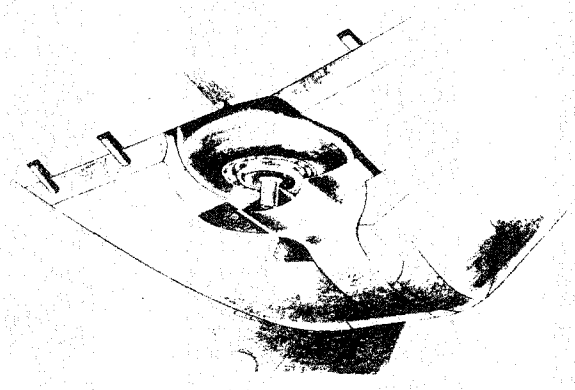

(b) Short-length fairing.

Figure D8.- Landing-gear installation on airplane 21 (Grumman F6F-3).

Removal of seals from the edges of the original full-length fairing over the retracted landing gear on airplane 21 increased the drag coefficient by 0.0009, indicating that air was leaking through the gaps around the cover plate. The short-length fairing, adopted for the production airplane, increased the drag coefficient by 0.0012 over that measured for the completely sealed fairing. This drag is due both to air leakage and to the airflow disturbance of the exposed parts.

APPENDIX E

DRAG DUE TO COCKPIT CANOPIES

Results of tests to reduce the drag increments produced by cockpit canopies are discussed herein.

(a) Original canopy.

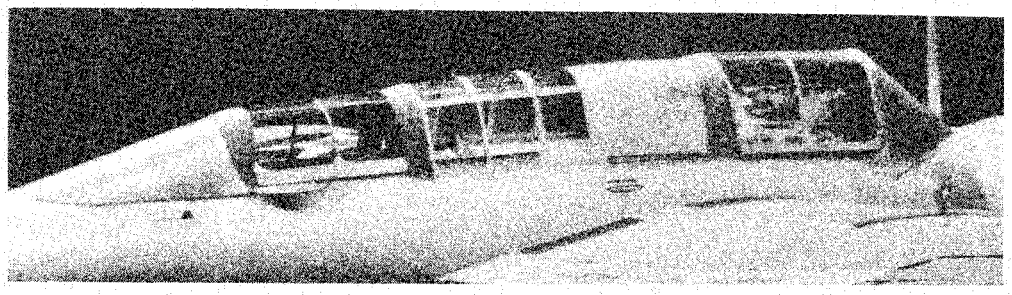

(b) Modified canopy.

L-76-177

Figure E1.- Cockpit canopies on airplane 6 (Brewster XSBA-1).

Rounding the windshield of airplane 6 and eliminating the sharp edge at the juncture of the windshield and the forward hood reduced the airplane drag coefficient by 0.0011. By replacing the quarter-spherical canopy tail section with a streamline shape, a net drag-coefficient reduction of 0.0019 was obtained.

APPENDIX E

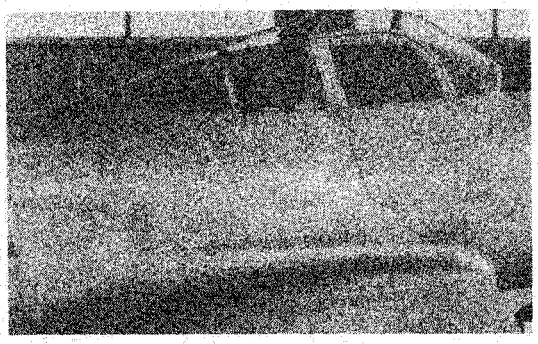

(a) Original canopy.

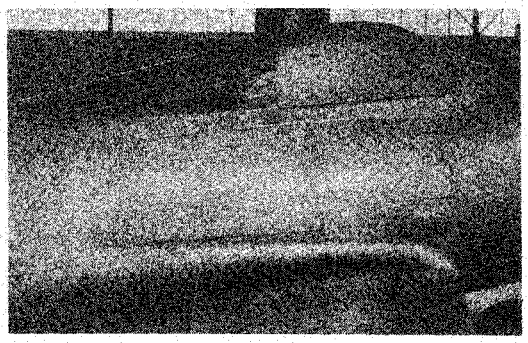

(b) Lowered canopy.

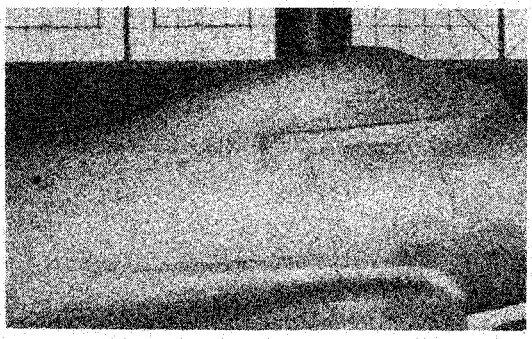

(c) Lowered canopy with reduced tail length.

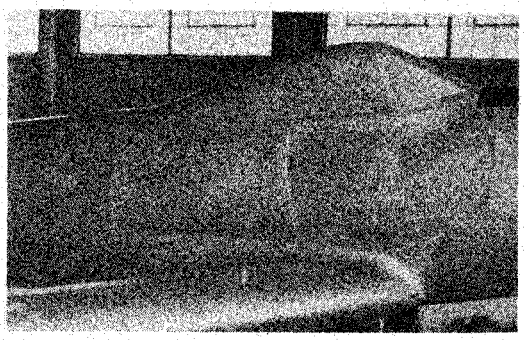

(d) Lowered canopy with reduced tail length and flat-sided windshield.

L-76-178

Figure E2.- Cockpit canopies on airplane 9 (Bell XP-39).

Comparison of data with and without the canopy for airplane 9 showed a drag-coefficient increment of only 0.0004. One modification, which consisted of reducing the height of the enclosure in order to decrease the expansion angle of the flow over the canopy tail, reduced the canopy drag-coefficient increment to 0.0002. Decreasing the length of the lowered canopy tail section resulted in a canopy drag-coefficient increment of 0.0003. Adding a flat-sided windshield to the lowered and shortened enclosure resulted in a canopy drag-coefficient increment of 0.0004.

APPENDIX E

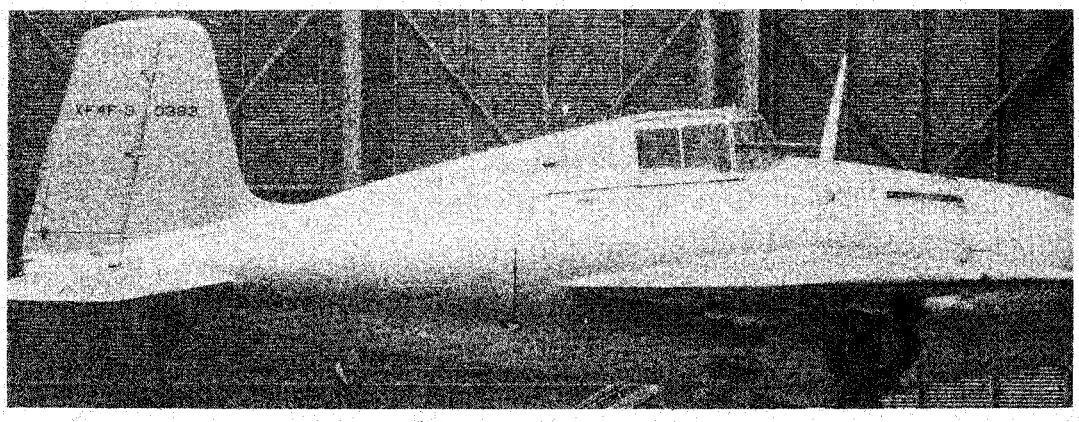

(a) Original canopy.

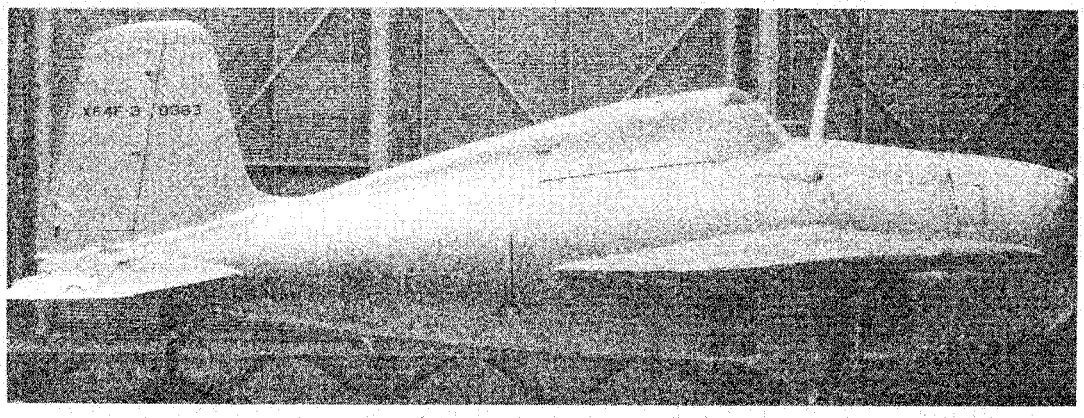

(b) Modified canopy.

L-76-179

Figure E3.- Cockpit canopies on airplane 10 (Grumman XF4F-3).

Increasing the radius of the juncture formed by the windshield and hood and reducing the windshield slope resulted in a reduction in drag coefficient of 0.0004 for airplane 10.

APPENDIX E

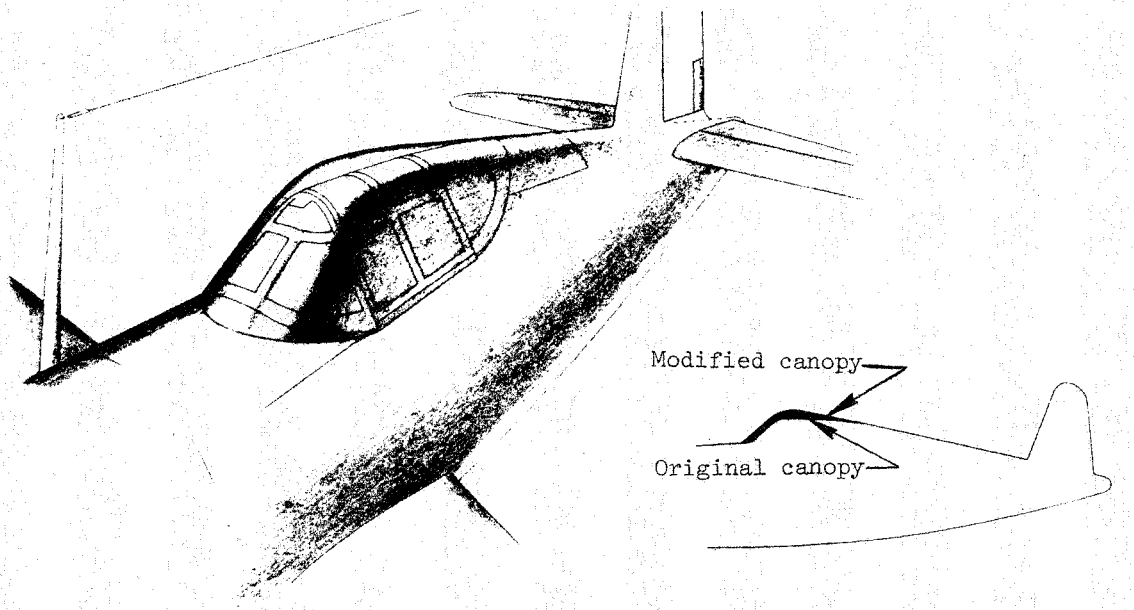

Figure E4.- Cockpit canopies on airplane 20 (Vought-Sikorsky F4U-1).

A well-rounded canopy was installed to eliminate the sharp peak of the original canopy of airplane 20 and to provide greater pilot visibility. Although the modified canopy was larger, the airplane drag coefficient was decreased by 0.0004.

APPENDIX F

DRAG DUE TO CONTROL-SURFACE GAPS

Drag coefficient increments due to control-surface gaps in the tails of three airplanes are discussed herein.

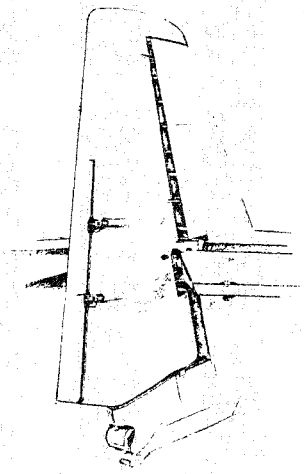

(a) Airplane 17; $\Delta C_D = 0.0009$.

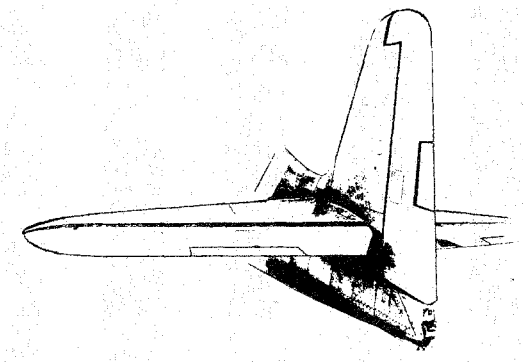

(b) Airplane 21; $\Delta C_D = 0.0005$.

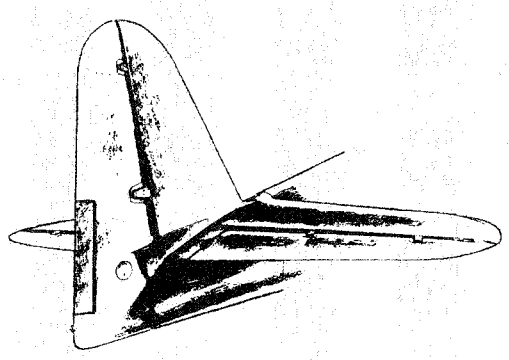

(c) Airplane 22; $\Delta C_D = 0.0007$.

Figure F1.- Tail-gap drag for airplanes 17 (Grumman XTBF-1), 21 (Grumman F6F-3), and 22 (Bell P-63).

An increase in drag was measured when the tape seals and metal fairings were removed from the gaps on the horizontal and vertical tail surfaces of airplanes 17, 21, and 22. Reduction of the drag due to these gaps may be obtained by sealing the lightening holes in the spars of the fixed portion of the tail and/or sealing the fuselage at the rear bulkhead. Further reductions may be obtained through careful attention to gap and contour details.

APPENDIX G

DRAG DUE TO ANTENNA INSTALLATIONS

Examples of drag-coefficient increments due to antenna installations are presented herein.

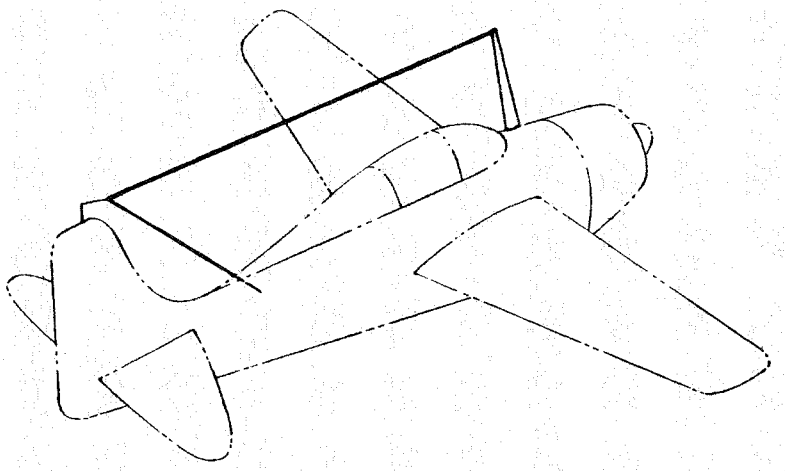

(a) Original antenna installation.

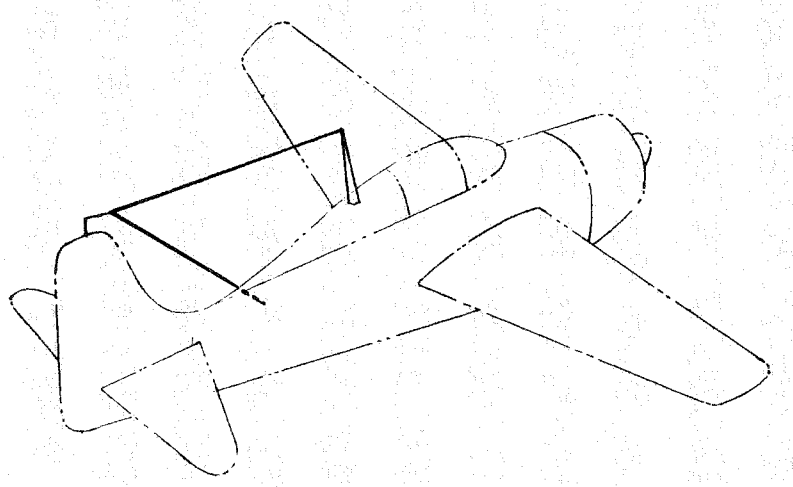

(b) Modified antenna installation.

Figure G1.- Antenna installations on airplane 10 (Grumman XF4F-3).

The antenna installation of airplane 10 produced an increment in drag coefficient of 0.0007. By shortening the mast and the wire length, this increment was reduced to 0.0002.

APPENDIX G

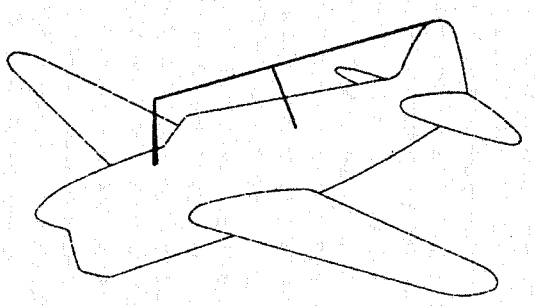

(a) Airplane 13; $\Delta C_D = 0.0004$.

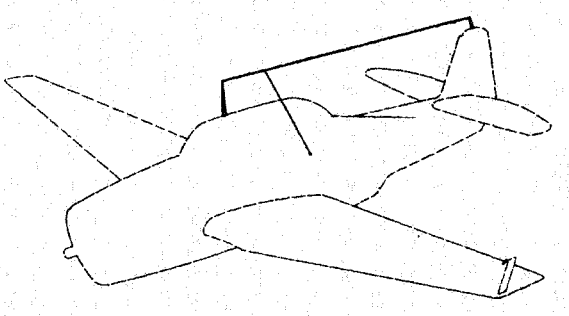

(b) Airplane 17; $\Delta C_D = 0.0004$.

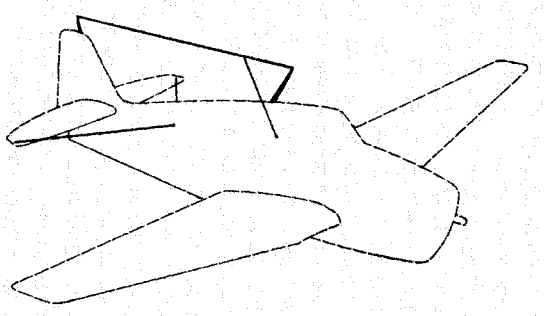

(c) Airplane 21; $\Delta C_D = 0.0003$.

Figure G2.- Antenna drag on airplane 13 (Curtiss XSO3C-1), 17 (Grumman XTBF-1), and 21 (Grumman F6F-3).

The drag-coefficient increments were measured as the difference in the drag with antennas installed and removed. Therefore the drag of these installations included contributions from both the masts and the wires of the antenna.

APPENDIX G

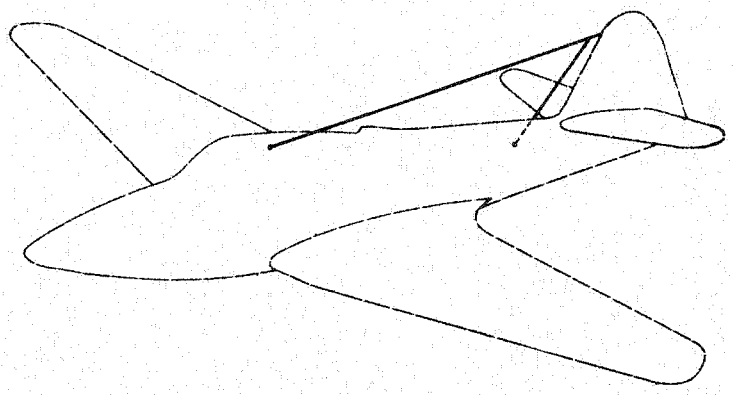

(a) Airplane 22.

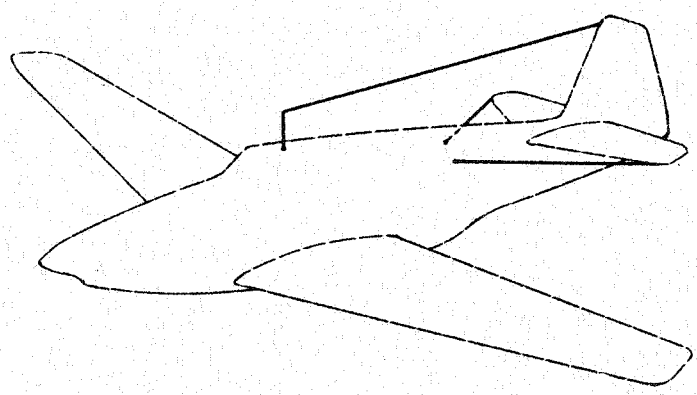

(b) Airplane 23.

Figure G3.- Antenna installations on airplanes 22 (Bell P-63) and 23 (North American P-51B).

No increase in drag was measured for these antenna installations.

REFERENCES

1. Roskam, Jan, ed.: Proceedings of the NASA/Industry/University General Aviation Drag Reduction Workshop. Univ. Kansas, July 1975.
2. Dearborn, C. H.; and Silverstein, Abe: Drag Analysis of Single-Engine Military Airplanes Tested in the NACA Full-Scale Wind Tunnel. NACA WR L-489, 1940. (Formerly NACA ACR, Oct. 1940.)
3. Lange, Roy H.: A Summary of Drag Results From Recent Langley Full-Scale-Tunnel Tests of Army and Navy Airplanes. NACA WR L-108, 1945. (Formerly NACA ACR L5A30.)
4. DeFrance, Smith J.: The N.A.C.A. Full-Scale Wind Tunnel. NACA Rep. 459, 1933.
5. Goett, Harry J.: Experimental Investigation of the Momentum Method for Determining Profile Drag. NACA Rep. 660, 1939.
6. Silverstein, Abe; and Becker, John V.: Determination of Boundary-Layer Transition on Three Symmetrical Airfoils in the N.A.C.A. Full-Scale Wind Tunnel. NACA Rep. 637, 1939.
7. Silverstein, Abe: Experiments on the Recovery of Waste Heat in Cooling Ducts. NACA ACR, May 1939.
8. Küchemann, Dietrich; and Weber, Johanna: Aerodynamics of Propulsion. First ed. McGraw-Hill Book Co., Inc., 1953.
9. Hood, Manley J.: The Effects of Some Common Surface Irregularities on Wing Drag. NACA TN 695, 1939.
10. Hoerner, Sighard F.: Fluid-Dynamic Drag. Publ. by the author (148 Busteed Drive, Midland Park, New Jersey 07432), 1965.

TABLE I.- BASIC GEOMETRIC CHARACTERISTICS OF AIRPLANES TESTED

Airplane	Weight, N (lb)	Wing area, m^2 (ft^2)	Span, m (ft)	Reference chord, m (ft)	Overall length, m (ft)	Wing section
1	21 937 (4 932)	19.42 (209.0)	10.67 (35.0)	2.15 (7.04)	7.81 (25.61)	Root: NACA 23018 Tip: NACA 23009
2	24 233 (5 448)	21.66 (233.2)	10.36 (34.0)	2.49 (8.17)	8.13 (26.67)	Root: NACA 23015 Tip: NACA 23009
3	19 918 (4 478)	24.71 (266.0)	9.75 (32.0)	1.52 (5.00)	6.75 (22.14)	Clark Y-H
4	27 889 (6 270)	28.36 (305.3)	12.80 (42.0)	2.54 (8.33)	10.36 (33.98)	Root: NACA 23015 Tip: NACA 23009
5	32 261 (7 253)	29.60 (318.6)	12.65 (41.5)	2.92 (9.58)	9.68 (31.75)	Root: NACA 2415 Tip: NACA 2409
6	26 337 (5 921)	23.97 (258.0)	10.06 (33.0)	2.43 (7.96)	8.47 (27.79)	Root: Clark Y-H 18% thick Tip: Clark Y-H 11.8% thick
7	30 171 (6 783)	21.93 (236.0)	11.37 (37.3)	2.64 (8.67)	9.66 (31.70)	Root: NACA 2215 Tip: NACA 2209
8	30 046 (6 755)	20.78 (223.7)	10.97 (36.0)	2.33 (7.64)	8.41 (27.60)	Root: Seversky 3, 16.7% thick Tip: Seversky 3, 8.2% thick
9	27 355 (6 150)	19.79 (213.0)	10.36 (34.0)	2.54 (8.33)	9.07 (29.75)	Root: NACA 0015 Tip: NACA 23009
10	25 910 (5 825)	24.15 (260.0)	11.58 (38.0)	2.48 (8.14)	8.53 (28.00)	Root: NACA 23015 Tip: NACA 23009
11	29 357 (6 600)	15.79 (170.0)	9.94 (32.6)	2.23 (7.33)	8.33 (27.33)	Root: NACA 23016.5 Tip: NACA 23009
12	26 688 (6 000)	21.93 (236.0)	11.37 (37.3)	2.74 (9.00)	9.30 (30.51)	Root: NACA 2215 Tip: NACA 2209
13	24 713 (5 556)	26.94 (290.0)	11.58 (38.0)	3.05 (10.00)	10.44 (34.24)	Root: NACA 23017 Tip: NACA 23009
14	85 179 (19 150)	43.20 (465.0)	18.69 (61.3)	3.35 (11.00)	14.63 (48.00)	Root: NACA 23018 Tip: NACA 23009
15	64 496 (14 500)	30.43 (327.5)	15.85 (52.0)	2.13 (7.00)	11.53 (37.83)	Root: NACA 23016 Tip: NACA 23009
16	249 088 (56 000)	97.36 (1048.0)	33.53 (110.0)	4.26 (14.00)	20.22 (66.33)	Root: Consolidated 22% thick Tip: Consolidated 9.3% thick
17	64 282 (14 452)	45.52 (490.0)	16.51 (54.2)	3.63 (11.92)	12.47 (40.92)	Root: NACA 23015 Tip: NACA 23009
18	28 912 (6 500)	15.79 (170.0)	9.48 (31.1)	2.20 (7.21)	8.87 (29.10)	Root: NACA 23016.5 Tip: NACA 23009
19	56 832 (12 777)	41.06 (442.0)	15.15 (49.7)	3.66 (12.00)	11.18 (36.67)	Root: NACA 23017 Tip: NACA 23009
20	48 928 (11 000)	29.17 (314.0)	12.49 (41.0)	2.67 (8.75)	10.16 (33.34)	Root: NACA 23015 Tip: NACA 23009
21	50 890 (11 441)	30.03 (334.0)	13.05 (42.8)	3.03 (9.93)	10.31 (33.83)	Root: NACA 23015.6 (Modified) Tip: NACA 23009
22	34 081 (7 662)	23.04 (248.0)	11.68 (38.3)	2.54 (8.33)	10.02 (32.87)	Root: NACA 66 series Tip: NACA 66 series
23	37 417 (8 412)	21.66 (233.2)	11.29 (37.0)	2.64 (8.67)	9.83 (32.25)	NACA-NAA compromise low drag

TABLE II.- POWER-PLANT INSTALLATION OF AIRPLANES

Airplane	Engine characteristics					
	Propeller diameter, m (ft)	Propeller gear ratio	Power, altitude, and rpm (a)			Type
			kW (hp)	m (ft)	rpm	
1	3.12 (10.25)	Direct drive	559 (750)	4633 (15 200)	2100	Single-row radial, air cooled
2	3.05 (10.0)	3:2	671 (900)	3048 (10 000)	2550	Twin-row radial, air cooled
3	2.74 (9.0)	Direct drive	611 (820)	3658 (12 000)	2100	Single-row radial, air cooled
4	3.35 (11.0)	3:2	559 (750)	4328 (14 200)	2550	Twin-row radial, air cooled
5	3.28 (10.75)	16:11	597 (800)	4887 (16 000)	2300	Single-row radial, air cooled
6	2.74 (9.0)	Direct drive	559 (750)	4572 (15 000)	2100	Single-row radial, air cooled
7	3.35 (11.0)	2:1	746 (1000)	4877 (16 000)	2600	Inline, liquid cooled
8	3.35 (11.0)	16:9	820 (1100)	4572 (15 000)	2700	Twin-row radial, air cooled with geared supercharger
9	3.17 (10.4)	9:5	858 (1150)	6096 (20 000)	2950	Inline, liquid cooled with turbosupercharger
10	2.97 (9.75)	3:2	746 (1000)	6096 (20 000)	2550	Twin-row radial, air cooled with two-stage geared supercharger
11	3.20 (10.5)	2:1	858 (1150)	3658 (12 000)	3000	Inline, liquid cooled
12	3.05 (10.0)	16:9	746 (1000)	4420 (14 500)	2700	Twin-row radial, air cooled
13	2.82 (9.25)	3:2	336 (450)	3658 (12 000)	3000	Inverted V-12, air cooled
14	3.43 (11.25)	16:9	2 at 1044 (1400)	3505 (11 500)	2400	Twin-row radial, air cooled
15	3.56 (11.67)	2:1	2 at 1044 (1400)	7620 (25 000)	3000	Inline, liquid cooled with supercharger
16	3.66 (12.0)	16:9	4 at 895 (1200)	7620 (25 000)	2600	Twin-row radial, air cooled with two-speed supercharger
17	3.81 (12.5)	16:9	2 at 1007 (1350)	3962 (13 000)	2400	Twin-row radial, air cooled with two-speed supercharger
18	3.05 (10.0)	2:1	858 (1150)	3658 (12 000)	3000	Inline, liquid cooled
19	3.66 (12.0)	16:9	1007 (1350)	3962 (13 000)	2400	Twin-row radial, air cooled with two-speed supercharger
20	4.06 (13.33)	2:1	1156 (1550)	7772 (25 500)	2550	Twin-row radial, air cooled with two-stage supercharger
21	3.99 (13.08)	2:1	1230 (1650)	7620 (25 000)	2700	Twin-row radial, air cooled with two-stage supercharger
22	3.38 (11.08)	2.23:1	858 (1150)	6828 (22 400)	3000	Inline, liquid cooled with auxiliary-stage supercharger
23	3.40 (11.17)	44:21	969 (1300)	7376 (24 200)	3000	Inline, liquid cooled with supercharger

[a] Power at specified altitude and rpm.

TABLE III.- SUMMARY OF DRAG RESULTS

[Numbers in parentheses refer to figure or table numbers]

(a) Airplanes 1 to 11 at $C_L = 0.15$ (ref. 2)

Item	Airplanes										
	1	2	3	4	5	6	7	8	9	10	11
	Drag coefficient, C_D										
Airplane in original condition	0.0377	0.0328	0.0390	0.0267	0.0320	0.0362	0.0257	0.0275	0.0329	0.0269	0.0201
	Drag-coefficient increment, ΔC_D										
Cooling							0.0034 [a].0017 (A4)		0.0023 [a].0008 (A1)		0.0011 (A5)
Cowling								0.0020 (A8)		0.0013 (A9)	
Cowling leakage					0.0008 (B1)			0.0009 (B1)		0.0003 (B1)	
Carburetor air scoop		[b]0.0010 (A13)						0.0006 (IV)	0.0019 (A14)	[b]0.0006 (A15)	0.0001 (A16)
Oil cooler		0.0020 (A17)	0.0007 (A18)	0.0007 [a].0003 (A19)				0.0017 [a].0009 (A20)	0.0040 [a].0011 (A21)	0.0008 (A22)	
Intercooler								0.0011 (IV)		0.0012 (A12)	
Exhaust stack	0.0016 (Similar to airplane 5)				0.0010 (A26)		0.0003 (2(g))	0.0005 (A26)	0.0014 (A26)		0.0003 (A26)
Supercharger									0.0033 (A30)		
Landing gear	0.0016 (D1)		0.0007 (2(c))	0.0019 [a].0005 (D2)			[b]0.0009 (D3)	0.0002 (D4)	0.0019 [a].0016 (D5)		
Cockpit canopy						[b]0.0019 (E1)			0.0004 (E2)	[b]0.0004 (E3)	
Antennas								0.0008 (IV)		0.0007 [a].0002 (G1)	

[a] Drag-coefficient increment of the modified installation.

[b] Difference in airplane drag coefficients for the original and the modified installations.

TABLE III.- Concluded

(b) Airplanes 12 to 23 at C_L as required for high-speed flight condition (ref. 3)

Item	Airplanes											
	12	13	14	15	16	17	18	19	20	21	22	23
Drag coefficient, C_D												
Airplane in original condition	0.0243	0.0337	0.0386	0.0293	[c] 0.0361	0.0264		0.0280	0.0284	0.0293	0.0221	0.0208
Airplane in sealed and faired condition	0.0203	0.0313	0.0282	0.0222		0.0183	0.0160	0.0219	0.0215	0.0210	0.0171	0.0173
Drag-coefficient increment, ΔC_D												
Cooling	0.0040 [a] .0012 (A6)	[b] 0.0004 (A7)					[a] 0.0011 (A2)				[b] 0.0005 (A3)	
Cowling			[a] 0.0041 (A10)									
Cowling leakage						0.0004 (B1)		0.0005 (B1)		0.0005 (B1)		
Oil cooler			0.0018 [a] .0008 (A23)	0.0008 (A24)			[b] 0.0004 (A25)					
Exhaust stacks						0.0008 (A27)		0.0021 (A27)	0.0010 (A28)		0.0005 (A29)	0.0007 (A29)
Supercharger					0.0040 [a] .0027 (A31)							
Wing irregularities and wing leakage									0.0022 (C3)			
Landing gear						0.0014 [a] .0007 (D6)		0.0005 (D7)		0.0009 [a] .0012 (D8)		
Tail wheel and arresting hook										0.0005 (B2)		
Cockpit canopy									[b] 0.0004 (E4)			
Tail gap						0.0009 (F1)				0.0005 (F1)	0.0007 (F1)	
Antennas		0.0004 (G2)				0.0004 (G2)				0.0003 (G2)	0 (G3)	0 (G3)

[a] Drag-coefficient increment of the modified installation.

[b] Difference in airplane drag coefficient for the original and the modified installations.

[c] Estimated value.

Airplane condition

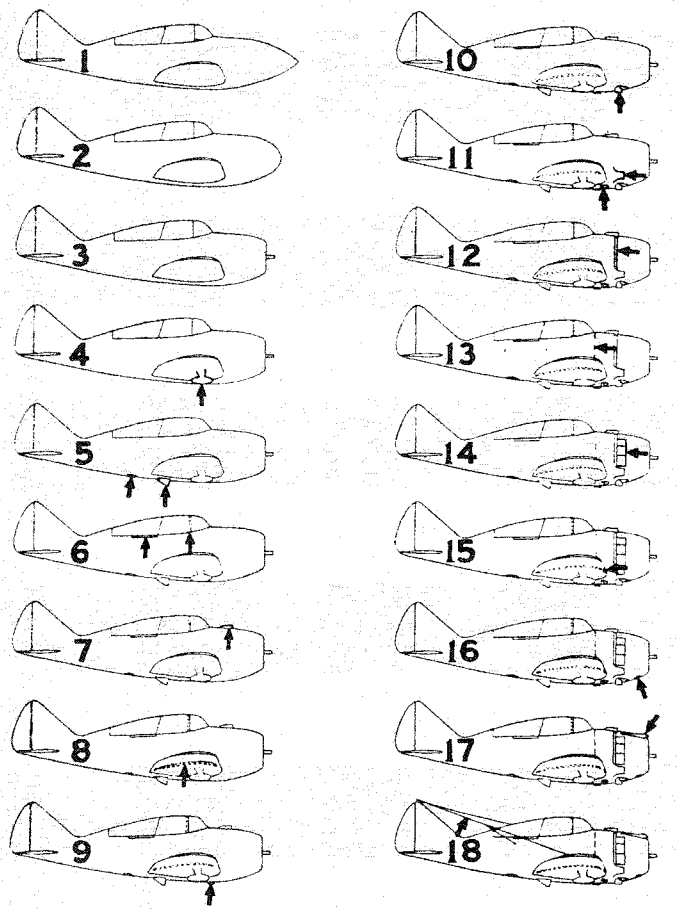

TABLE IV.- RESULTS OF TESTS TO IDENTIFY SOURCES OF DRAG FOR AIRPLANE 8 (SEVERSKY XP-41)

Condition number	Description	C_D $(C_L = 0.15)$	ΔC_D	ΔC_D, percent[a]
1	Completely faired condition, long nose fairing	0.0166		
2	Completely faired condition, blunt nose fairing	.0169		
3	Original cowling added, no airflow through cowling	.0186	0.0020	12.0
4	Landing-gear seals and fairing removed	.0188	.0002	1.2
5	Oil cooler installed	.0205	.0017	10.2
6	Canopy fairing removed	.0203	-.0002	-1.2
7	Carburetor air scoop added	.0209	.0006	3.6
8	Sanded walkway added	.0216	.0007	4.2
9	Ejector chute added	.0219	.0003	1.8
10	Exhaust stacks added	.0225	.0006	3.6
11	Intercooler added	.0236	.0011	6.6
12	Cowling exit opened	.0247	.0011	6.6
13	Accessory exit opened	.0252	.0005	3.0
14	Cowling fairing and seals removed	.0261	.0009	5.4
15	Cockpit ventilator opened	.0262	.0001	.6
16	Cowling venturi installed	.0264	.0002	1.2
17	Blast tubes added	.0267	.0003	1.8
18	Antenna installed	.0275	.0008	4.8
Total			0.0109	

[a] Percentages based on completely faired condition with long nose fairing.

TABLE V.- PROFILE DRAG AND LOCATION OF TRANSITION POINT FOR THE WINGS OF AIRPLANES 1 TO 11

Airplane	Description of wing	$\frac{s}{c}$ (a)	$\frac{y}{b/2}$ (b)	$\frac{t}{c}$ (c)	Measured $C_{D,w,o}$	Calculated[d] $C_{D,w,o}$	$\Delta C_{D,w,o}$
1	Metal covered, brazier-head rivets; larger rivets on forward portion of wing; laps facing back				0.0090	0.0058	0.0032
2	Metal covered, brazier-head rivets; row of larger rivets on upper surface about 0.15c behind L.E.; laps facing back				.0083	.0062	.0021
3	Fabric covered, raised stitching; drag measured on lower wing				.0084	.0070	.0014
4	Front portion of wing metal covered, flush rivets; rear portion fabric covered, flush stitching				.0070	.0063	.0007
5	Metal covered, flush rivets to about 0.18c behind L.E., remainder brazier-head rivets; perforated dive and landing flaps				.0109	.0072	.0037 ΔC_D due to perforated flaps, 0.0020
6	Metal covered, flush rivets on front half of wing, laps facing back; fabric covering on rear half; perforated dive and landing flaps				.0106	.0065	.0041 ΔC_D due to perforated flaps, 0.0016
7	Metal covered, flush rivets, laps facing forward	0.176	0.48	0.126	.0079	.0060	.0019
8	Metal covered, flush rivets, joggled laps	.198	.41	.134	.0070	.0059	.0011
9	Metal covered, flush rivets, filled joints	.180	.42	.135	.0073	.0060	.0013 See figure C2
10	Metal covered, flush rivets, filled joints				.0077	.0061	.0016
11	Wood, filled and polished	.180	.35	.130	.0074	.0061	.0013

[a] Chordwise location of transition point.

[b] Spanwise location where transition point was measured.

[c] Maximum wing section thickness at spanwise location where transition point was measured.

[d] Calculated values based on smooth airfoil data.

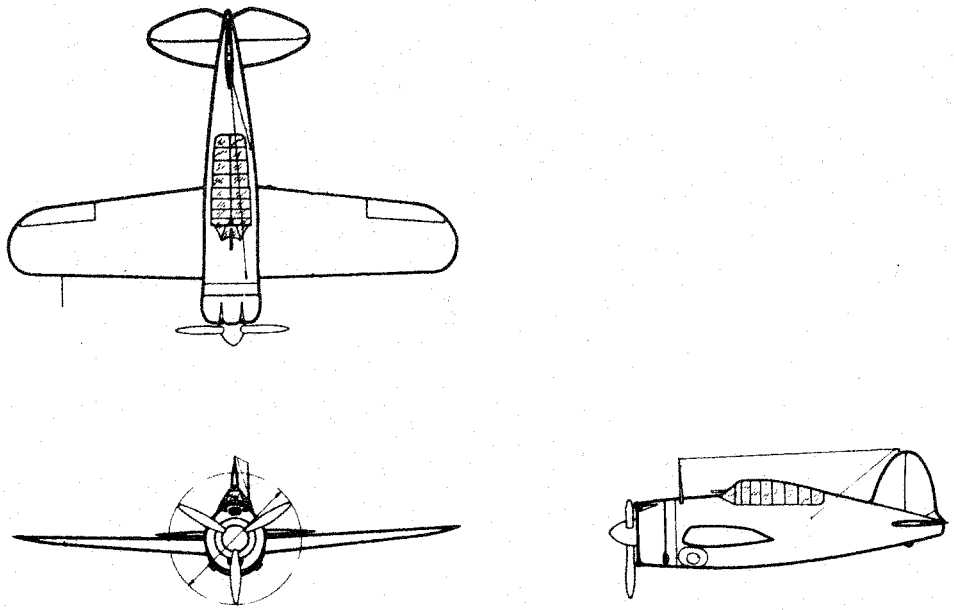

(a) Airplane 1 (Brewster XF2A-1).

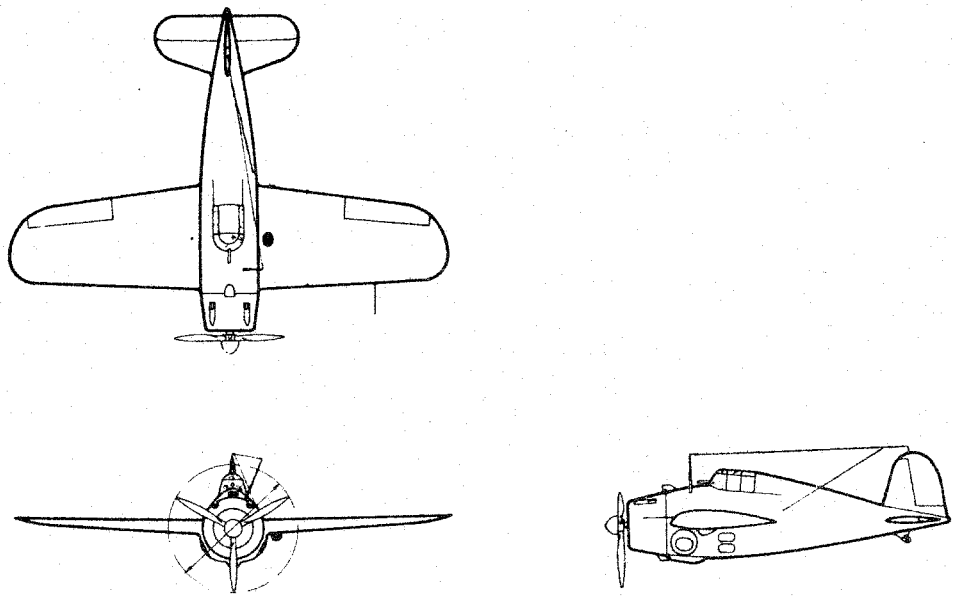

(b) Airplane 2 (Grumman XF4F-2).

Figure 1.- Three-view sketches of the airplanes tested.

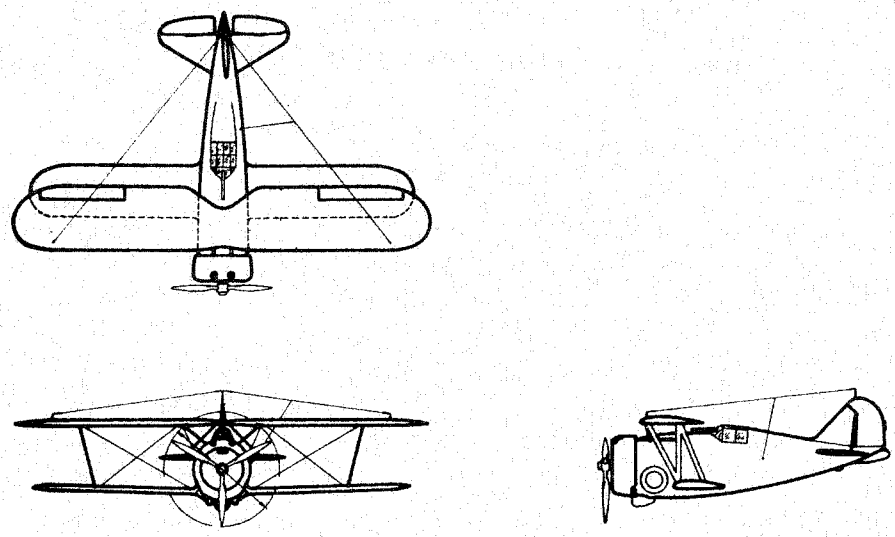

(c) Airplane 3 (Grumman F3F-2).

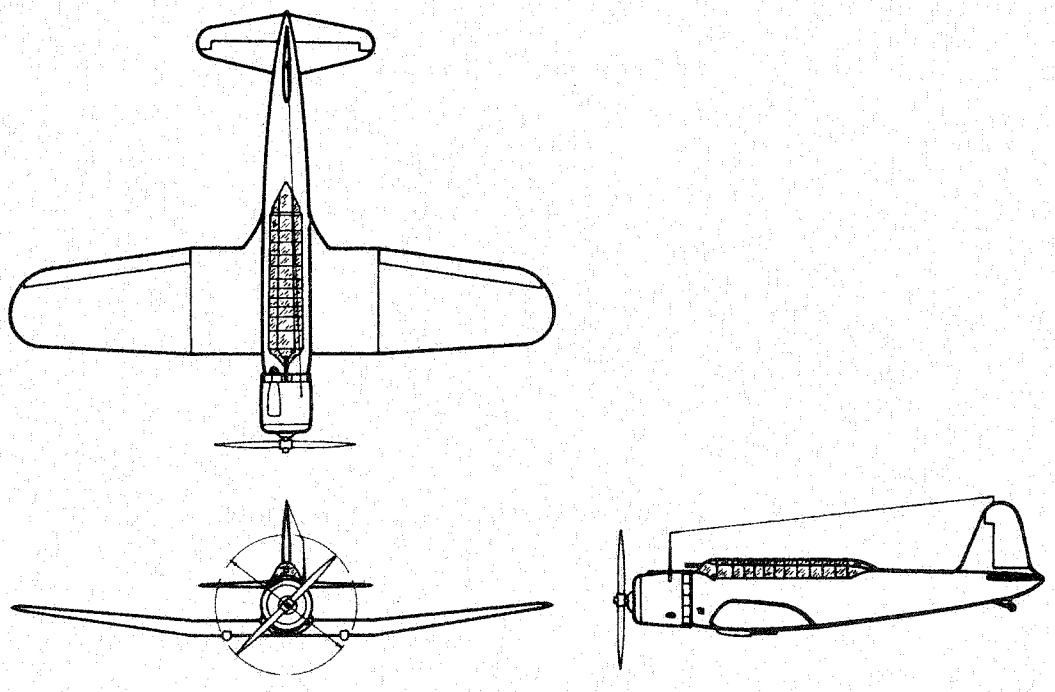

(d) Airplane 4 (Vought SB2U-1).

Figure 1.- Continued.

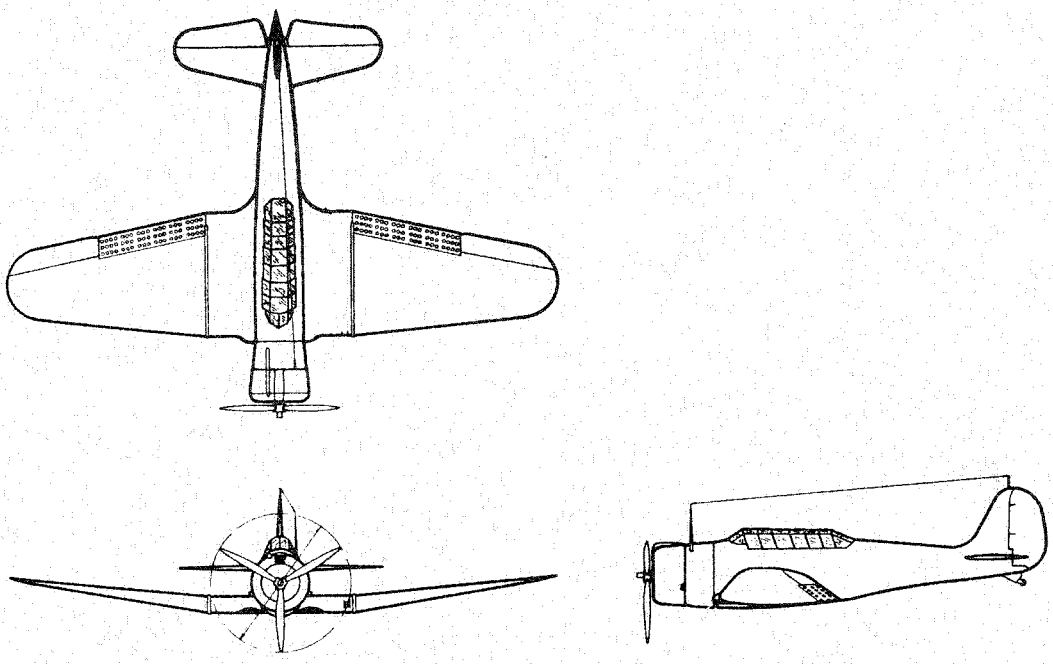

(e) Airplane 5 (Douglas XBT-2).

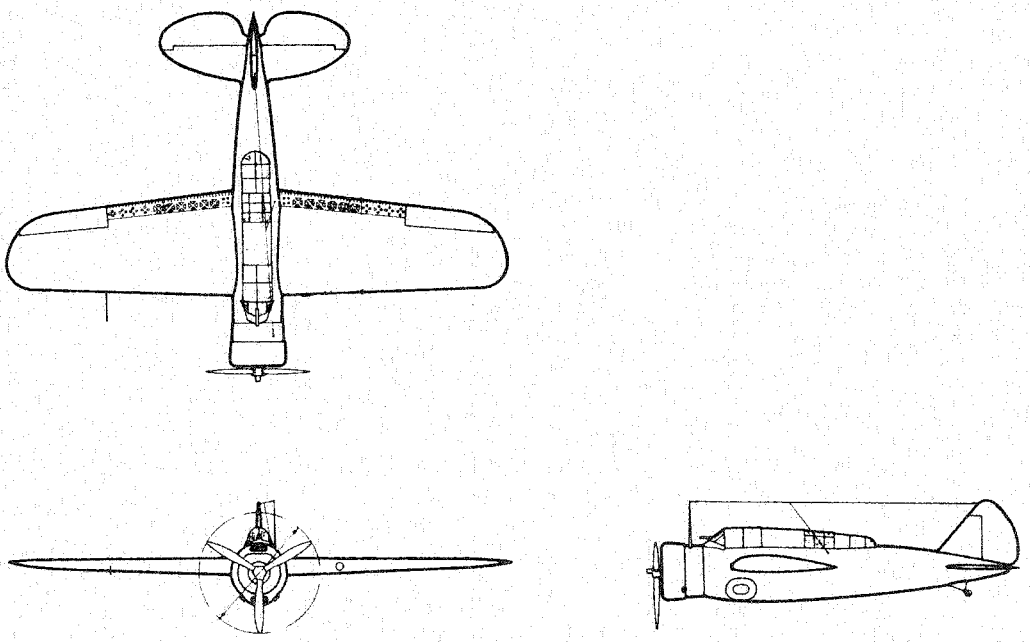

(f) Airplane 6 (Brewster XSBA-1).

Figure 1.- Continued.

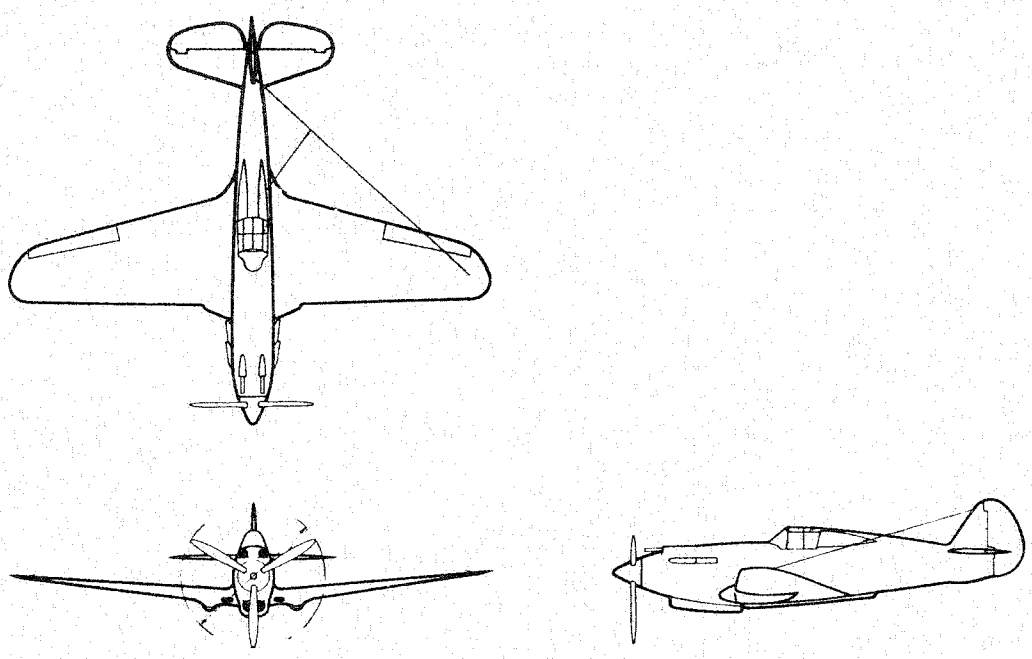

(g) Airplane 7 (Curtiss XP-40).

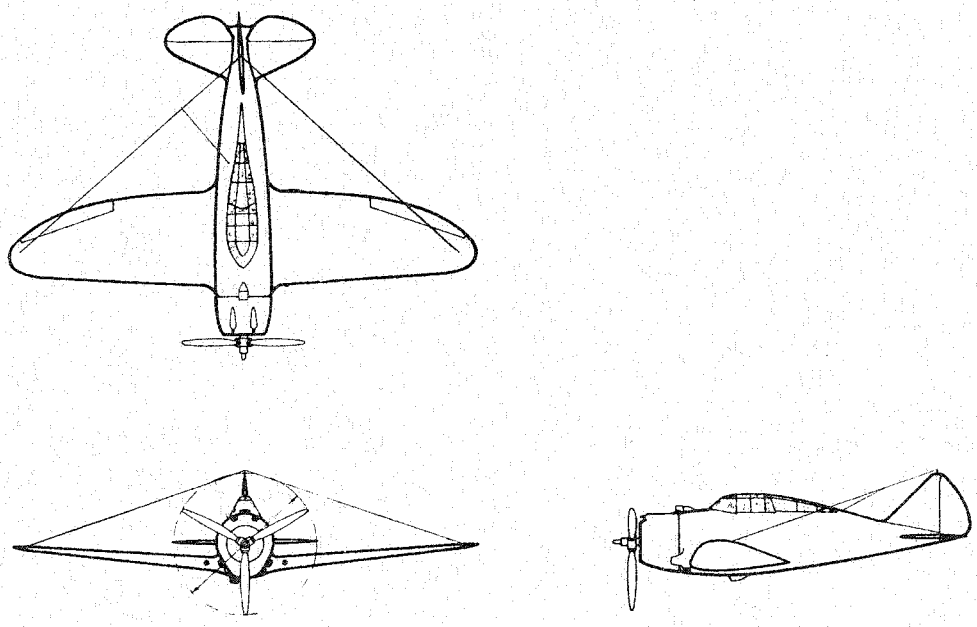

(h) Airplane 8 (Seversky XP-41).

Figure 1.- Continued.

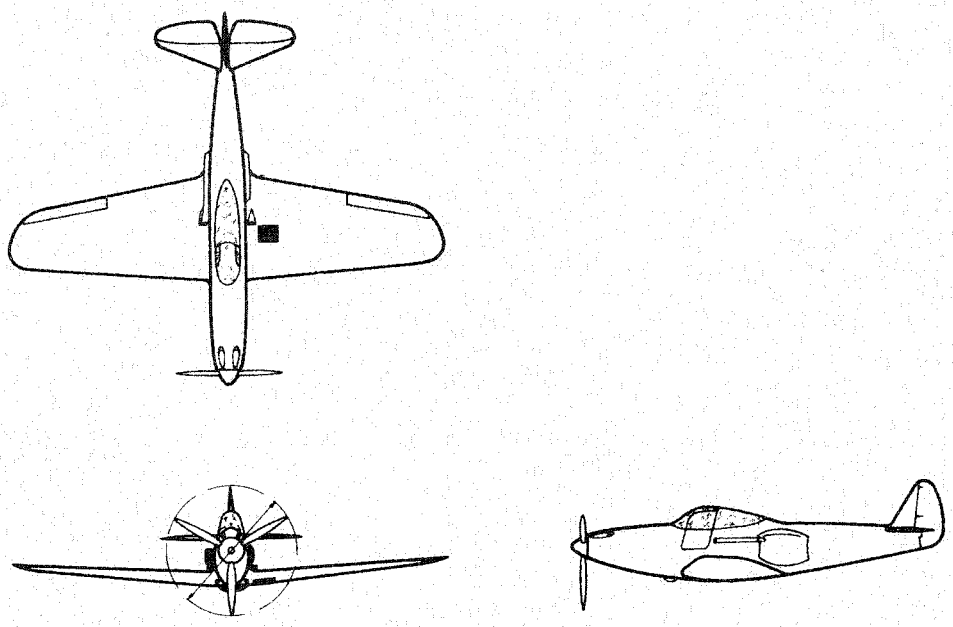

(i) Airplane 9 (Bell XP-39).

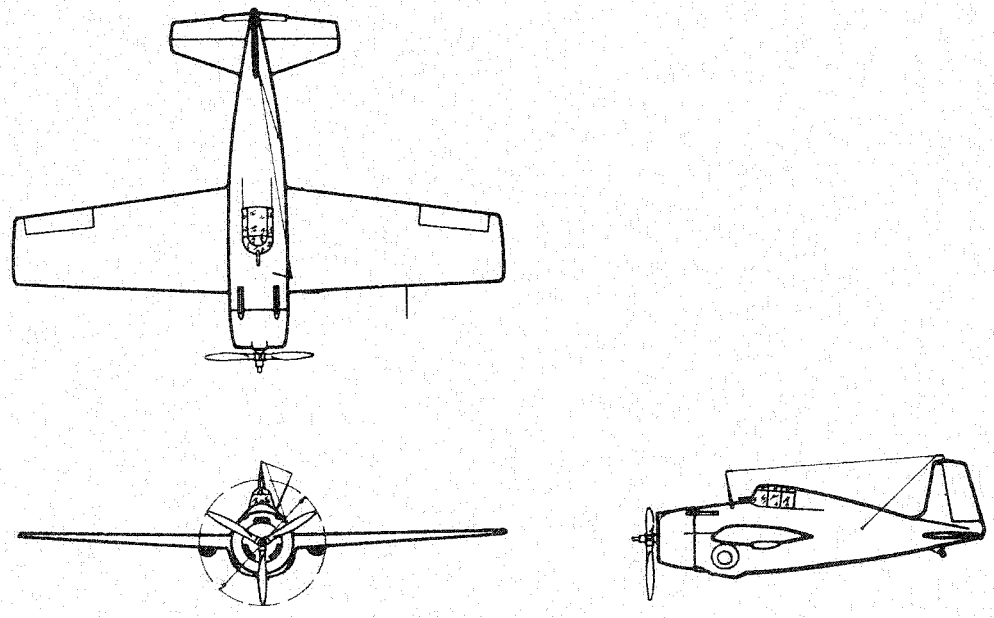

(j) Airplane 10 (Grumman XF4F-3).

Figure 1.- Continued.

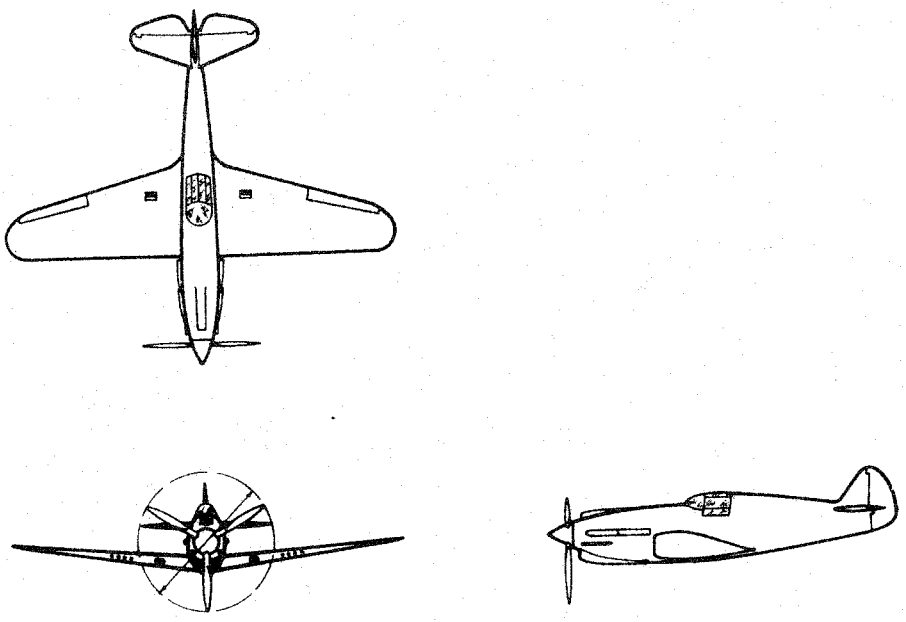

(k) Airplane 11 (Curtiss XP-46).

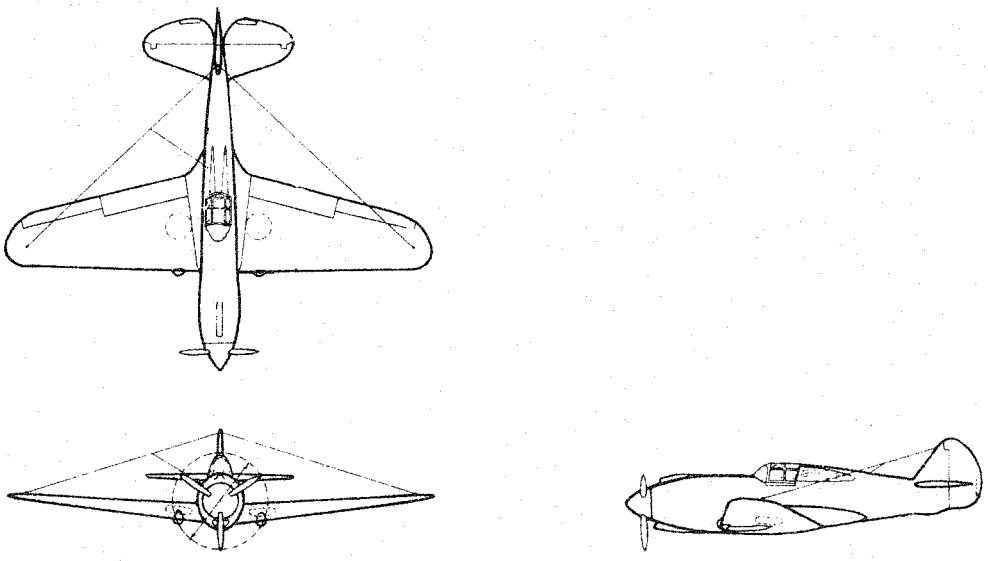

(l) Airplane 12 (Curtiss XP-42).

Figure 1.- Continued.

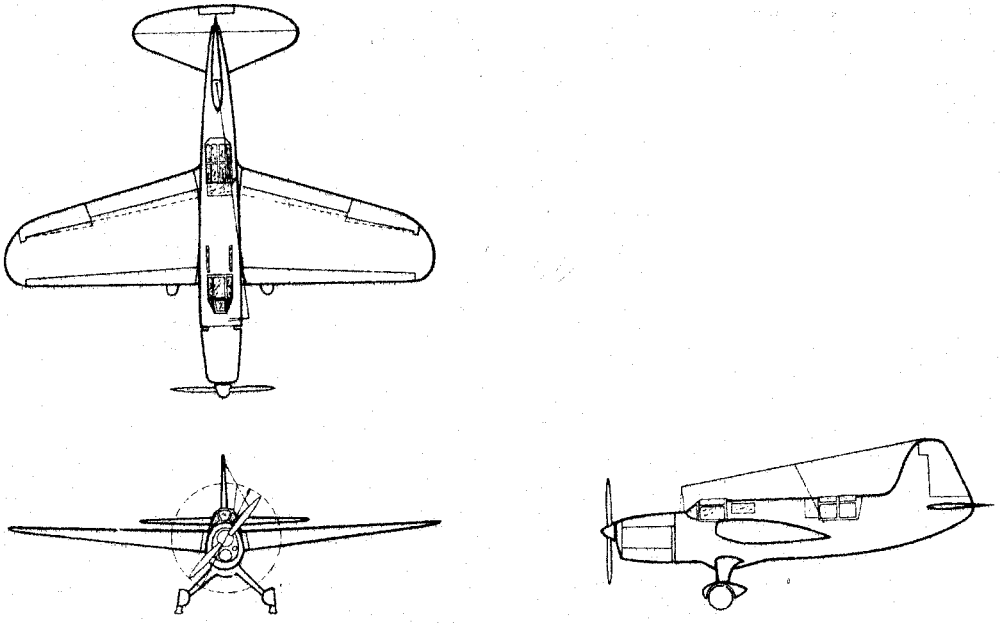

(m) Airplane 13 (Curtiss XSO3C-1).

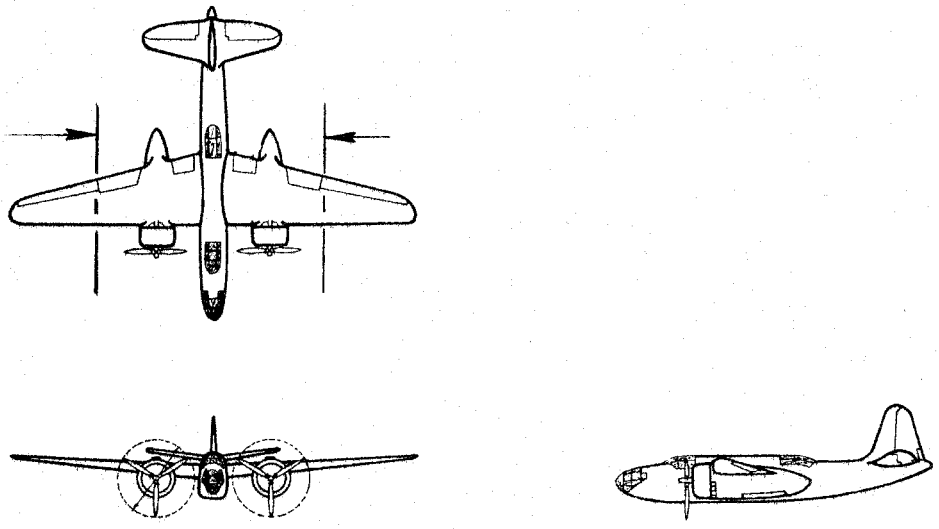

(n) Airplane 14 (Douglas A-20A). Note that airplane 14 was tested with outer wing panels removed as indicated.

Figure 1.- Continued.

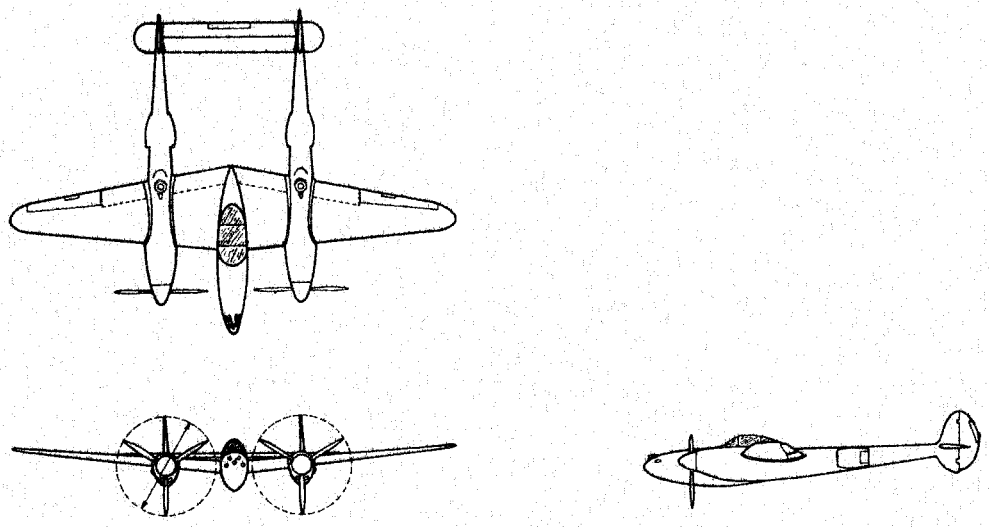

(o) Airplane 15 (Lockheed YP-38).

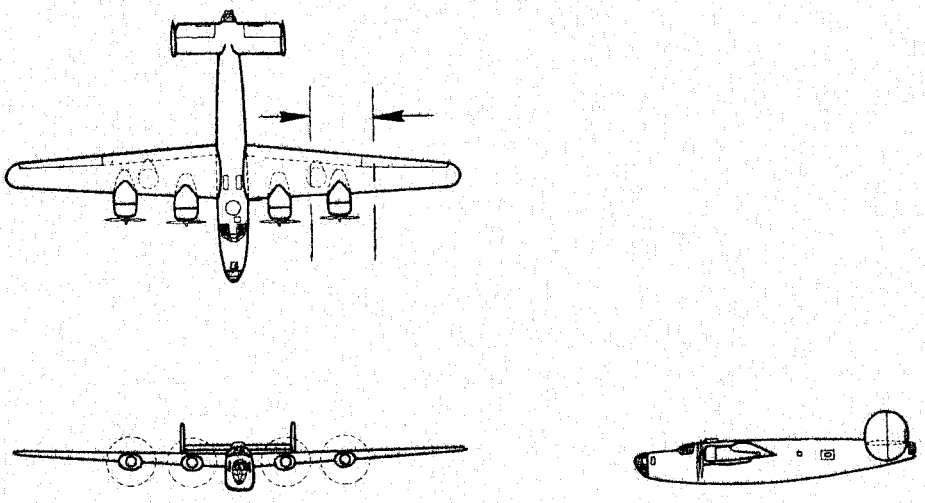

(p) Airplane 16 (Consolidated B-24D). Note that isolated engine nacelle of airplane 16 was tested as indicated.

Figure 1.- Continued.

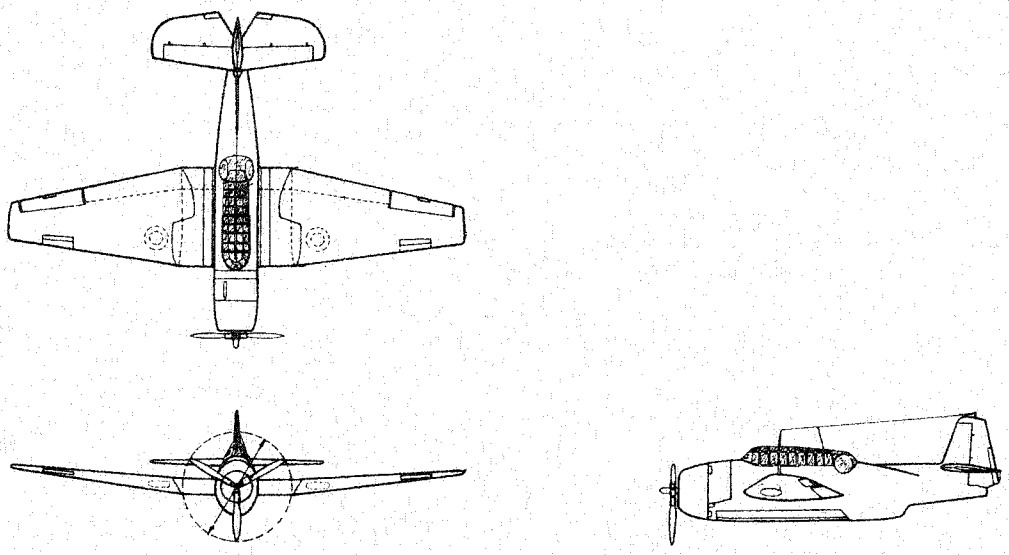

(q) Airplane 17 (Grumman XTBF-1).

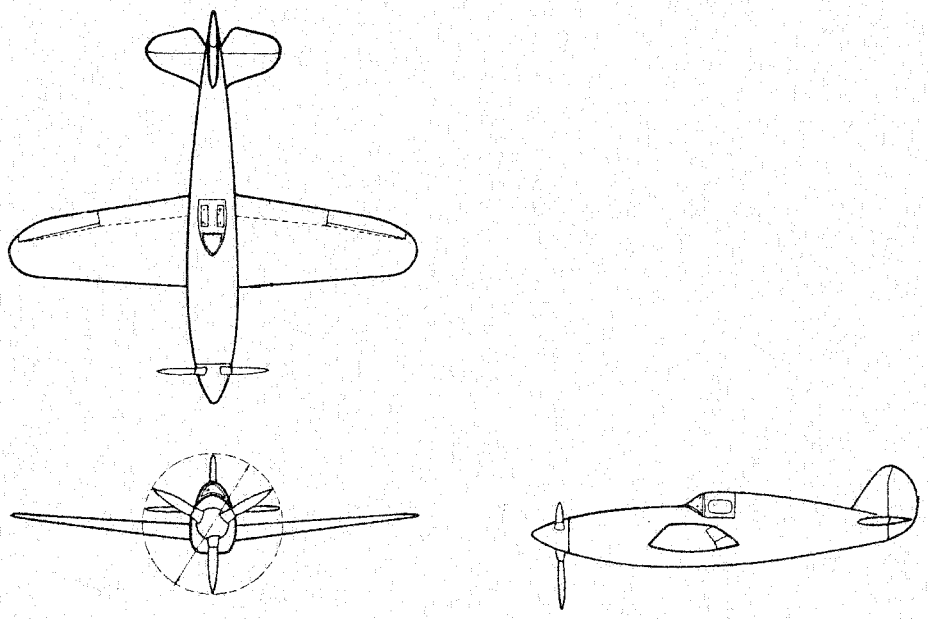

(r) Airplane 18 (General Research Model).

Figure 1.- Continued.

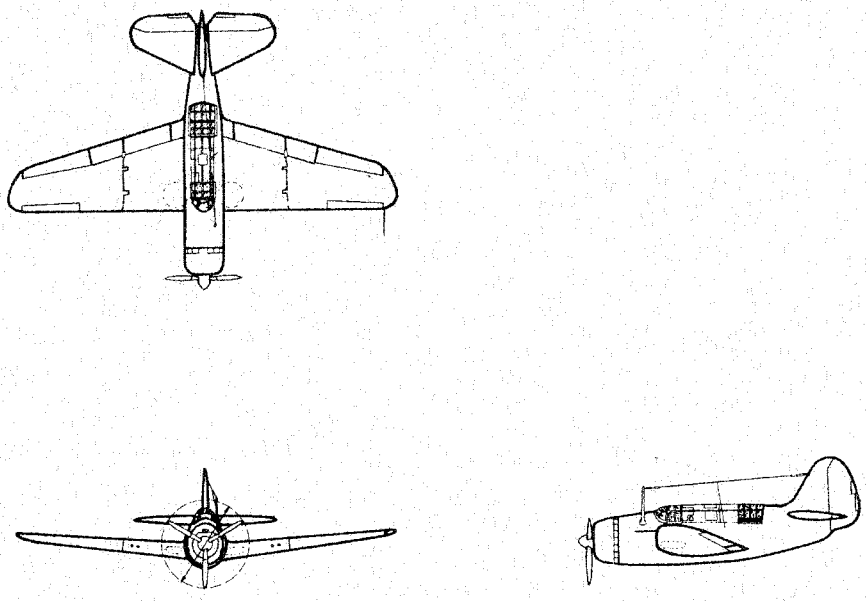

(s) Airplane 19 (Curtiss SB2C-1).

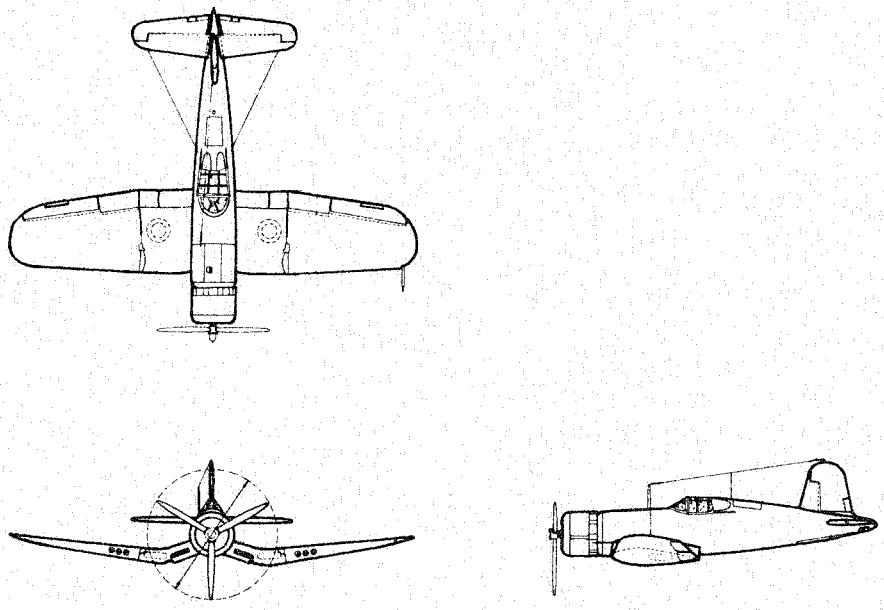

(t) Airplane 20 (Vought-Sikorsky F4U-1).

Figure 1.- Continued.

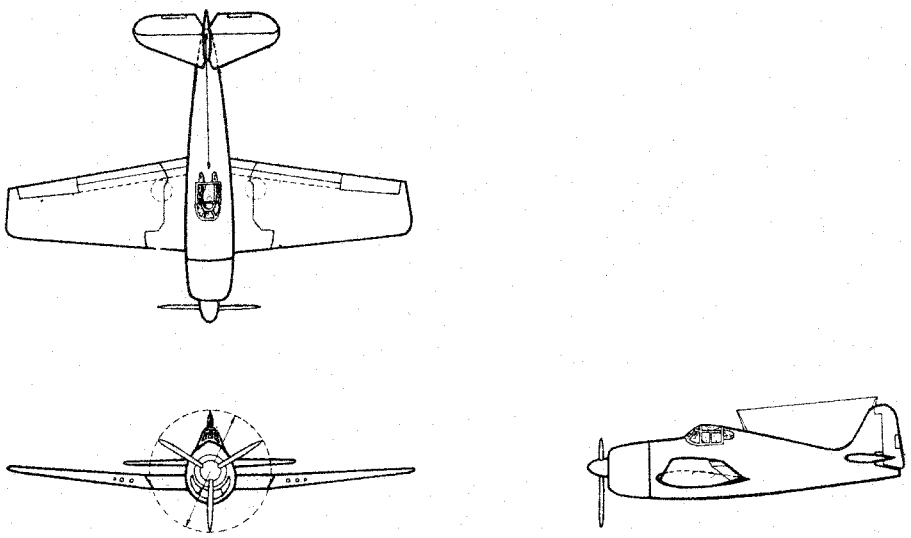

(u) Airplane 21 (Grumman F6F-3).

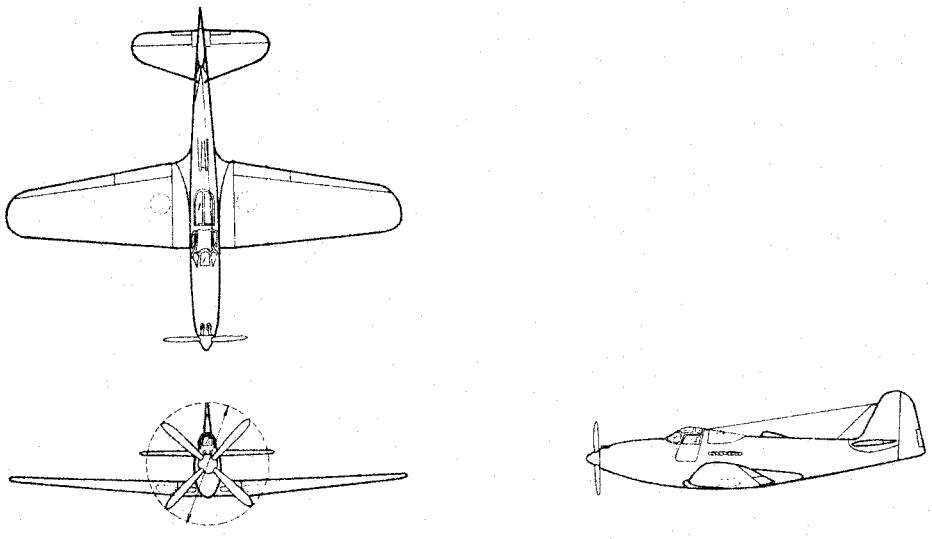

(v) Airplane 22 (Bell P-63).

Figure 1.- Continued.

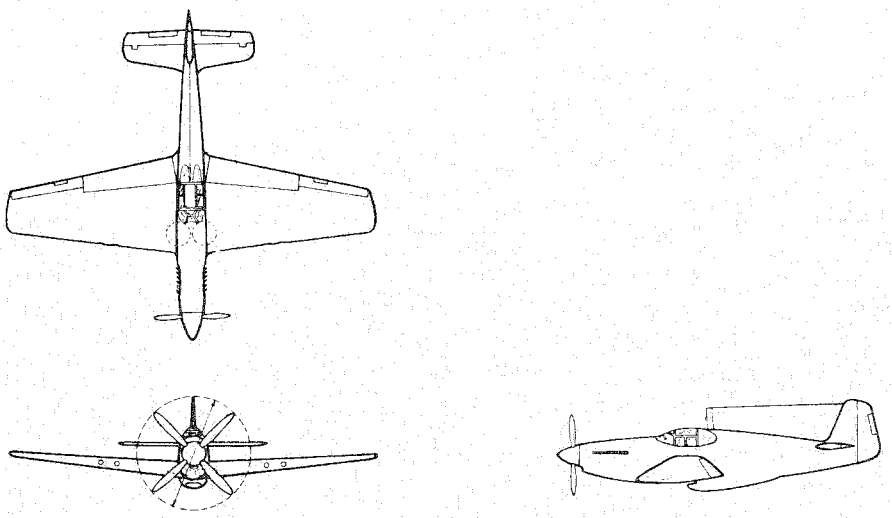

(w) Airplane 23 (North American P-51B).

Figure 1.- Concluded.

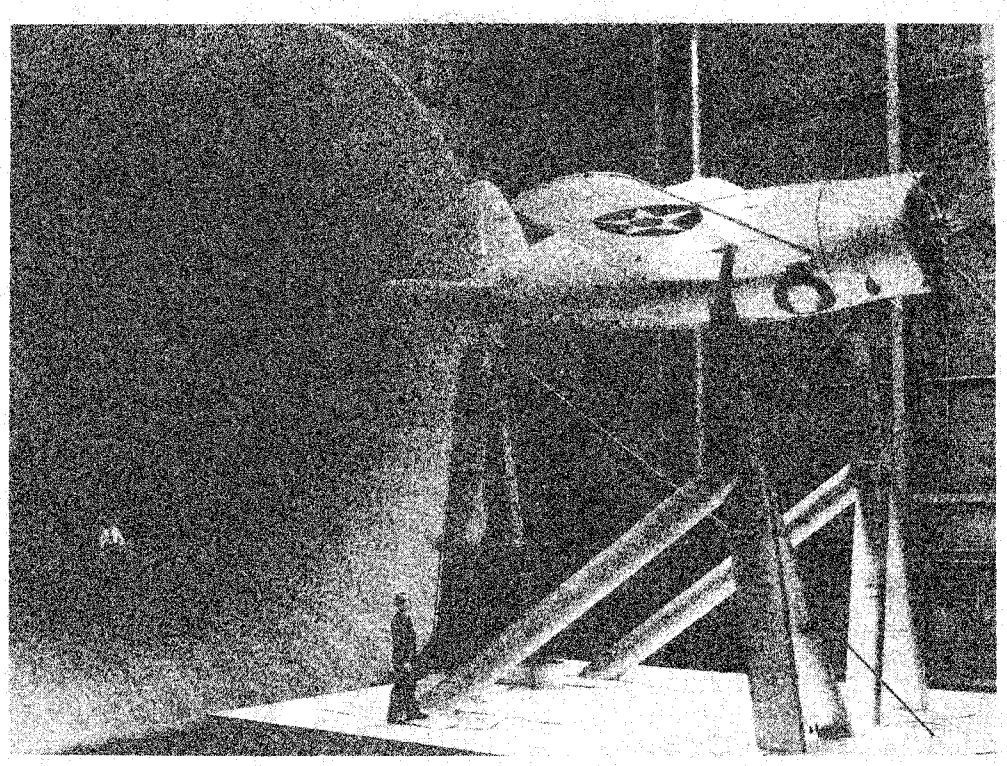

(a) Airplane 1 (Brewster XF2A-1).

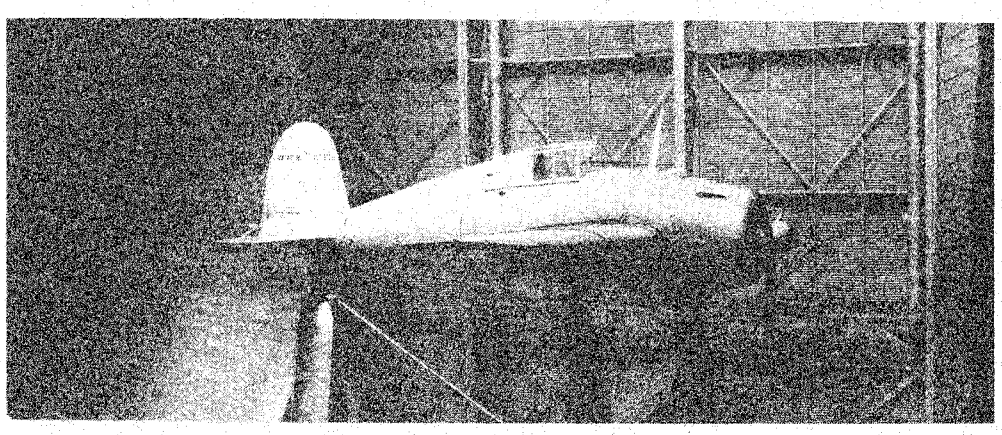

(b) Airplane 2 (Grumman XF4F-2).

L-76-180

Figure 2.- Photographs of airplanes mounted for tests in Langley full-scale tunnel.

(c) Airplane 3 (Grumman F3F-2).

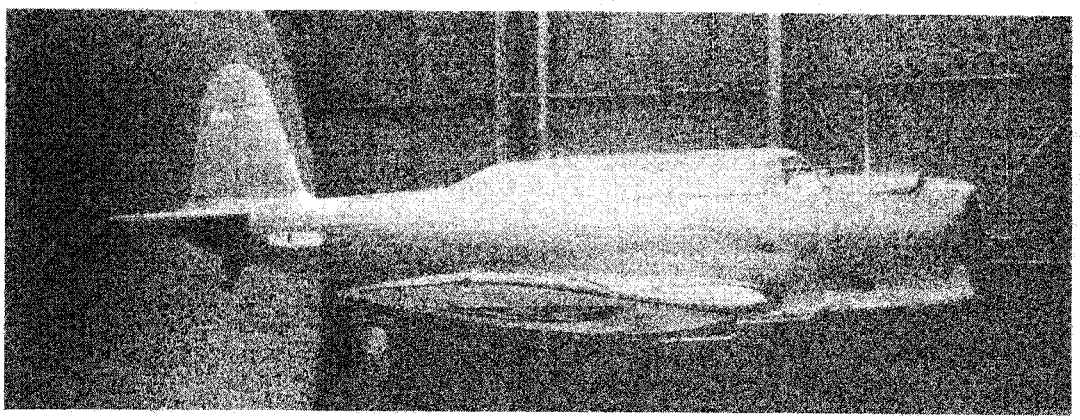

(d) Airplane 4 (Vought SB2U-1).

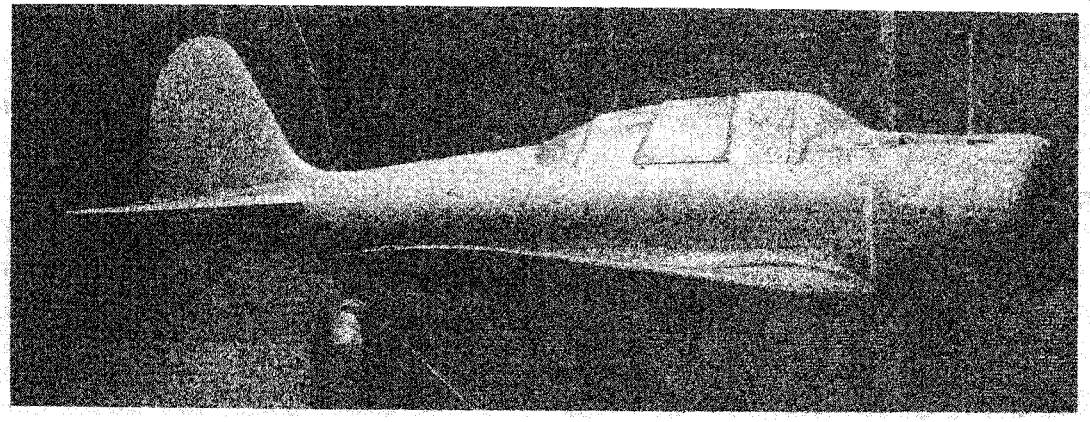

(e) Airplane 5 (Douglas XBT-2) with modified cockpit canopy.

Figure 2.- Continued. L-76-181

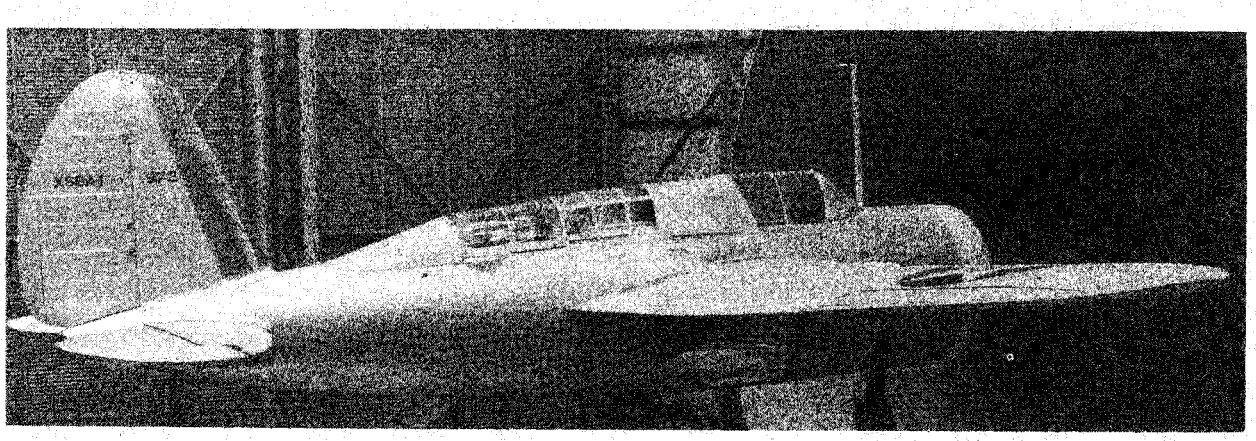

(f) Airplane 6 (Brewster XSBA-1) with modified cockpit canopy.

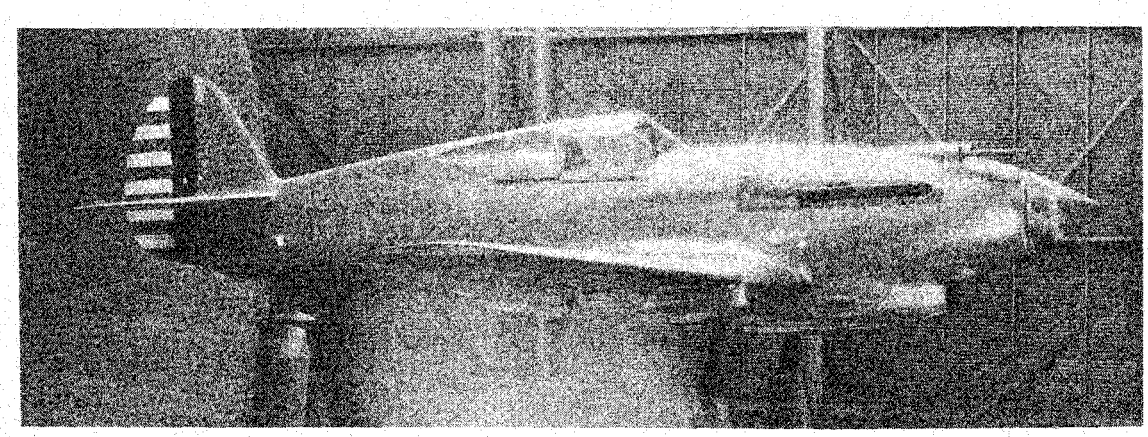

(g) Airplane 7 (Curtiss XP-40).

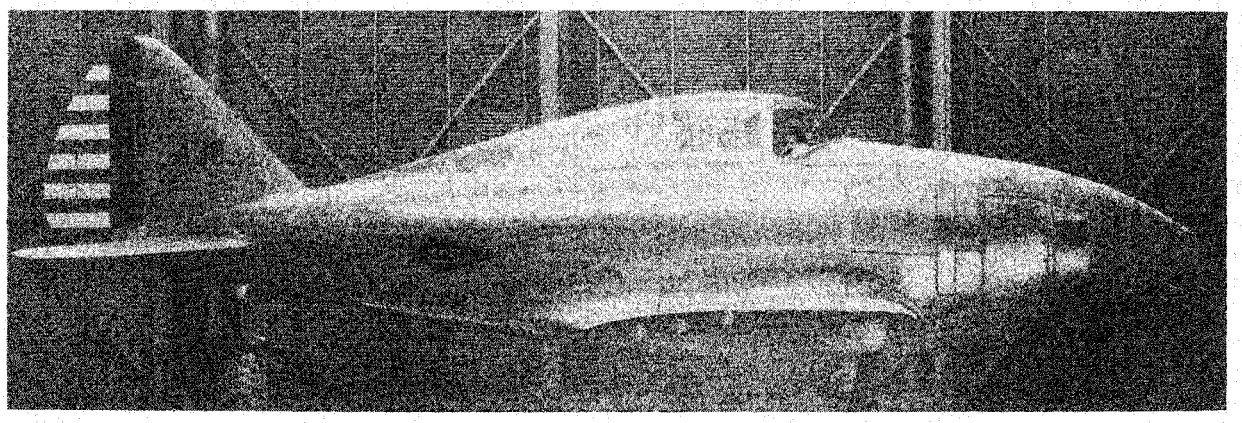

(h) Airplane 8 (Seversky XP-41) with streamlined nose fairing.

Figure 2.- Continued. L-76-182

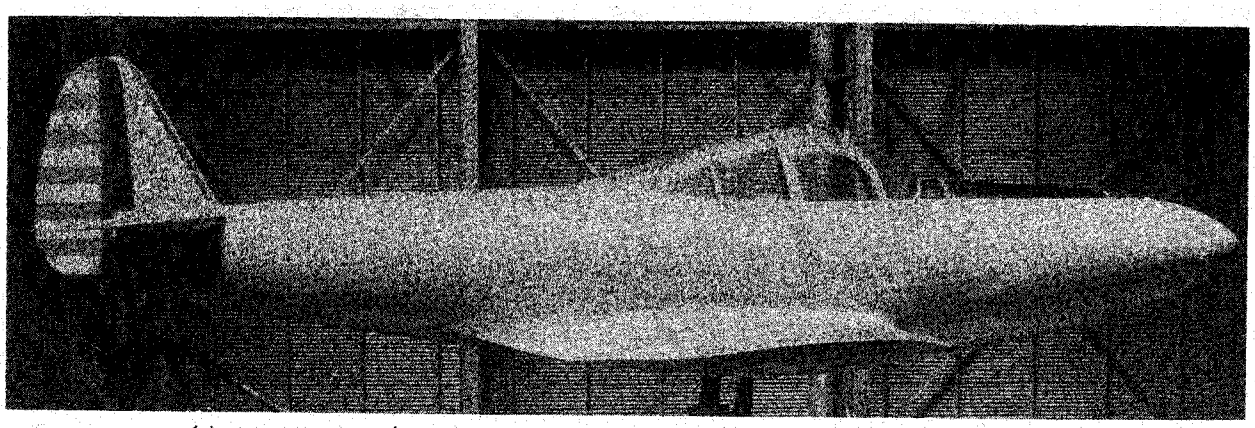

(i) Airplane 9 (Bell XP-39) with external protrusions removed.

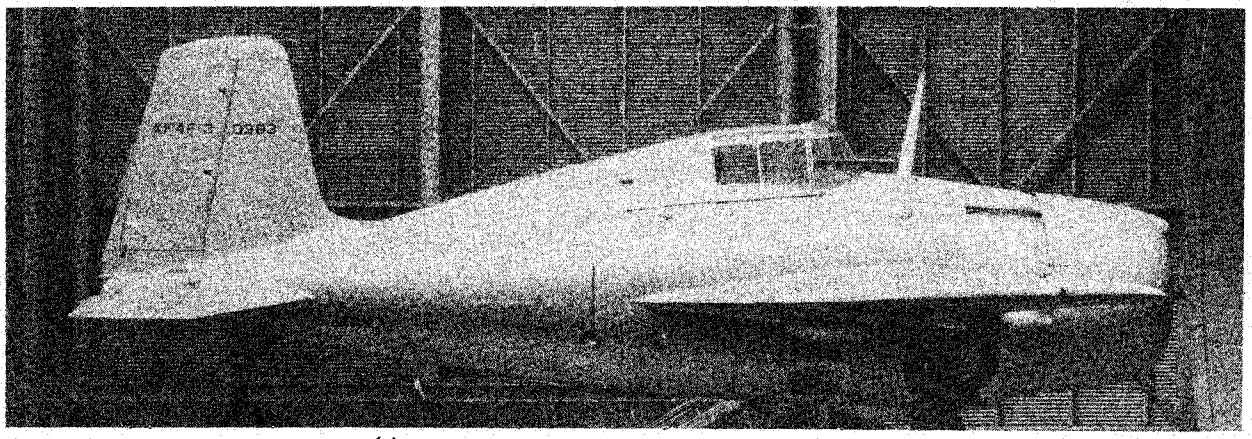

(j) Airplane 10 (Grumman XF4F-3).

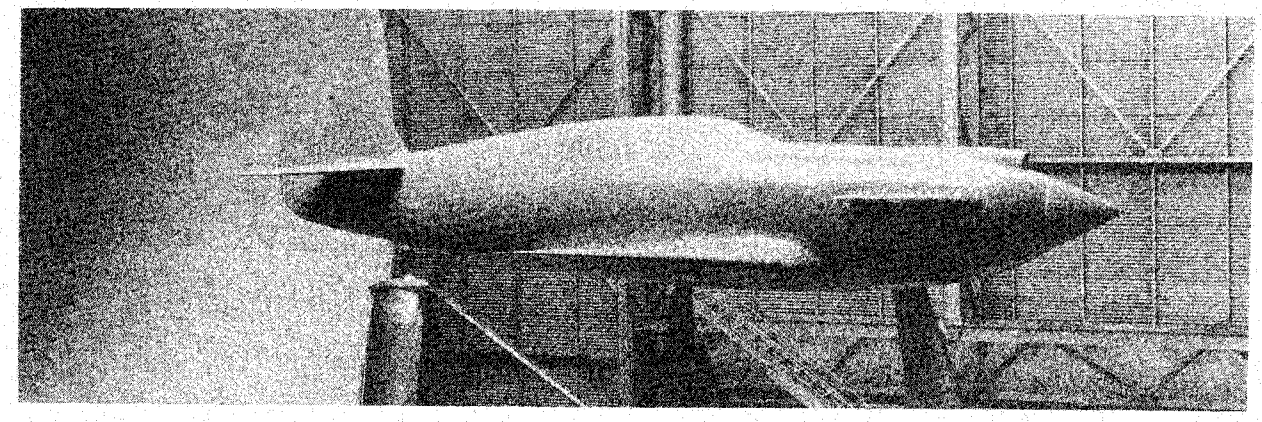

(k) Airplane 11 (Curtiss XP-46).

Figure 2.- Continued. L-76-183

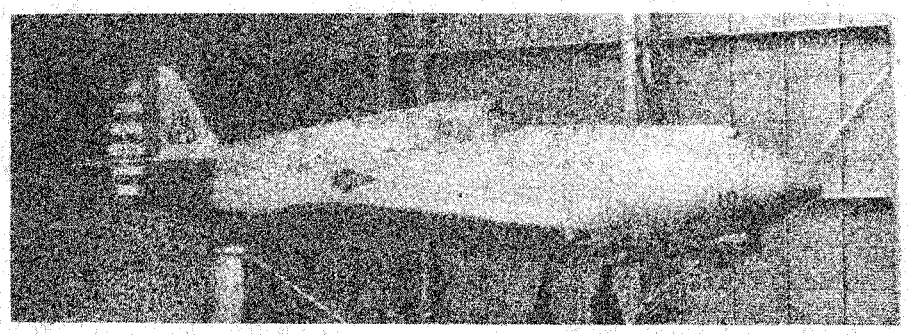

(l) Airplane 12 (Curtiss XP-42).

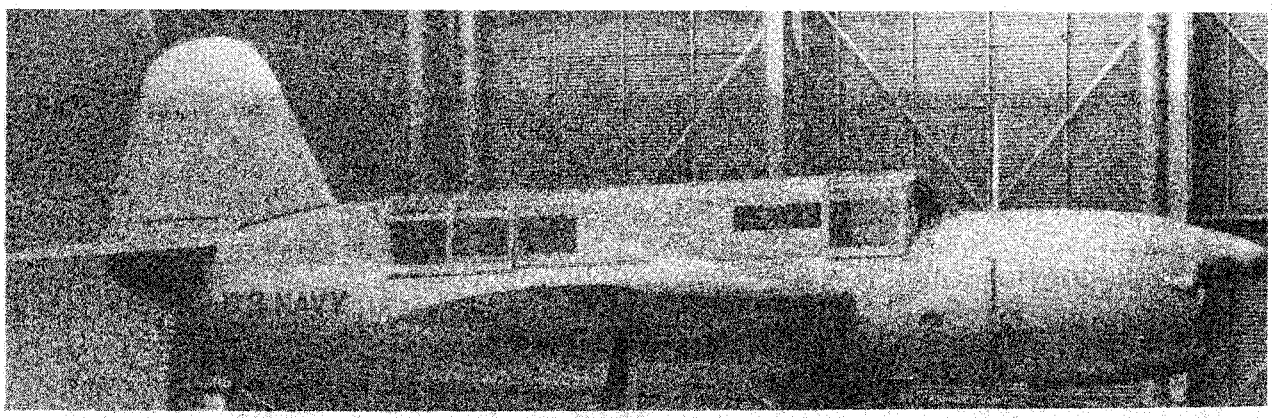

(m) Airplane 13 (Curtiss XSO3C-1).

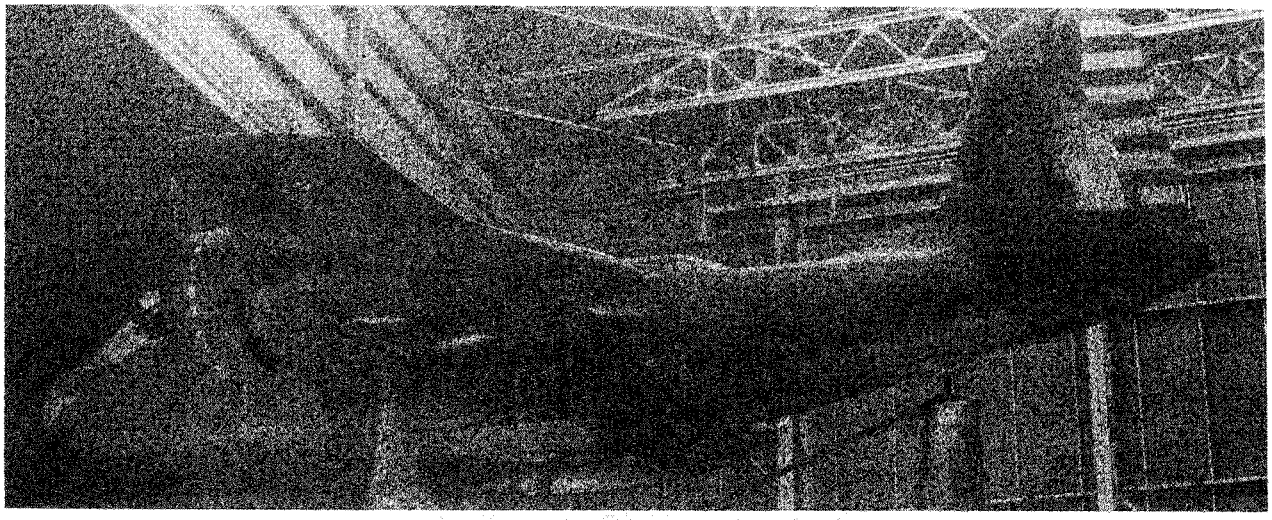

(n) Airplane 14 (Douglas A-20A) with outer wing panels removed.

Figure 2.- Continued. L-76-184

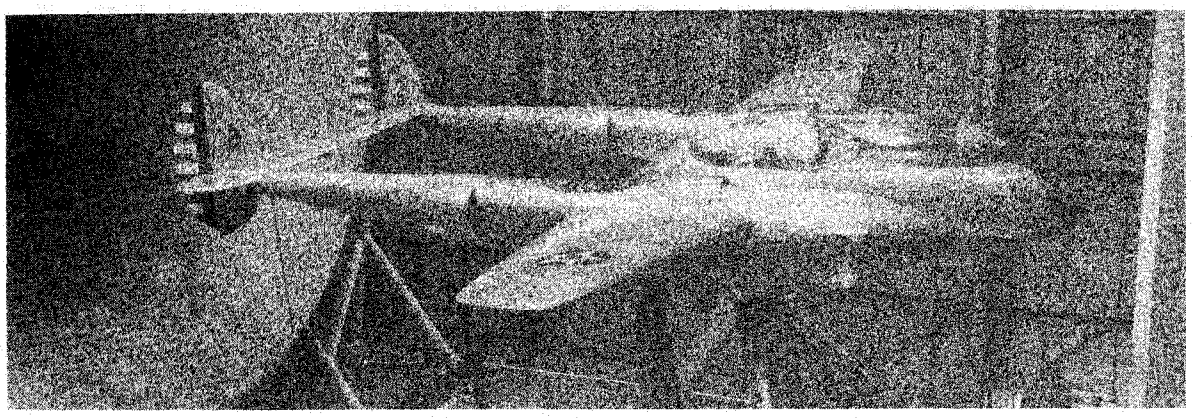

(o) Airplane 15 (Lockheed YP-38).

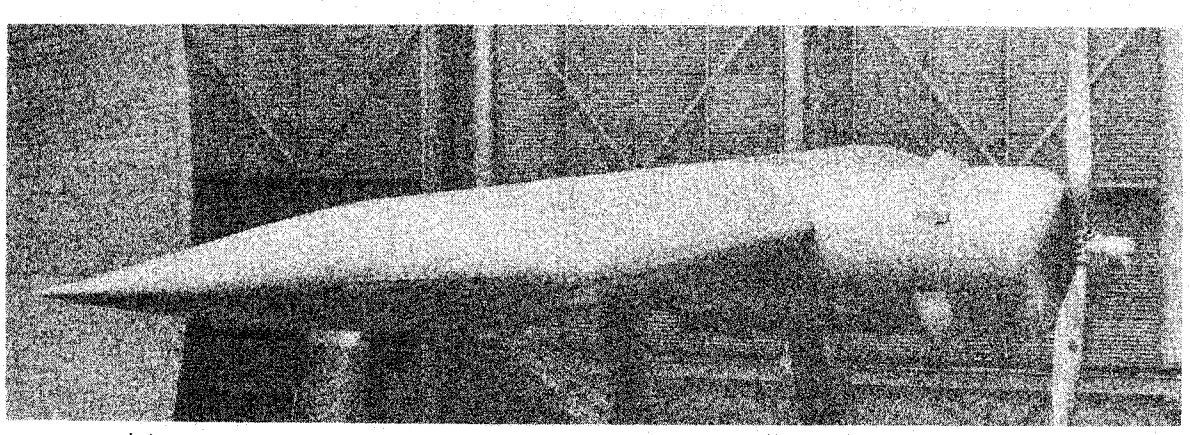

(p) Engine-nacelle installation of airplane 16 (Consolidated B-24D).

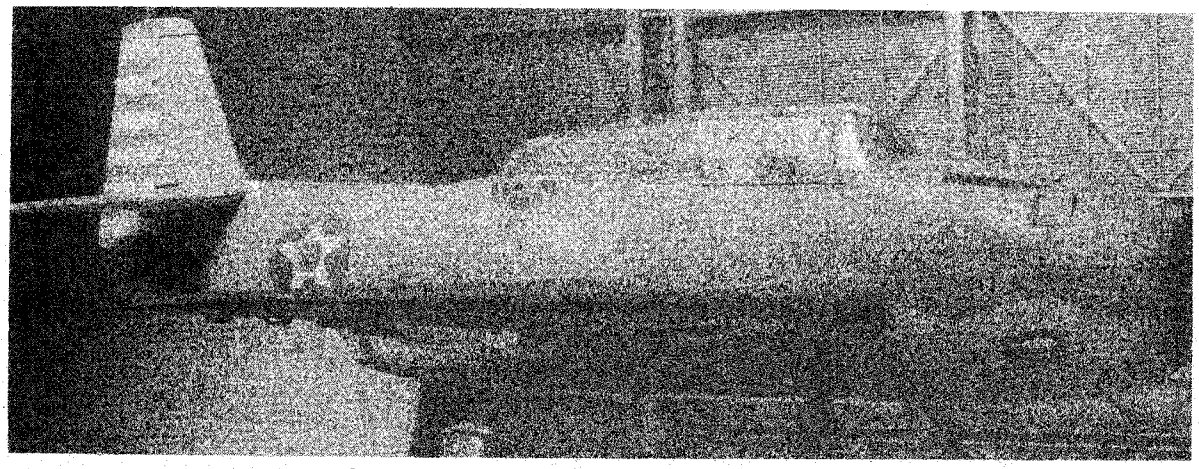

(q) Airplane 17 (Grumman XTBF-1).

Figure 2.- Continued. L-76-185

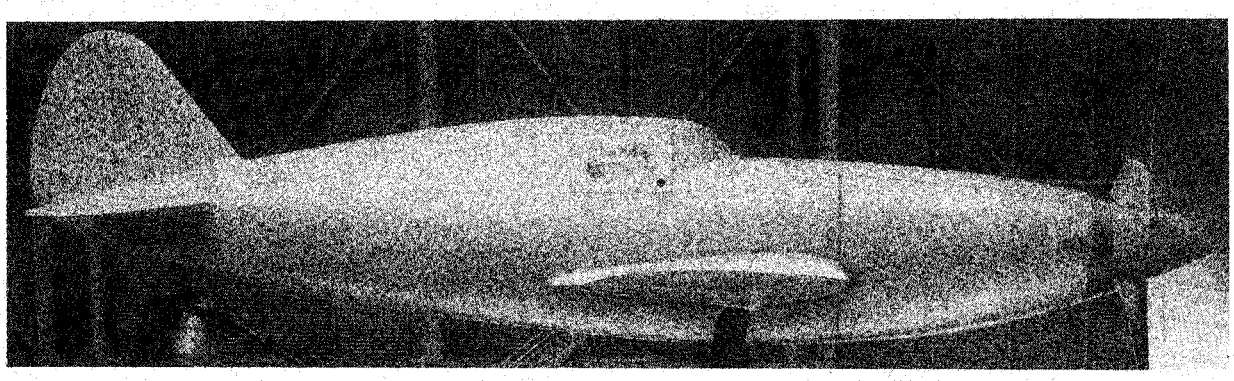

(r) Airplane 18 (General Research Model).

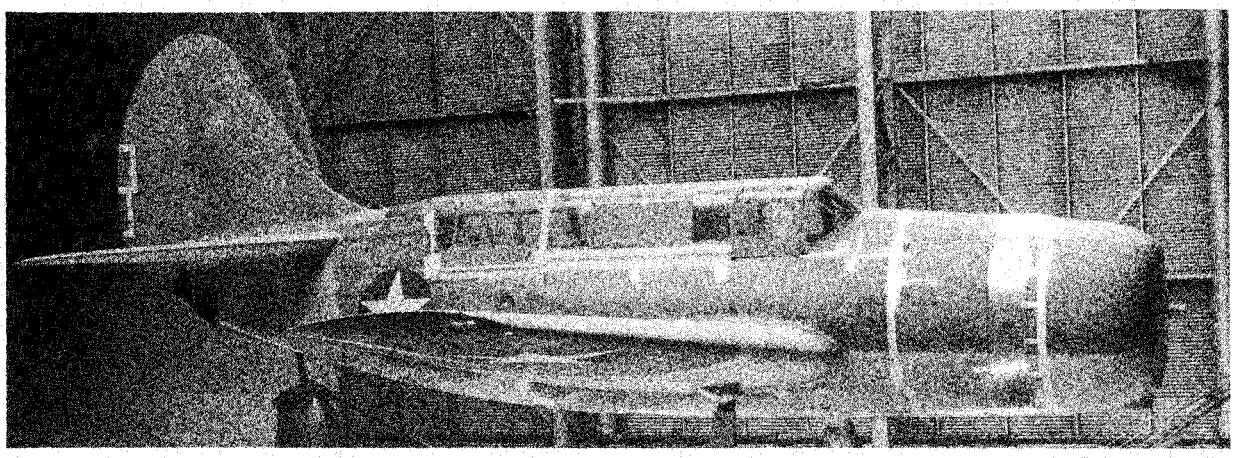

(s) Airplane 19 (Curtiss SB2C-1).

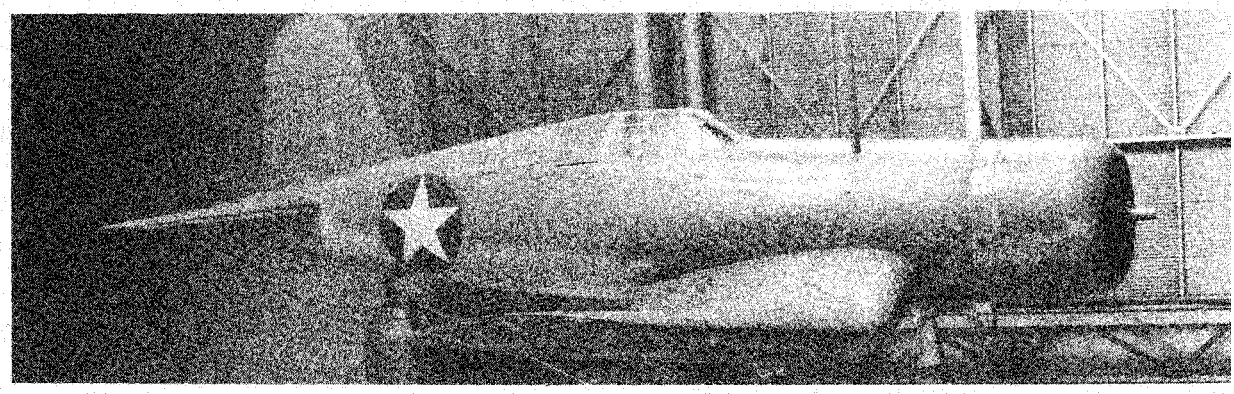

(t) Airplane 20 (Vought-Sikorsky F4U-1).

Figure 2.- Continued. L-76-186

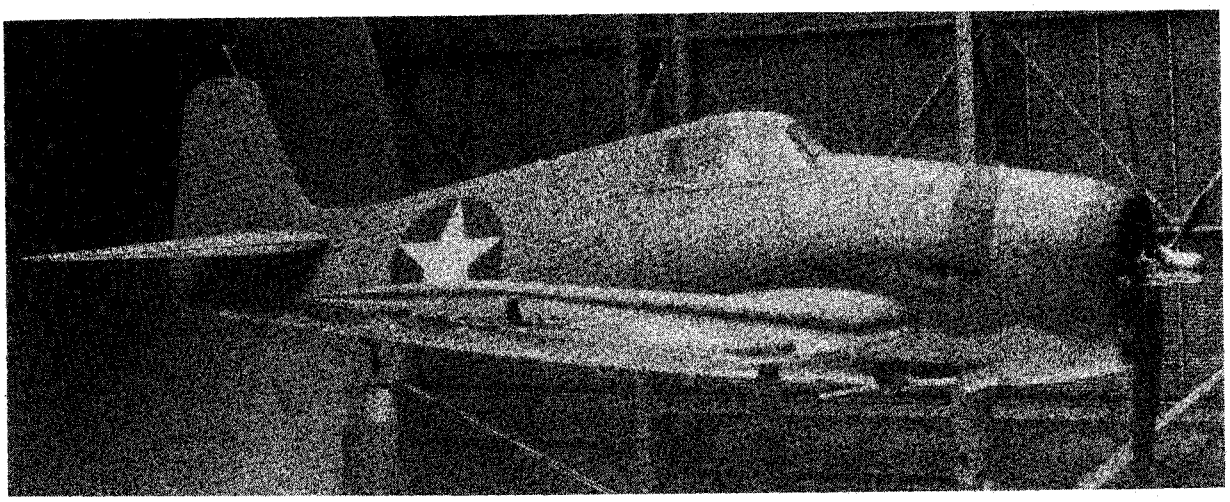

(u) Airplane 21 (Grumman F6F-3).

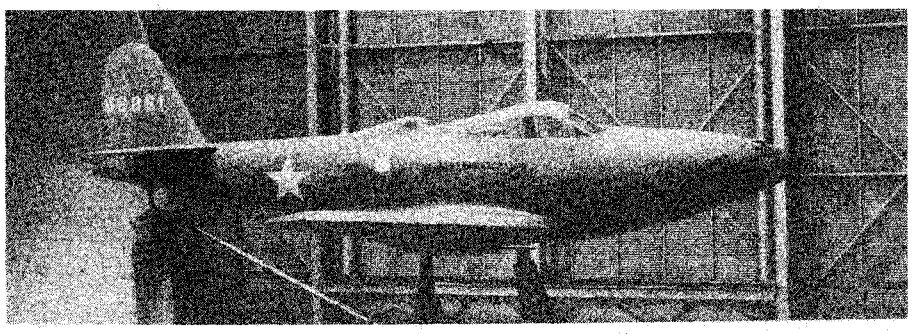

(v) Airplane 22 (Bell P-63).

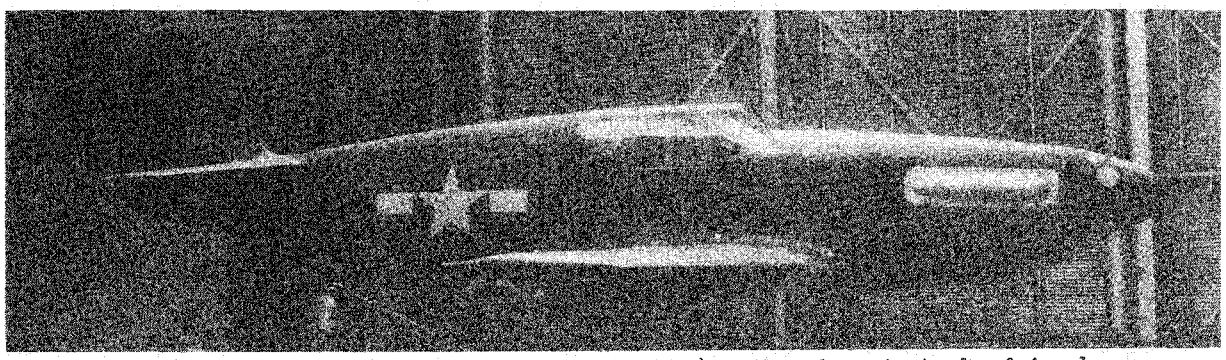

(w) Airplane 23 (North American P-51B) with exhaust stacks faired.

Figure 2.- Concluded. L-76-187